THEORETICAL STUDIES OF SGEMP FIELD GENERATION

Systems, Science and Software

PREPARED FOR
Defense Nuclear Agency

December 1974

DNA 3654F

THEORETICAL STUDIES OF SGEMP FIELD GENERATION

Systems, Science and Software
P.O. Box 1620
La Jolla, California 92037

December 1974

Final Report for Period November 1973—November 1974

CONTRACT No. DNA 001-74-C-0043

APPROVED FOR PUBLIC RELEASE;
DISTRIBUTION UNLIMITED.

THIS WORK SPONSORED BY THE DEFENSE NUCLEAR AGENCY
UNDER SUBTASK R99QAXEB089-46.

Prepared for
Director
DEFENSE NUCLEAR AGENCY
Washington, D. C. 20305

UNCLASSIFIED

SECURITY CLASSIFICATION OF THIS PAGE (When Data Entered)

REPORT DOCUMENTATION PAGE		READ INSTRUCTIONS BEFORE COMPLETING FORM
1. REPORT NUMBER DNA 3654F	2. GOVT ACCESSION NO.	3. RECIPIENT'S CATALOG NUMBER
4. TITLE (and Subtitle) THEORETICAL STUDIES OF SGEMP FIELD GENERATION		5. TYPE OF REPORT & PERIOD COVERED Final Report for Period Nov 73—Nov 74
		6. PERFORMING ORG. REPORT NUMBER SSS-R-75-2469
7. AUTHOR(s) Andrew Wilson		8. CONTRACT OR GRANT NUMBER(s) DNA 001-74-C-0043
9. PERFORMING ORGANIZATION NAME AND ADDRESS Systems, Science and Software P.O. Box 1620 La Jolla, California 92037		10. PROGRAM ELEMENT, PROJECT, TASK AREA & WORK UNIT NUMBERS NWED Subtask R99QAXEB089-46
11. CONTROLLING OFFICE NAME AND ADDRESS Director Defense Nuclear Agency Washington, D.C. 20305		12. REPORT DATE December 1974
		13. NUMBER OF PAGES<br~~100~~ 129
14. MONITORING AGENCY NAME & ADDRESS(if different from Controlling Office)		15. SECURITY CLASS. (of this report) UNCLASSIFIED
		15a. DECLASSIFICATION/DOWNGRADING SCHEDULE

16. DISTRIBUTION STATEMENT (of this Report)

Approved for public release; distribution unlimited.

17. DISTRIBUTION STATEMENT (of the abstract entered in Block 20, if different from Report)

18. SUPPLEMENTARY NOTES

This work sponsored by the Defense Nuclear Agency under Subtask R99QAXEB089-46.

19. KEY WORDS (Continue on reverse side if necessary and identify by block number)

IEMP
Analytic

20. ABSTRACT (Continue on reverse side if necessary and identify by block number)

Analytic models of the generation of IEMP in cavities (at pressures below 1 torr) and external to conducting objects in free space are developed. A series of computer codes devised to extend the analytic approach to more complex situations is presented. Four areas of research are identified: (1) the effect of small conducting or dielectric objects on the potential distribution in a cavity in which space charge exists; (2) the development of an analytic method to treat space-charge dynamics before the onset of space-charge-limiting of a nonmonoenergetic current beam; (3) the

DD FORM 1 JAN 73 1473 EDITION OF 1 NOV 65 IS OBSOLETE

UNCLASSIFIED

SECURITY CLASSIFICATION OF THIS PAGE (When Data Entered)

20. ABSTRACT (Continued)

formation and time-dependent behavior of a plasma sheath outside a (planar, cylindrical or spherical) conductor; (4) the conditions for pinching to occur in a finite cavity. Numerical examples of each of the four topics are presented. Finally, the dynamics of a heavily space-charge-limited current in the SPI beam injection facility is examined with the electrostatic particle code.

PREFACE

The following S^3 personnel contributed to the work described in this report:

James Harvey
Ira Katz
Donald Parks
Albert Petschek
Robert Vik
Andrew Wilson

CONTENTS

ILLUSTRATIONS

ILLUSTRATIONS (Cont'd)

ILLUSTRATIONS (Cont'd)

1. SCOPE OF WORK

The work described in this report is concerned primarily with the calculation of IEMP and SGEMP fields in low-density media. Thus, problems related to the photoemission of electrons or to the transport of photons and electrons through dense materials form no part of this work. Rather, the plasma aspects of IEMP and SGEMP are emphasized.

A variety of problems are addressed here. In Chapter 2 analytic models of IEMP and SGEMP in vacuo are developed. Much of this research is the outgrowth of the work described in Reference 2.1.1. First (Section 2.1), the basic problem of the calculation of the electric fields and potentials in an evacuated cavity is considered. Questions related to boundary conditions (conducting or insulating) are examined. Also, the effect of the angle and energy dependence of the electrons emitted into the cavity is discussed. Next (Section 2.2), the effect of placing small dielectric objects in a cavity is examined. The objects are assumed to be small in comparison with the length scale of the variation of the fields. The Child-Langmuir treatment of space-charge limited current flow in a diode has served as a valuable scaling relationship for many applications in IEMP research. In Section 2.3 an analytic treatment of cases where the electrons emitted are not monoenergetic and where the emitted pulse is time-dependent is presented. It is based upon a perturbation expansion of the electron transport equation. In Section 2.4 the fields generated outside, rather than within a conductor are analyzed. This work is related to satellite SGEMP problems. The formation of plasma sheaths is examined and a method is presented

for calculating the size, density and time dependence of such sheaths in plane, cylindrical and spherical geometries.

In Chapter 3 the conditions for the pinch effect to be important in IEMP environments are examined. Pinching in dense, collision-dominated plasmas is well understood and, more recently, pinching of intense, relativistic electron beams has been observed. However, the magnetic constriction of diffuse, low-energy IEMP electron beams is less well understood. Only recently have experiments been initiated in which the effect might be observed.

It is possible to derive simple analytic conditions for pinching in two limiting cases--namely, at zero density and secondly, when the space charge is neutralized. However, under intermediate conditions a numerical treatment is necessary. A 2-D computer code was written to examine the IEMP pinch effect. Calculations of weak pinching in the presence of a partially neutralized space-charge field are presented in Chapter 3.

Two computer codes were developed for application to problems where analytic methods are not useful. They are described in Chapter 4. Both are axisymmetric, two-dimensional, particle codes. Both use the Fast Fourier Method to decompose a 2-D problem into a finite set of uncoupled 1-D equations. The codes are much faster in operation than those based on the Green's Function method. They are also less cumbersome and hence faster than the fully electromagnetic treatment used in some IEMP particle codes. They employ the capacitance matrix technique to solve the boundary value problem. As a result they have a greater range of application than other IEMP codes, inasmuch as they could be coded to apply to arbitrary boundaries and, indeed, to arbitrary potentials on the boundaries. Of the two codes, one solves electrostatic problems (Poisson's

equation) while the other solves magnetostatic problems (Poisson's equation and Ampere's Law). The electrostatic code has been applied to space-charge limited flow in axisymmetric geometry. Also, it has been used to examine the effects of nonconducting boundaries on the beam transport in cylinders. These calculations are discussed in Chapter 5. The magnetostatic code has been applied to pinch problems (Chapter 3).

Thus, a considerable range of work is presented here. The electrodynamic aspects of IEMP and SGEMP are emphasized. Of particular interest is the cavity field generation problem under a wide range of conditions--from very low densities where the current flow may be limited by the electrostatic potential to higher densities where it may be limited by the magnetic potential. This work is applicable not only to real environments but also to simulation experiments. Finally, the analytic work in Chapter 2, in addition to having direct application to a number of problems (dielectric objects, satellite sheaths, etc.), could also provide the impetus for numerical studies of such effects.

2. FIELD GENERATION IN A VACUUM

2.1 GENERAL CONSIDERATIONS

The problem of calculating the electric and magnetic fields either within an evacuated cavity or outside an object in free space is a topic of perennial interest to IEMP and SGEMP workers. Much effort has been expended toward understanding such problems and this has led to a variety of techniques — both numerical and analytical.

In this chapter we shall deal only with analytical methods and shall discuss in Sections 2.2 through 2.4 three topics in which appreciable progress can be made without resorting to the computer. This section will be an introduction to those sections. The notation used will be introduced and the basis for the models used will be considered.

To begin, it is assumed that Poisson's equation is applicable to the problems under examination. The use of this equation is valid provided the length scale of interest, L, is traversed by photons in a time L/c that is much less than the time t_r characteristic of the pulse duration. Here c is the velocity of light. That is, we require

$$L << ct_r \quad . \tag{2.1.1}$$

Thus, for a pulse duration $t_r = 10^{-8}$ sec it is clear that this condition is satisfied for systems as large as one meter. In addition to this condition it is also necessary that the electrons have essentially non-relativistic velocities βc. That is, we require that $\beta << 1$. Otherwise the electrons would interact directly with the electromagnetic waves — a feature which is not taken into account if we use Poisson's equation alone.

In one dimension Poisson's equation is written

$$d^2\psi/dz^2 = -4\pi\rho \quad . \tag{2.1.2}$$

The charge density ρ is related to the current density j_{esu} by

$$\rho\beta c = -j_{esu}$$

or

$$\rho = -j_{esu}/\beta c = -0.1j/\beta \tag{2.1.3}$$

where j is in amperes/cm^2 ($j > 0$). If the electrons are not limited by space charge β may be taken as constant and $j(z)$ is just the emitted current density $j(0)$ at $z = 0$. With ψ expressed in volts the Poisson equation is then written

$$d^2\psi/dz^2 = 120\pi j/\beta \quad . \tag{2.1.4}$$

This is easily integrated and, with grounded boundaries

$$\psi(0) = \psi(L) = 0$$

the potential is given by

$$\psi(z,t) = -(60\pi/\beta)\, j(0,t)\, z(L - z) \quad . \tag{2.1.5}$$

This simple result will be referred to on numerous occasions throughout this report. This potential is negative and has its greatest magnitude at $z = L/2$,

$$\psi_{max} = - (15\pi/\beta)\, jL^2 \quad . \tag{2.1.6}$$

Thus, with $\beta \sim 1/3$, $L = 10$ cm and $j = 1$ A/cm^2 the maximum potential is approximately 14.5 kilovolts. If, instead of grounded boundaries, we have prescribed values $\psi(0,t)$, $\psi(L,t)$ which may be time-dependent the result is

$$\psi(z,t) = (60\pi/\beta)\, j(0,t)\, z(L - z) + [\psi(L,t) - \psi(0,t)]\, z/L + \psi(0,t) \quad .$$

Consequently, if the emitting surface $z = 0$ is grounded but the receiving plate $z = L$ becomes charged in the course of the pulse then the absolute value $|\psi|$ is increased. As a result, an insulating plate (or more generally insulating boundaries) will cause the potential $|\psi|$ to increase and hence may lead to the onset of space-charge limited flow under otherwise nonspace-charge dominated conditions.

In two-dimensional axisymmetric geometry the Poisson equation reads

$$\left(\frac{1}{r}\frac{\partial}{\partial r}\, r\, \frac{\partial}{\partial r} + \frac{\partial^2}{\partial z^2}\right) \psi = -1200\, \pi\rho \tag{2.1.7}$$

where ψ is expressed in volts and ρ is in electrostatic units. With the walls of a cylinder, of radius R and length L, the solution to this equation is

$$\psi(r,z,t) = 300 \int_0^R dr'\, r' \int_0^L dz'\, G(r,r',z,z')\, \rho(r',z',t) \tag{2.1.8}$$

where the Green's function G is written (Ref. 2.1.2)

$$G(r,r',z,z') = \frac{8\pi}{R} \sum_{n=1}^{\infty} F(z,z')\, \frac{J_0\left(\alpha_n \frac{r}{R}\right) J_0\left(\alpha_n \frac{r'}{R}\right)}{\alpha_n J_1^2(\alpha_n) \sinh \alpha_n \frac{L}{R}} \tag{2.1.9}$$

where

$$F(z,z') = \sinh \frac{\alpha_n z}{R} \sinh \alpha_n \frac{L - z'}{R} \quad , \quad z \leq z'$$

$$= \sinh \frac{\alpha_n (L - z)}{R} \sinh \frac{\alpha_n z'}{R} \quad , \quad z \geq z'$$

where

$$J_0(\alpha_n) = 0 \quad , \quad n = 1, 2, \ldots \; .$$

The emitted current can be expanded in terms of the functions appropriate to cylindrical symmetry, namely Bessel functions

$$j(r,0,t) = g(t) \sum_{s=1}^{\infty} a_s J_0(\alpha_s r/R) \quad . \qquad (2.1.10)$$

In some cases only a few terms of this expression need be retained (Ref. 2.1.2).

In the case where electrons are injected normal to the $z = 0$ surface the one-dimensional relationship (Eq. 2.1.3) between the charge density ρ and the emitted current density j can be used, as done above. We shall now generalize the treatment given in Ref. 2.1.1 to include both angular and energy dependence.

At a point $(r,0)$ on the emitting surface of a cylinder (Figure 2.1.1) let the number of electrons be

$$n(r,0) = \int dv_0 \, v_0^2 \, d\theta_0 \sin\theta_0 \, d\phi_0 \, f(r,0,v_0,\theta_0,\phi_0)$$

where f is the distribution function, θ_0 and ϕ_0 are the polar and azimuthal angles, respectively, and v_0 is the velocity.

In order to calculate the charge density $\rho(r,z)$ at an arbitrary point within the cylindrical cavity it is necessary to first obtain the distribution function from the Vlasov equation

$$\frac{\partial f}{\partial t} + \vec{v} \cdot \nabla f - \frac{e}{m} \vec{E} \cdot \frac{\partial f}{\partial \vec{v}} = 0$$

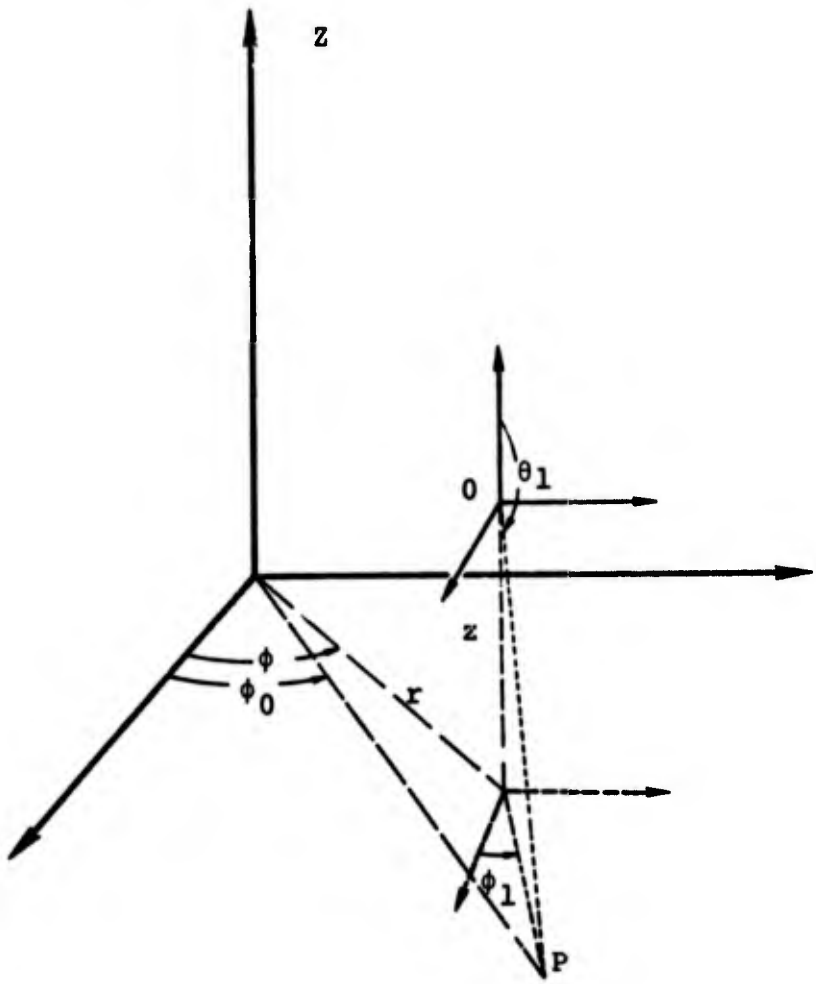

Figure 2.1.1 Showing the local coordinate system angles (θ_1, ϕ_1) of an observer O at point (R = r, Z = z, $\Phi = \phi$) with respect to a point P at (R = r_o, Z = 0, $\Phi = \phi_0$) from which electrons are emitted.

where E is the electric field. Since there is no absorption nor source of electrons in the cavity it is easier to obtain the solution by noting that the Vlasov equation is really a statement about the conservation of electrons in phase-space. At a point (r,z) the number of electrons f is obtained by integrating back along their trajectories to the point of emission $(r_0,0)$. Secondly, in the quasistatic approximation where electrons traverse a distance L in a time much less than that characterizing changes in the emitted current the time derivative in the Vlasov equation can be neglected. This precludes discussion of space-charge limited currents.

It is now useful to introduce the angles θ_1, ϕ_1 (Figure 2.1.1) in the local frame of an observer at a point (r,z,ϕ). In terms of these quantities the charge density can be expressed as

$$\rho(r,z,\phi) = -e\int dv\ v^2\ d\phi_1\ d\theta_1\ \sin\theta_1\ f(r_o,o,v,\pi-\theta_1,\pi+\phi_1) \qquad (2.1.11)$$

where

$$r_o^{\,2} = r^2 + z^2\tan\theta_1 - 2rz\ \tan\theta_1\ \cos(\phi-\phi_1)$$

which follows from some straightforward algebra.

At this point we must make some assumptions about the form of the distribution function of the emitted electrons. First, we shall assume that f is separable:

$$f(r_0,0,v_0,\theta_0,\phi_0) = f_0(r_0,0)\ f_v(v_0)\ f_\Omega(\theta_0,\phi_0) \qquad (2.1.12)$$

That is, the distribution of electrons emitted is independently a function f_0 of position on the $z = 0$ surface, a function

f_v of the emission velocity v_0 and a function f_Ω of the angle of emission. Let us now consider a few specific models of the emission.

1. Energy (velocity) dependence:

a. Maxwellian

$$f_v(v) = \frac{4n_0}{\sqrt{\pi}} \frac{\exp - (v/v_T)^2}{v_T^3} \tag{2.1.13}$$

b. Monoenergetic

$$f_v(v) = n_0 \frac{\delta(v - v_T)}{v^2} \tag{2.1.14}$$

Note that in either case

$$\int_0^\infty dv\, v^2 f_v(v) = n_0 \tag{2.1.15}$$

2. Angular dependence:

We shall always assume azimuthal symmetry in the angle of emission, i.e.,

$$f_\Omega(\theta_0,\phi_0) = \frac{f_\Omega}{2\pi}(\theta_0) \quad . \tag{2.1.16}$$

This is not a very restrictive assumption and is true in most circumstances. Hereafter, $\rho(r,z,\phi)$ will be written as $\rho(r,z)$. Two models of angular emission are:

a. Isotropic

$$f_\Omega(\theta_0) = \frac{f_{\Omega_0}}{2\pi} \tag{2.1.17}$$

b. Unidirectional normal to surface

$$f_\Omega(\theta_0) = \frac{f_\Omega}{2\pi}\,\delta(\cos\theta_0) \tag{2.1.18}$$

Note that in either case

$$\int d\phi_0\, d\theta_0 \sin\theta_0\, f_\Omega = 1 \tag{2.1.19}$$

From Eqs. (2.1.11), (2.1.12) and (2.1.16) the charge density can now be written as

$$\rho(r,z) = -\frac{en_0}{2\pi}\int d\phi_1\, d\theta_1 \sin\theta_1\, f_o(r_o,0)\, f_\Omega(\pi-\theta_1) \tag{2.1.20}$$

The limits on the θ_1 integral are zero and $\theta_c(\phi_1)$ where

$$\cos\theta_c(\phi_1) = \frac{z}{\left[z^2 + r_c^2(\phi_1)\right]^{1/2}} \tag{2.1.21}$$

where

$$r_c(\phi) = -r \cos \phi + \sqrt{R^2 - r^2 \sin^2 \phi} \qquad (2.1.22)$$

The cut-off angle θ_c arises on account of the finite dimensions of the cylinder. It is assumed that electrons are emitted only from the $z = 0$ plane and that once they strike another wall they are absorbed.

If $f_0(r_0,0)$ is independent of r_0 we then have

$$\rho(r,z) = -\frac{e\, n_0\, f_0}{2\pi} \int_0^{2\pi} d\phi_1 \int_0^{\theta_c(\phi_1)} d\theta_1 \sin\theta_1\, f_\Omega(\pi-\theta_1) \quad . (2.1.23)$$

With the angular emission model (2a) above (see Eq. 2.1.17) we have

$$\rho(r,z) = -e\, n_0\, f_0\, f_{\Omega_0} \int_0^{2\pi} \frac{d\phi_1}{2\pi} \left[1 - \cos\theta_c(\phi_1)\right] \qquad (2.1.24)$$

and for model (2b) (see Eq. 2.1.18),

$$\rho(r,z) = -e\, n_0\, f_0\, f_\Omega(0) \quad . \qquad (2.1.25)$$

In each of these equations time dependence may enter independently through n_0, f_0 or the angular function f_Ω.

Equation (2.1.25) is simply a generalization of the result (2.1.3) to take account of the energy dependence. Equations (2.1.24) and (2.1.25) can be used to check the accuracy and statistical fluctuations in a particle simulation code with isotropic and normal emission, respectively, for arbitrary energy dependence.

It is now possible to use one of these emission models to calculate $\rho(r,z)$ and to substicute the result in Equation (2.1.8). Apart from the simple angular emission case (2b) (see page 12), the calculations are quite complex and are better treated by a direct numerical scheme. In addition, they are applicable to situations where dynamics are dominated by space charge.

2.2 FIELD DISTORTION BY SMALL OBJECTS

2.2.1 General Considerations

In this section we investigate the distortion of field lines in cavities when small dielectric objects are inserted therein. Before doing this we shall discuss the various effects produced by such insertions. The electric field will be modified for any of the following reasons:

1. The body will become charged. If it is an insulator, the nonuniform charge distribution will lead to additional fields. The time required for the charge distribution in an insulator to become uniform is of order σ^{-1} where σ is the conductivity (in sec^{-1} in esu). If the body is a conductor its surface becomes an equipotential surface.

2. In an electric field, a small body will become polarized, either because of the polarization of the dielectric or the flow of current on a conductor. The resulting multipole moments will affect the external fields.

In either Case 1 or 2, the charges or moments of charge on the body will induce image charges in the cavity walls. The effect of the image charges on the fields in the cavity may be appreciable if the distance of the small object from a cavity wall is of the same order of magnitude as the dimensions of the body.

3. If the body has an atomic number different from that of the walls, or if its thickness is of the order of or greater than a mean free path for the radiation creating the pulse, then there will be shadowing effects that lead to a reduction in the current behind the object.

Let us now consider the relative importance of these three effects. Ignoring space-charge limitations and the divergence of the exciting radiation the current in a cavity is just equal to the current in the adjacent material. This is a consequence of the fact that at low densities in the cavity there is no source of electrons and no absorption of them either. The current in the material depends strongly on its average atomic number because the attenuation of the incident photons rises rapidly with atomic number while the range of electrons is not strongly affected. Thus, we expect the current in a body placed in a cavity to be similar to that in the cavity as long as the body has an atomic number similar to that of the cavity walls. Also, we expect the current emerging from the far side of the body to be similar to that elsewhere in the cavity for similar atomic numbers unless the attenuation of the body is appreciable. The net total charge delivered per unit cross section of the body is therefore expected to be small for similar atomic numbers and thin bodies, but of the same order as the time integral of the current density to the cavity walls.

If the body is insulated from the wall or connected by a high inductance path (e.g., via a long thin wire), the charge on it may exceed the charge on the walls. Its effect on the field in its vicinity may be correspondingly larger. That is, the perturbation due to Cause 1 above may exceed the ambient field. It will decrease as r^{-1} or r^{-2} depending upon whether the object is essentially cylindrical or spherical.

It is well-known that a cylinder or a sphere placed in an electric field concentrates it so that the field at the pole may be several times the field far from the pole. Thus,

for a cylinder the ratio of the two fields is $2\varepsilon/(\varepsilon + 1)$ as we shall presently see. Since for considered matter the dielectric constant ε is typically between 1 and 100 and for conductors it is infinite the ratio is of order unity. Thus, the perturbation of the fields due to Cause 2 is of the same order as that due to Cause 1. In this case the field drops off as r^{-2} or r^{-3} for cylindrical and spherical geometries, respectively.

As regards Case 3, the reduction of the current resulting from shadowing presumably affects the field in the entire cavity but is of order (small body cross section)/(cavity area). Since the electric field is proportional to the integral of the charge density the shadowing effect of a small body should not produce large local changes and, as an effect, it does not compete with the ambient field anywhere.

To summarize, we conclude that (a) for small bodies with an atomic number similar to that of the cavity walls, the photons do not liberate much free charge. However, if the body is insulated from the cavity walls, charge may collect on it as a result of the electron current. The charge thus collected may change the field in its vicinity by an appreciable amount. (b) The polarization produced by the small body placed in an electric field will also change the field appreciably in its vicinity. (c) The effect of shadowing by small bodies is of less importance because influence is not localized.

We shall now see what progress can be made analytically in situations where Causes 1 and 2, respectively, are important.

2.2.2 Cause 1--Charged Bodies

In this case we shall calculate the field and potential produced by a charged body placed between two conducting plates. We shall then compare this with the field and potential produced by a uniform charge density between the same plates.

The plates are infinite and positioned at $x = 0$ and $x = L$. A wire, thin in comparison with the interplate distance, is placed at a distance x_0 from the $x = 0$ plate. The wire is normal to the x-y plane.

The calculation of the potential produced by a charge per unit length q on the wire is straightforward (see, for instance, Ref.2.2.1). The complex potential at (x,y) is

$$F(x,y) = 2\,q\,\ln\left[\frac{\sin \pi(x_0 + z)/2L}{\sin \pi(x_0 - L)/2L}\right]$$

where

$$z = x + iy \quad .$$

The potential $\psi(x,y)$ is related to F by

$$\psi(x,y) = \mathrm{Re}\, F(x,y) \quad .$$

It is largest close to the wire. At a distance r given by

$$r^2 = (x - x_0)^2 + (y - y_0)^2$$

the potential (call it ψ_w) is

$$\psi_w \approx 2q \ln\left|\frac{\sin \pi x_0/L}{\pi r/2L}\right|$$

where we have assumed that

$$r \ll x_0 \quad , \qquad r \ll L \quad .$$

This result may be compared with the potential ψ_u due to a uniform space charge (per unit volume) ρ in the space between the two plates

$$\psi_u(x,y) = 2\pi\rho\left(L - \frac{x}{2}\right)x \quad , \quad \text{all} \quad y \quad .$$

The charge per unit length q on an insulated wire can be estimated as follows. Assuming that all incident charge "sticks" to the insulating wire (of radius r) then after a time t the charge accumulated per unit length on the wire is

$$q = \rho v t \, 2\pi r$$

where v is the velocity at which the charge density moves. With this (over-) estimate of the charge accumulated by the wire, the potential in the two cases can be compared:

$$\frac{\psi_w(x,y)}{\psi_u(x,y)} \approx \frac{2\ vrt}{\left(L - \frac{x}{2}\right)x} \ln\left[\frac{\sin \pi x_0/2L}{\pi r/2L}\right] \quad .$$

It is assumed that the wire has a dimension r that is much less than the diode width L. Consequently, the above ratio

is generally small compared with unity until a time t_0 has elapsed where

$$t_0 = \frac{\left(L - \frac{x}{2}\right) x}{2\ vr} \quad .$$

The logarithmic term is slowly varying and is assumed to be of order unity. Thus, if the electrons move with an average velocity of 10^{10} cm/sec (which is typical of 30 keV electrons) the potentials ψ_u, ψ_w become comparable at a point midway across the gap (x = L/2) after a time

$$t_0 = 0.1\ L^2/8\ r \quad \text{nsec} \quad .$$

With L = 10 cm and with a wire radius of 0.1 cm, t_0 is approximately 12 nsec.

It is difficult to proceed much further with this problem on a purely analytic basis. The assumption that all electrons striking the wire must stick may not be valid. More important, as the charge on the wire builds up it will distort the space charge in its vicinity and electrons may be repelled from the vicinity of high potential next to the wire. Nevertheless, it appears from the above calculation that the potential due to the uniform charge is dominant for most times of interest. Moreover, we have overestimated the effect due to the wire for two reasons, namely, the charge assumed here is an upper limit and the potential is calculated at the wire itself. Finally, if the current flow were limited by space charge the charge accumulating on the wire would be even smaller.

To summarize, the effect of small charged objects is not likely to be very important (particularly in space-charge-limited situations) until late in a typical IEMP problem. This somewhat qualitative remark should be tested numerically with a particle simulation code.

2.2.3 Cause 2--Dielectric Objects

In this section, we consider the effect which a dielectric object produces on the field in which it is placed. In this context by "small" we mean that the linear dimensions of the object are small in comparison with the length scale on which the unperturbed field varies.

The simplest case to consider is that of a wire (cylinder) inserted in a uniform field. We might imagine the uniform field to be created by diode plates separated by a distance L large in comparison with the wire radius a. This case is quite simple to calculate. The unperturbed potential ψ_0 is given by

$$\psi_0 = - E_0 x$$

$$= - E_0 r \cos \phi$$

where E_0 is the uniform field and x is the direction of the electric field. Here (r,ϕ) are the polar coordinates. The boundary conditions to be satisfied on the circle $r = a$ are

$$\frac{\partial \psi}{\partial r} (a,\phi)\Big|_{\text{outside}} = \varepsilon \frac{\partial \psi}{\partial r} (a,\phi)\Big|_{\text{inside}}$$

$$\psi (a,\phi)\Big|_{\text{outside}} = \psi (a,\phi)\Big|_{\text{inside}}$$

where ε is the dielectric constant. Since one of the boundary conditions involves a derivative and since the potential outside $r = a$ is not constant in r so the potential within $r = a$ cannot be constant. Also ψ cannot vary as r^{-k} with $k > 0$ if it is to remain finite at $r = 0$. The possible form for ψ is $Ar \cos \phi$. Outside the cylinder the solution can take form $Cr \cos \phi + (B/r) \cos \phi$ which becomes $Cr \cos \phi$ for large r--which is correct since the potential for the cylinder is the unperturbed solution $-E_0 r \cos \phi$. Thus, using the two boundary conditions above at $r = a$, we have

$$- Ea + B/a = Aa$$

$$- E - B/a^2 = \varepsilon A \quad .$$

Thus, we obtain

$$\psi(r,\phi) = \left(-r + \frac{\varepsilon - 1}{\varepsilon + 1} \frac{a^2}{r}\right) E_0 \cos \phi \qquad (r \geq a)$$

$$= - \frac{2r}{\varepsilon + 1} E_0 \cos \phi \qquad (r \leq a) \quad .$$

In Cartesian coordinates (x,y) this result is

$$\psi(x,y) = \left(- x + \frac{\varepsilon - 1}{\varepsilon + 1} \frac{a^2 x}{x^2 + y^2}\right) E_0 \qquad (x^2 + y^2 \geq a^2)$$

$$= - \frac{2x}{\varepsilon + 1} E_0 \qquad (x^2 + y^2 \leq a^2) \quad .$$

It is convenient to introduce the normalized potential

$$\Psi = \psi/aE_0$$

and the normalized field magnitude

$$\chi = I_m F/aE_0 \quad .$$

Similarly, the normalized electric field components ε_x, ε_y are defined

$$E_x/E_0 \equiv \varepsilon_x = - \partial\Psi/\partial\xi$$

$$E_y/E_0 \equiv \varepsilon_y = - \partial\Psi/\partial\gamma$$

where

$$\xi = x/a$$

$$\gamma = y/a \quad .$$

Thus, if a is measured in centimeters and E_0 in volts/cm then ψ, γ are in volts. For a variety of values of ε contours of constant potential Ψ and field magnitude χ are plotted in Figures 2.2.1 through 2.2.4. Similarly, contours of constant field components ε_x, ε_y are shown in Figures 2.2.5 through 2.2.12.

Let us take an example, simple as it may be, to illustrate the use of these plots. A dielectric cylinder (or wire) of radius $a = 0.25$ cm is placed in a uniform electric

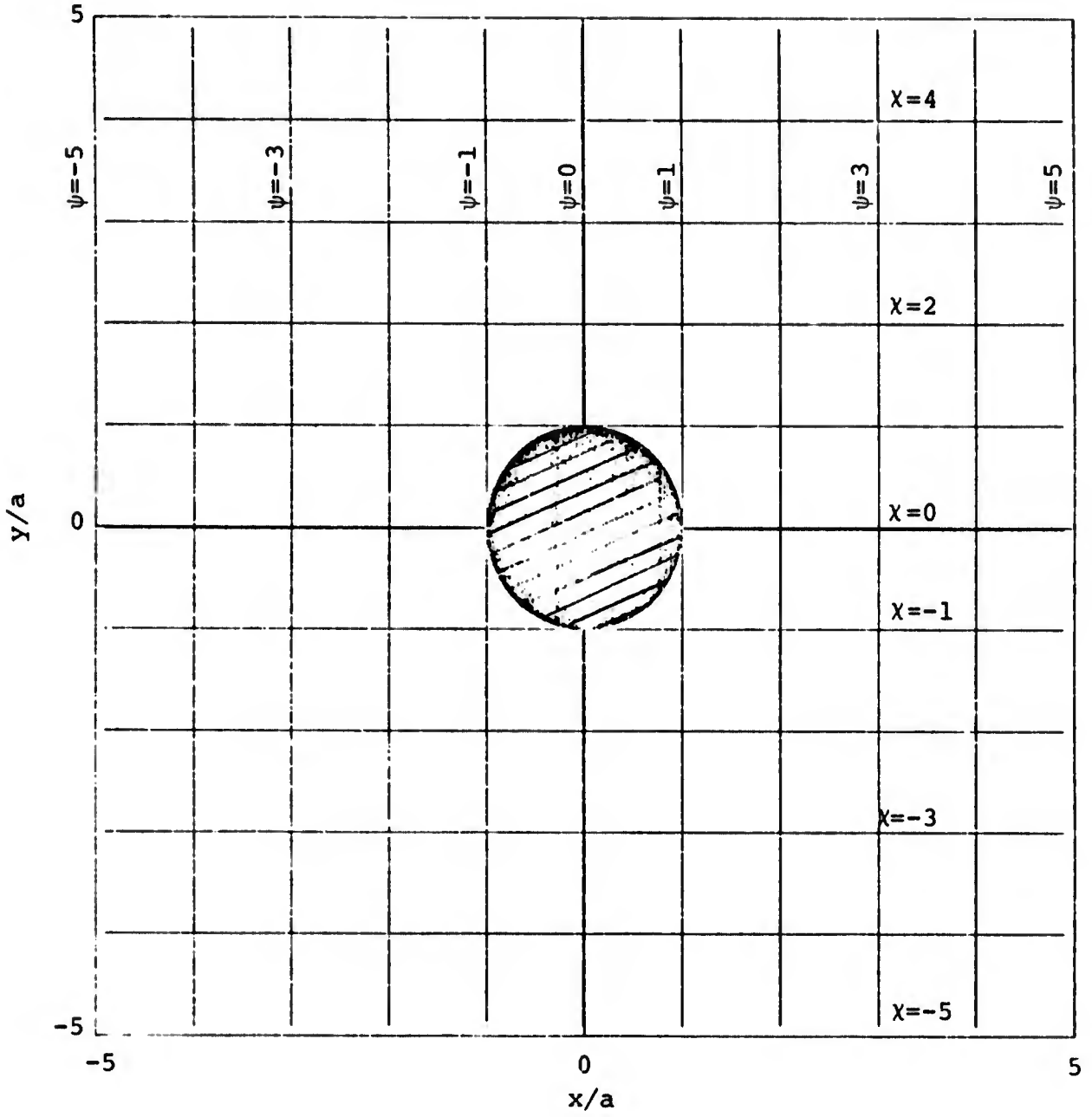

Figure 2.2.1 Contours of constant potential ψ and field magnitude χ for $\varepsilon = 1$.

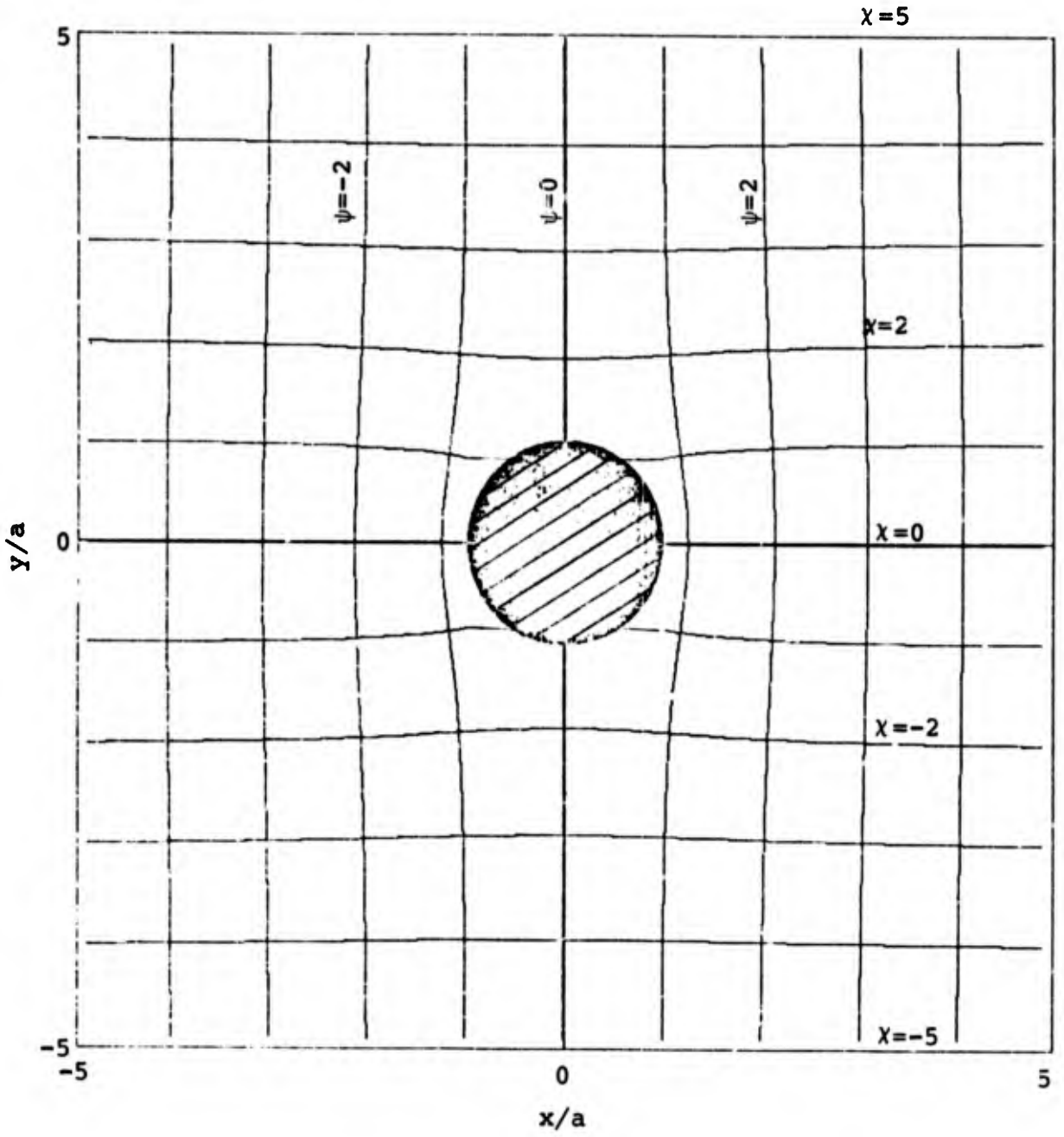

Figure 2.2.2 Contours of constant potential ψ and field magnitude χ for $\varepsilon = 2$.

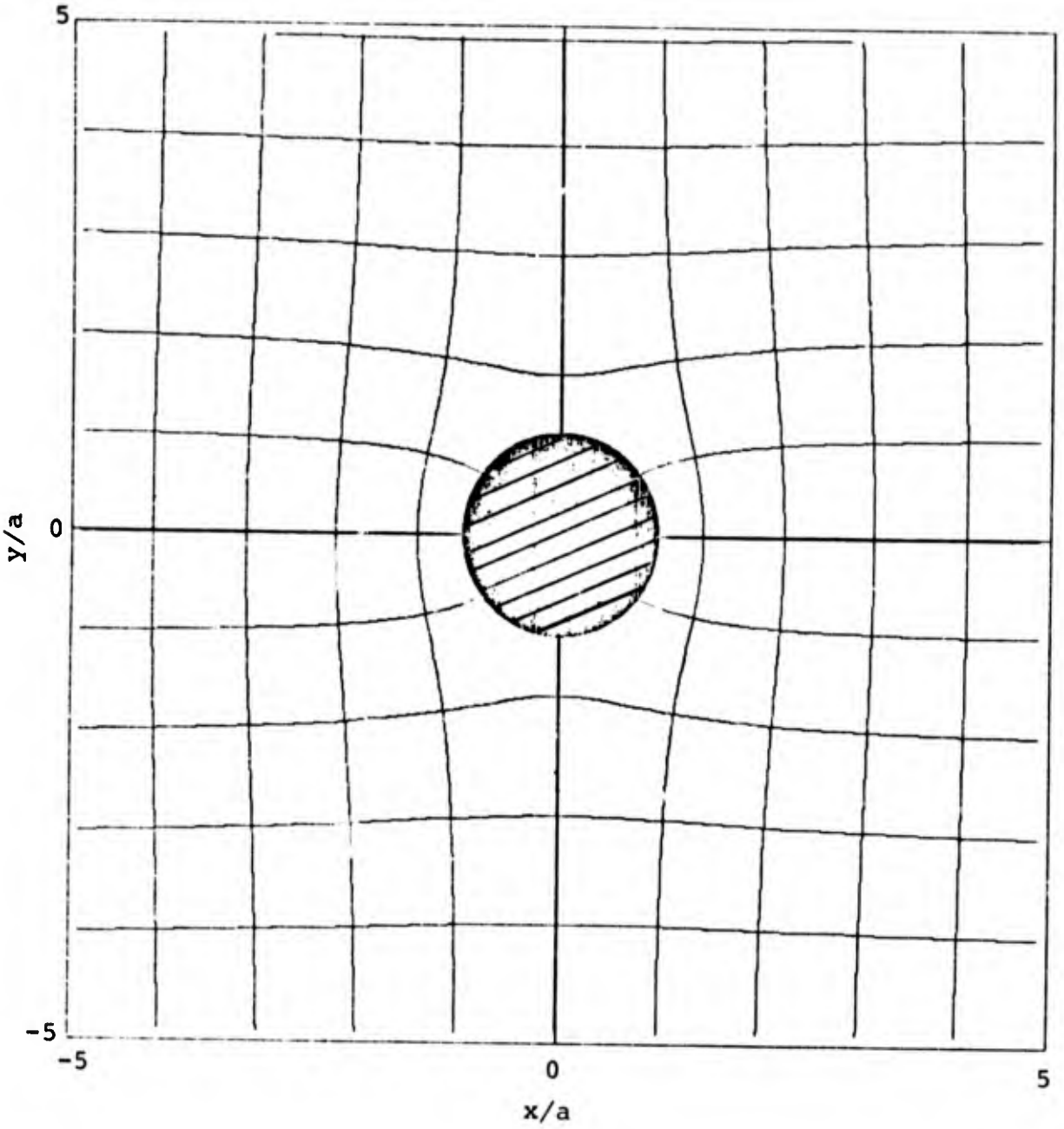

Figure 2.2.3 Contours of constant potential ψ and field magnitude χ for $\varepsilon = 5$.

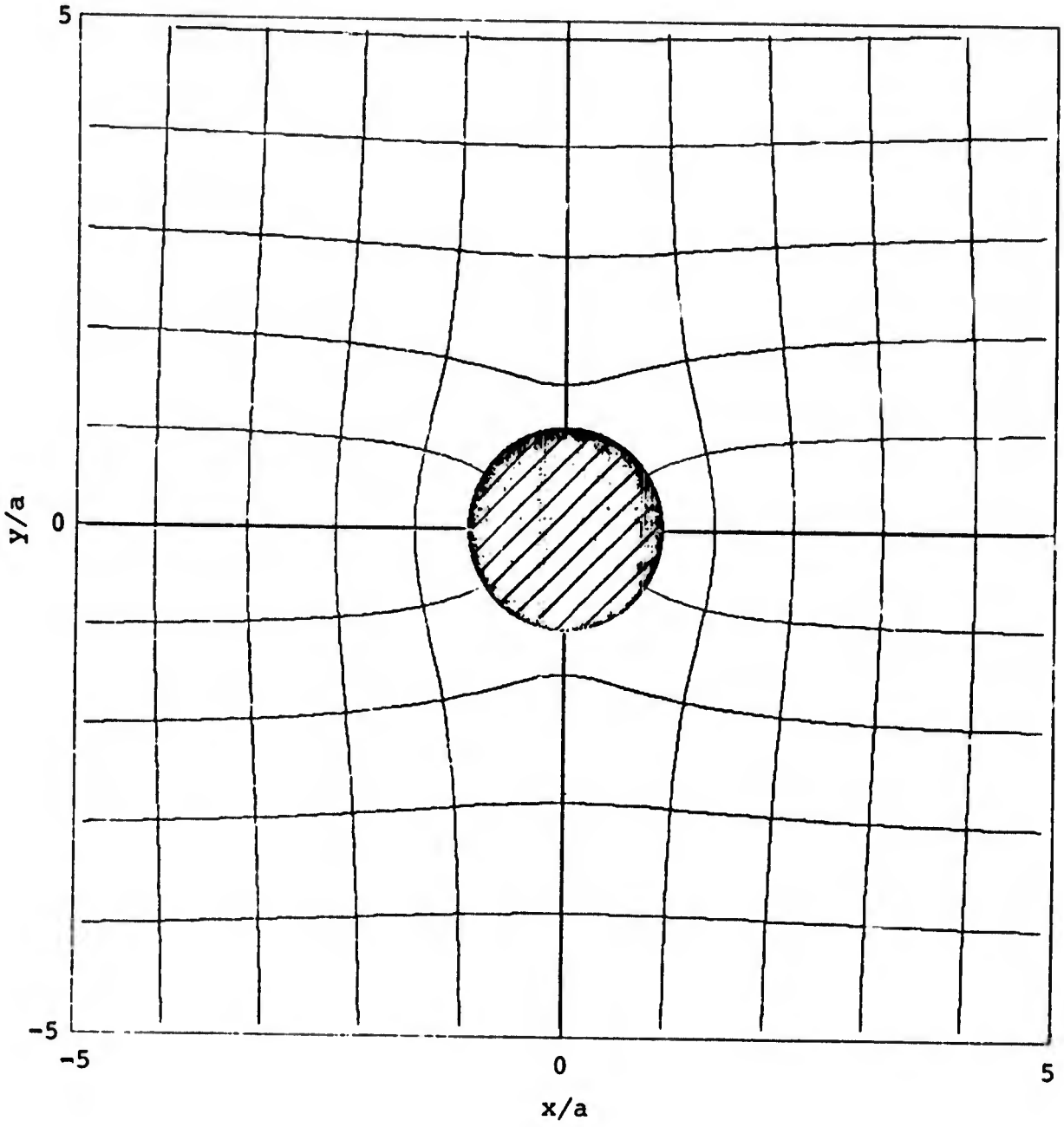

Figure 2.2.4 Contours of constant potential ψ and field magnitude χ for $\varepsilon = 10$.

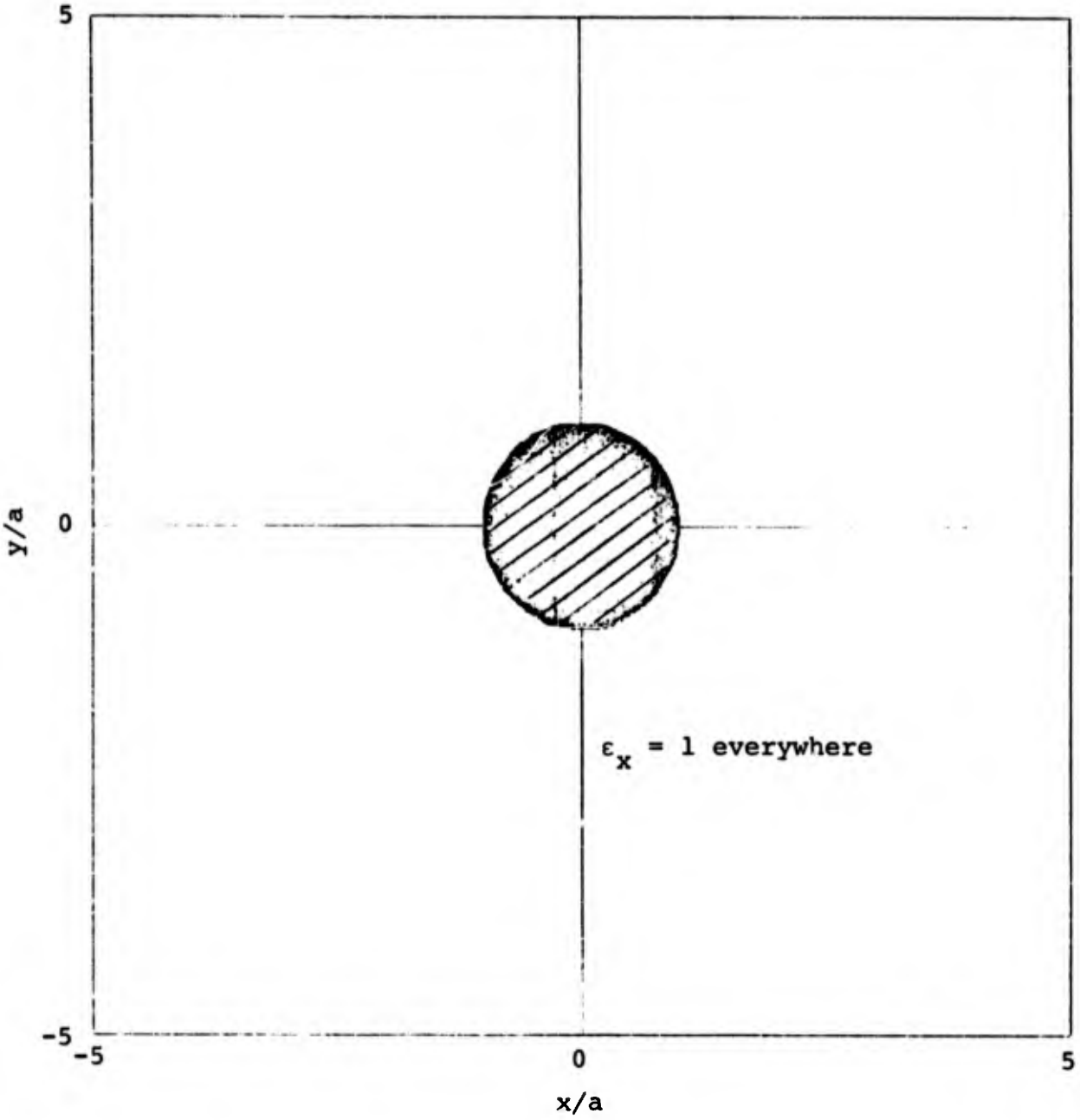

Figure 2.2.5 Contours of constant x-component of the electric field for $\varepsilon = 1$.

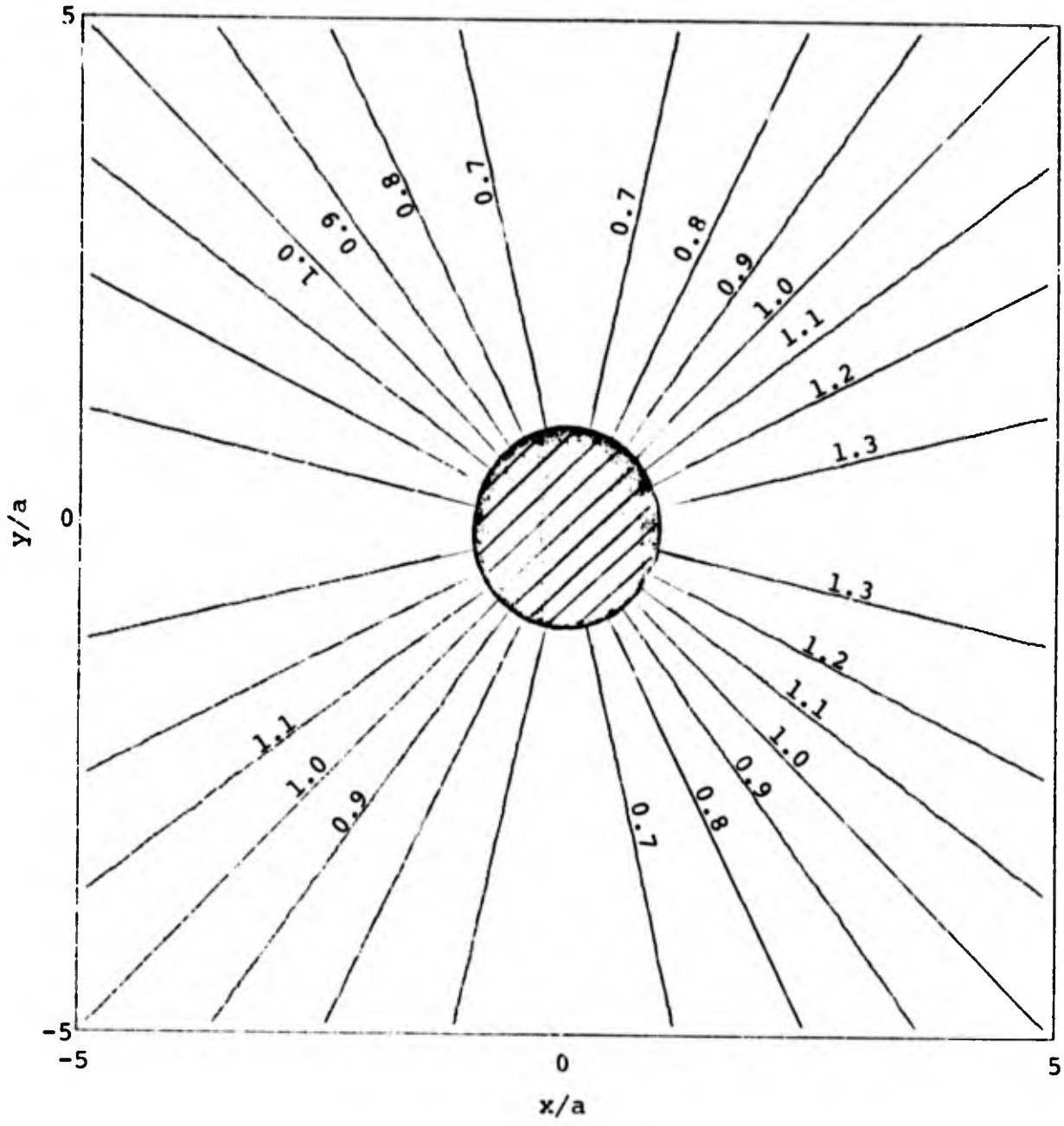

Figure 2.2.6 Contours of constant x-component of the electric field for $\varepsilon = 2$.

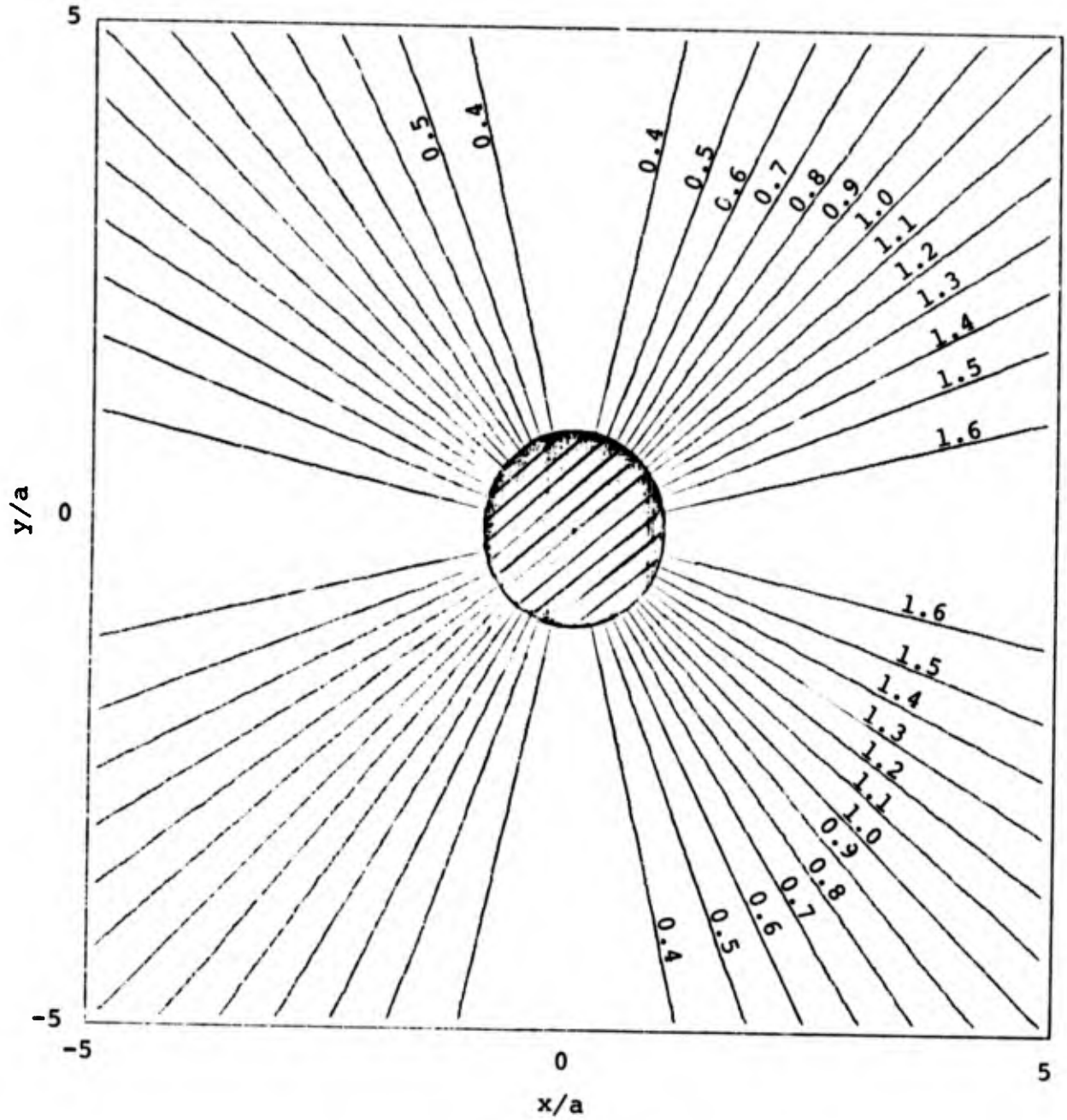

Figure 2.2.7 Contours of constant x-component of the electric field for $\varepsilon = 5$.

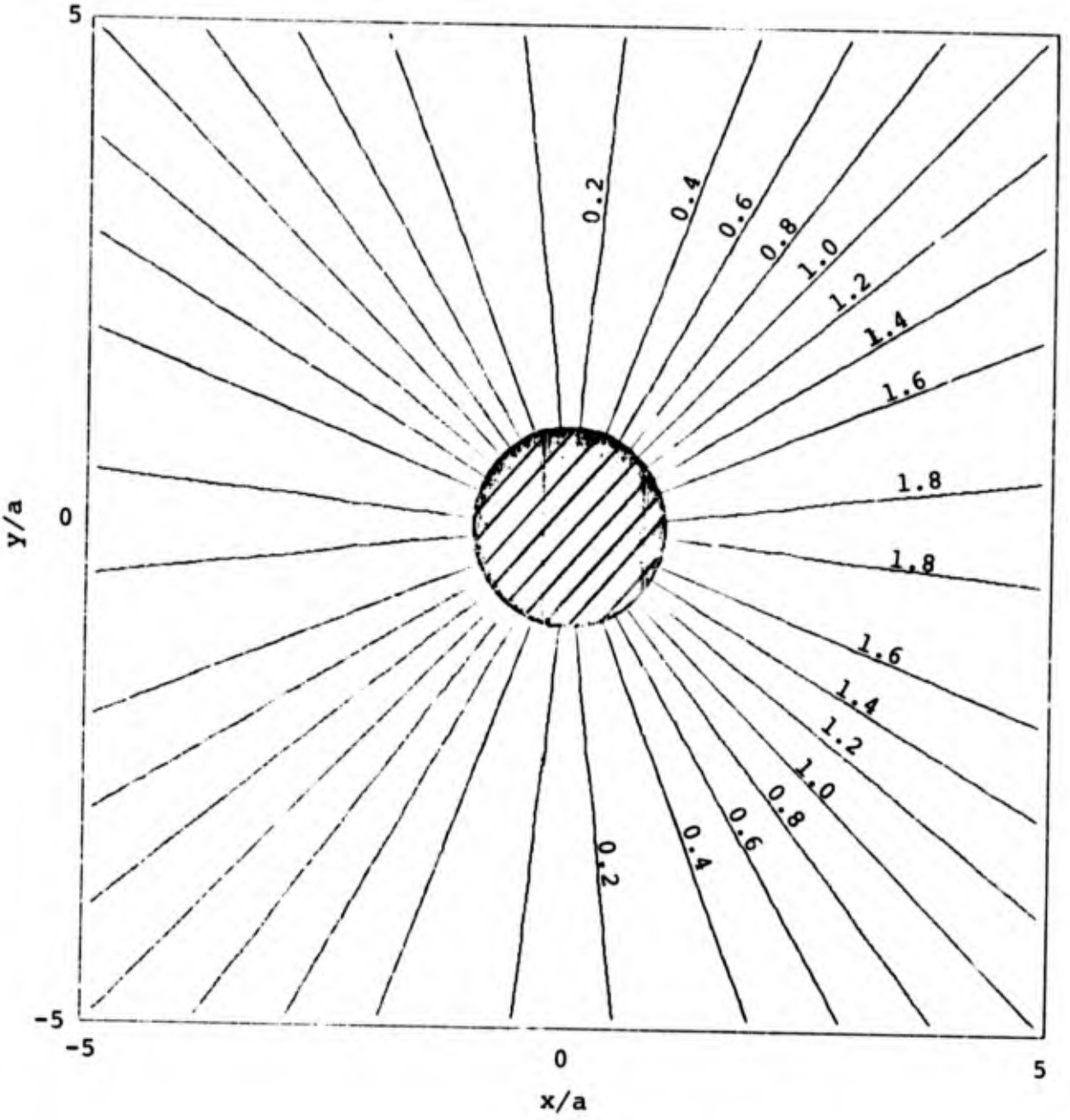

Figure 2.2.8 Contours of constant x-component of the electric field for $\varepsilon = 10$.

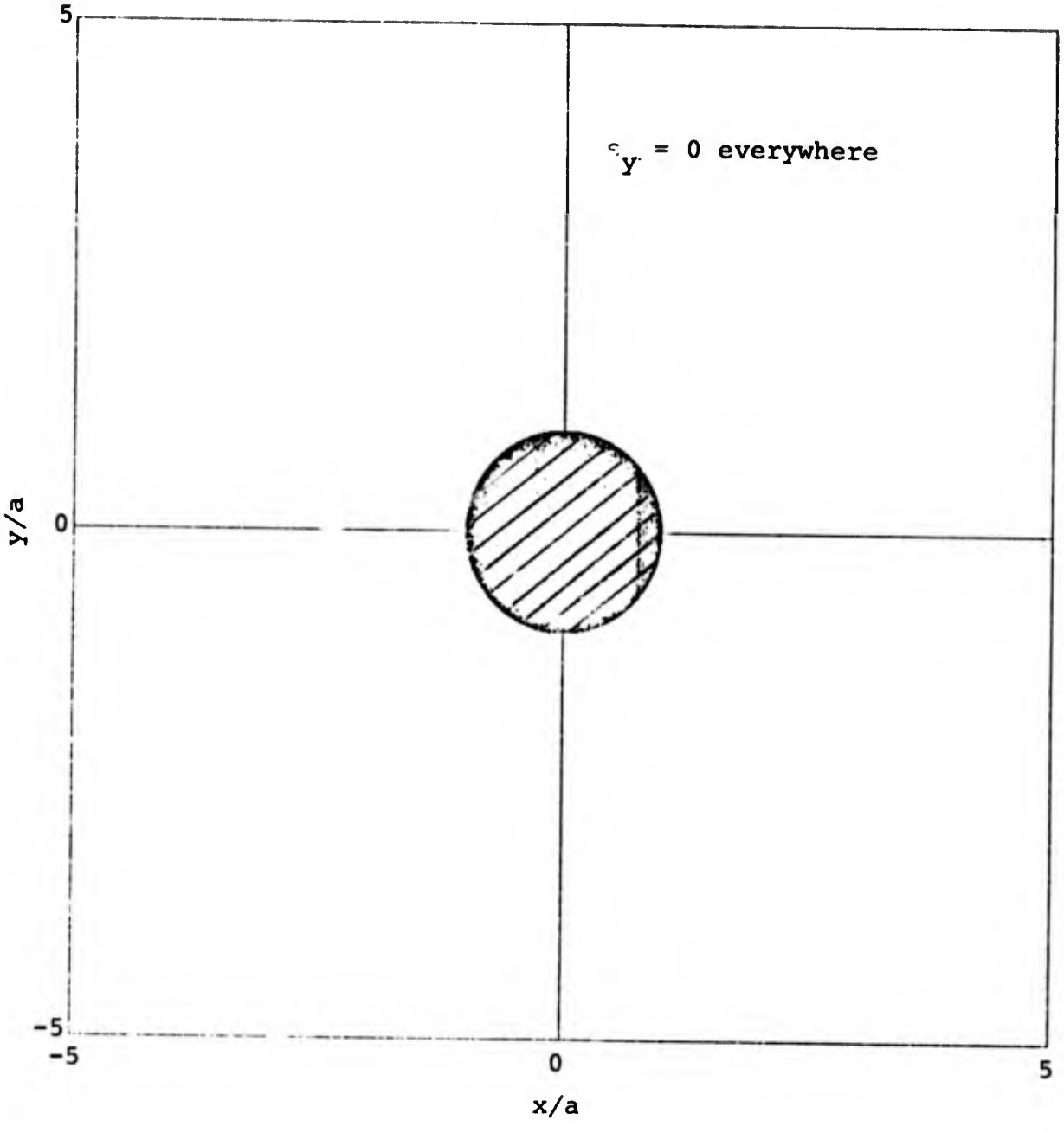

Figure 2.2.9 Contours of constant y-component of the electric field for $\varepsilon = 1$.

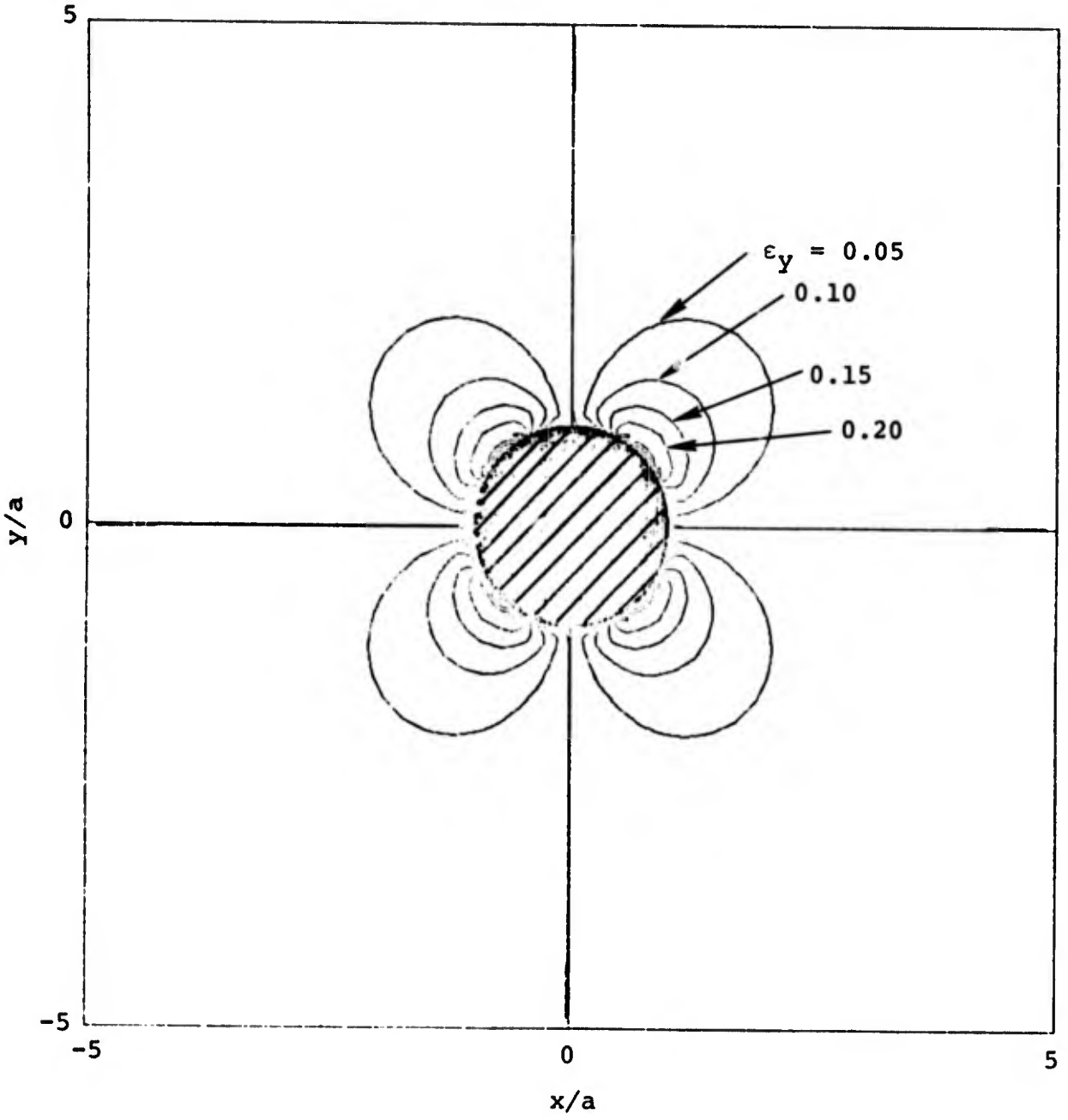

Figure 2.2.10 Contours of constant y-component of the electric field for $\varepsilon = 2$.

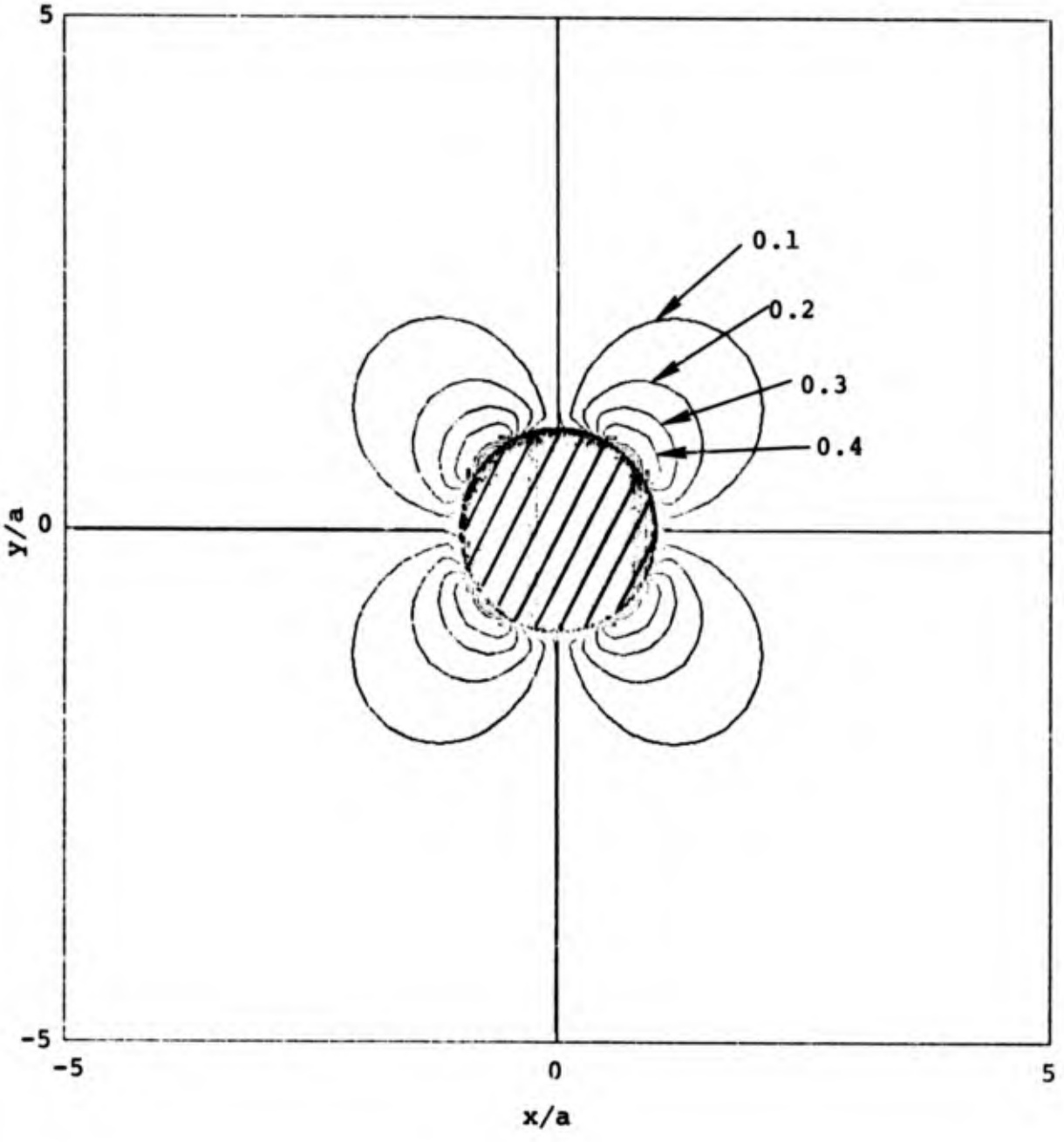

Figure 2.2.11 Contours of constant y-component of the electric field for $\varepsilon = 5$.

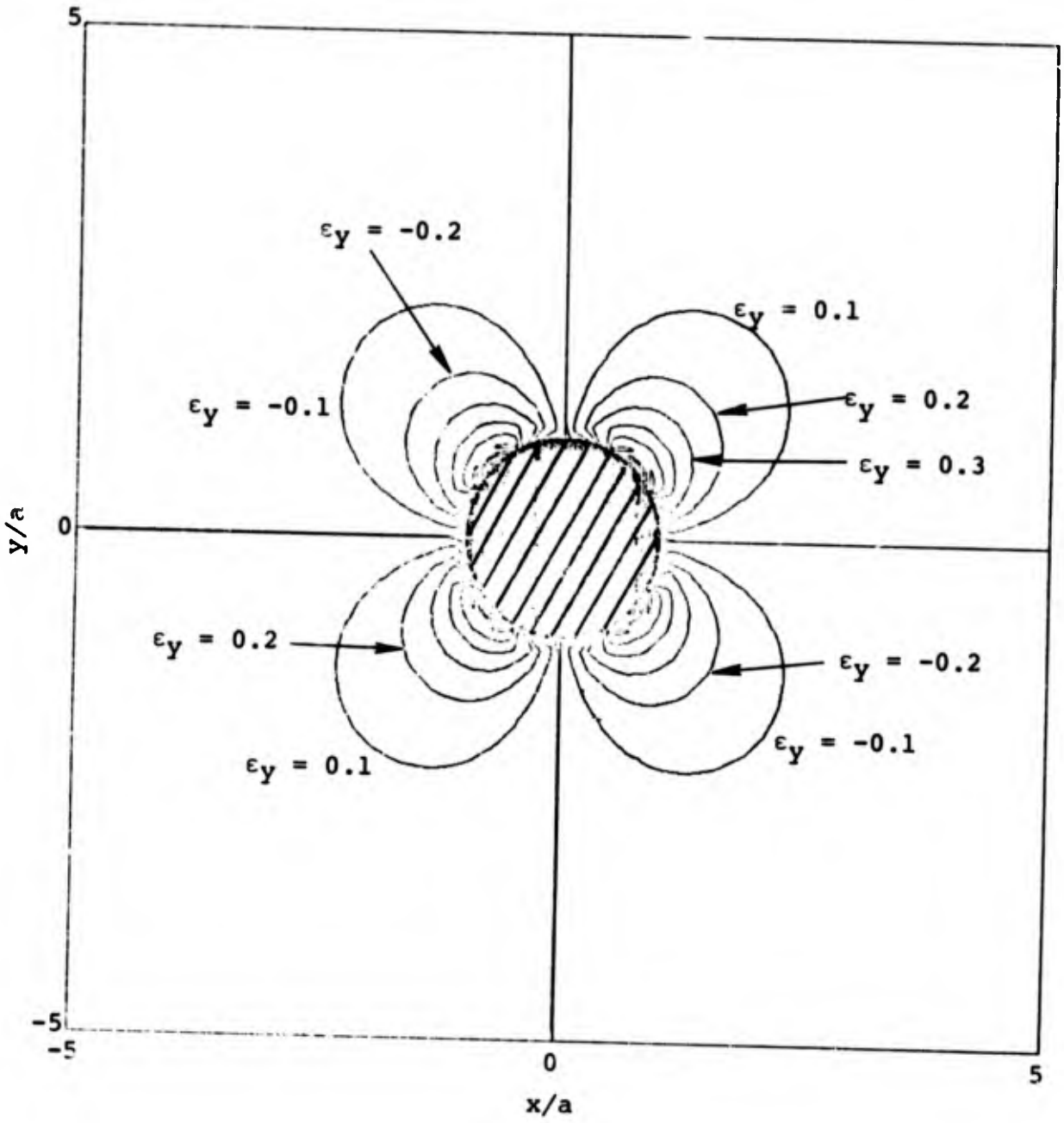

Figure 2.2.12 Contours of constant y-component of the electric field for $\varepsilon = 10$.

field $\hat{x}E_0$ of strength 1 kV/cm. Thus, to obtain values of the potential the normalized value should be multiplied by the scaling potential $aE_0 = 250$ volts. Positions in these plots (ξ,γ) are measured in units of the radius $a = 0.25$ cm. Thus, at the point $x = 0.25$ cm, $y = 0.5$ cm the potential is $250\ \Psi\ (1,2) \simeq 225$ V in the case where $\varepsilon = 5$ (Figure 2.2.3). Similarly, (Figures 2.2.7, 2.2.1) the x and y field components have values of

$$E_x\ (0.5,\ 0.25) = E_0\ \varepsilon_x\ (1.,\ 2.)$$

$$\simeq 600 \text{ volts/cm}$$

$$E_y\ (0.5,\ 0.25) = E_0\ \varepsilon_y\ (1.,\ 2.)$$

$$\simeq 100 \text{ volts/cm} \quad .$$

The uniform field E_0 might, for instance, have been produced at a distance of 7.5 cm from the emitting plate of a diode of width 10 cm in which a current density of ~ 0.35 A/cm^2 (produced by ~ 30 keV electrons) flowed. In this case, the field in the absence of the dielectric does not change appreciably on the length scale of the wire radius of 0.25 cm.

The treatment given here can be generalized to more complex geometries--a grid of wires, for instance. It is approximate in the sense that once the field lines have been distorted by the dielectric object, the electrons which produced the uniform field are, themselves, deflected by the equipotential contours. However, unless the electrons are nearly space-charge limited and have energies close to the

potential in the vicinity of the dielectric this correction is not of zero order. To treat the flow consistently in the neighborhood of dielectrics a numerical treatment is necessary and will form the subject of later work.

2.2.4 Summary

Three effects have been identified as causes for distorting field lines when small objects are inserted in an IEMP cavity. It was concluded that the photon shadowing by such objects was less important than the field line distortion resulting from charge build-up on the object or from field-line concentration by the dielectric properties of the object.

Formulas for the field distortion by simple, grounded dielectric objects were presented and equipotential surfaces for some configurations were generated. A similar program was not possible for the case of charged, insulated objects. Instead, the potential distribution produced by an insulated wire in a vacuum diode space was compared with the distortion resulting from a uniform space charge between the plates. This effect, unlike the grounded dielectric concentration of field, is essentially time-dependent and grows in importance as the object alters charge.

The treatment given here has been directed to uncovering the basic processes involved and giving approximate, simple answers. However, the effects are of real interest to the IEMP problem and deserve a more detailed numerical examination to provide consistent and accurate results.

2.3 PERTURBATION TREATMENT OF PARTIALLY SPACE-CHARGE-LIMITED DIODES

Much of the early work on one-dimensional IEMP field generation theory had, as its analytical model, the classic work of Langmuir and Child. In that model of space-charge-limited current flow in a diode, the electron emission is assumed to be (a) monoenergetic and (b) time-independent. Here a model is presented in which neither of these assumptions is required.

The work is based upon a perturbation theoretical expansion of the energy lost by an electron to the space-charge field during a transit across the diode. The method is quite simple and it leads to simple analytic results which are readily utilized.

Suppose we have a beam of electrons emitted from a plane surface $z = 0$. It is assumed that they are sufficiently energetic to pass from the cathode to anode without being limited by their own space charge. They obey the transport equation

$$\frac{\partial f}{\partial t} + v \frac{\partial f}{\partial z} - \frac{e}{m_o} E \frac{\partial f}{\partial v} = 0 \quad . \tag{2.3.1}$$

The first term of this equation is characterized by the time scale τ_p, the pulse length. The second term is characterized by the time $\tau_t = L/v_0$ taken to cross the cavity gap L where v_0 is the characteristic velocity. The third term in the above equation is scaled by the time for acceleration in the electric field $\tau_E = mv_0/eE$. It is assumed that the electrons are energetic and that the transit time is the least of the three time scales. Under those conditions, we define two small ordering parameters

$$\gamma_p = \frac{\tau_t}{\tau_p} = \frac{L}{v_0 \tau_p}$$

$$\gamma_E = \frac{\tau_t}{\tau_E} = \frac{eEL}{m_0 v_0^2} = \frac{e\phi}{1/2\ m_0 v_0^2}$$

where $\phi = EL/2$ is the characteristic electrostatic potential of the system. Let us now examine the relative magnitudes of these two parameters. In a one-dimensional cavity we have

$$\frac{d^2\phi}{dz^2} = -4\pi\rho = 4\pi\ j_{esu}/v_0 = \ 0.4\pi\ j_A/(v_0/c)$$

where j_A is the current in amp/cm^2. Then the maximum potential of the system is

$$\Phi = \phi(L/2) = \frac{0.4\pi\ j_A L^2}{8(v_0/c)}\ \text{esu} = \frac{15\pi c j_A L^2}{v_0}\ \text{volts} \quad .$$

By expressing the velocity v_0 in terms of the kinetic energy ε_0 (in eV) we have

$$\gamma_E = \frac{15\pi c j_A L^2}{5.93\text{x}10^7\ \varepsilon_0^{3/2}} = 2.38\ \text{x}\ 10^4\ \frac{j_A L^2}{\varepsilon_0^{3/2}}$$

$$\gamma_p = \frac{L}{5.93\text{x}10^7\ \varepsilon_0^{1/2}\tau_p} = \frac{1.69\text{x}10^{-8} L}{\varepsilon_0^{1/2}\ \tau_p} \quad .$$

We thus have four variables to consider in estimating the size of the two small parameters. If $\gamma_E << 1$ then γ_p can be considered small provided

$$\gamma_p \lesssim \gamma_E$$

that is, if

$$\frac{\varepsilon_0}{\tau_p L j_A} \lesssim 1.4 \times 10^{12} \quad .$$

Let us illustrate the relative magnitudes of γ_p, γ_E with a simple example. With $\varepsilon_0 = 9 \times 10^4$ eV, L = 5 cm, $j_A = 1$ A/cm^2

$$\gamma_E = 0.022$$

$$\gamma_p = 2.82 \times 10^{-10}/\tau_p$$

so that for $\tau_p \gtrsim 10^{-8}$ sec γ_p is also small. It is under conditions such as these that we can consider an expansion of the transport equation to be useful.

Introducing the variables

$$\tau = t/\tau_p$$

$$\zeta = z/L$$

$$w = v/v_0$$

the transport equation can be written

$$\gamma_p \frac{\partial f}{\partial \tau} + \frac{\partial f}{\partial \zeta} - \gamma_E \frac{\partial f}{\partial w} = 0 \quad .$$

To the zeroth order, we have

$$\frac{\partial f_0}{\partial \zeta} = 0 \quad .$$

That is, the electron density is uniform to lowest order. To next order, we have

$$\gamma_p \frac{\partial f_0}{\partial \tau} + \frac{\partial f_1}{\partial \zeta} - \gamma_E \frac{\partial f_0}{\partial w} = 0 \quad ,$$

from which we obtain the solution

$$f_1(\zeta) - f_1(0) = \int_0^{\zeta} d\zeta' (\gamma_E \frac{\partial}{\partial w} - \gamma_p \frac{\partial}{\partial \tau}) f_0 \quad .$$

At the boundary $\zeta = 0$ ($z = 0$), we impose the condition that

$$f_1(\zeta = 0) = 0 \quad , \qquad \text{for all } w > 0.$$

That is, the source of electrons enters only through f_0. The solution above in terms of t,z now reads

$$f_1(z) = \int_0^{z} dz' (\frac{eE(z')}{m_0 v_0} \frac{\partial}{\partial v_0} - \frac{1}{v_0} \frac{\partial}{\partial t}) f_0$$

$$= - \frac{e\phi(z)}{m_0 v_0} \frac{\partial f_0}{\partial v_0} - \frac{z}{v_0} \frac{\partial f_0}{\partial t} \quad .$$

We are now in a position to calculate the first-order charge density ρ_1. Before doing so let us define the current and charge density of both first- and zero-order magnitudes. Thus,

$$\rho_0 = -e\int dv_x\, dv_y\, dv_z\, f_0 \quad .$$

Since there is no motion normal to the z-axis we shall set

$$f_0 = f_0(v_z)\ \delta(v_x)\ \delta(v_y) \quad .$$

The function $f_0(v_z)$ is arbitrary. We shall select a function resembling the photoemission results of Dellin and McCallum[2.3.1]

$$f_0(v) = \frac{n_0}{v_T^3}\,\frac{2}{\sqrt{\pi}}\,v^3 \exp - \frac{v^2}{v_T^2}$$

where n_0 is the electron number density and v_T is characteristic velocity. With this definition

$$\rho_0 = -n_0 e$$

and

$$j_0 = -e\int dv_z\, v_z\, f_0(v_z)$$

$$= -n_0 e\bar{v} \ , \quad \text{where } \bar{v} = \frac{2}{\sqrt{\pi}}\,v_T \quad .$$

The zero-order potential ϕ_0 is given by

$$\frac{d^2\phi_0}{dz^2} = -4\pi\rho_0 = 4\pi n_0 e \quad .$$

With boundary conditions

$$\phi_0(0) = \phi_0(L) = 0$$

we obtain the result

$$\phi_0(z) = 2\pi n_0 e\, z(L-z) \quad .$$

The first-order potential ϕ_1 then satisfies the equation

$$\frac{d^2\phi_1}{dz^2} = -4\pi\rho_1 = 4\pi e[a_1\phi_0(z) + a_2 z]$$

where

$$a_1 = -\frac{e}{m_0}\int\frac{dv}{v}\frac{\partial f_0}{\partial v} = -\frac{n_0 e}{m_0 v_T^2}$$

$$a_2 = -\frac{\partial}{\partial t}\int\frac{dv}{v} f_0 = -\frac{\partial}{\partial t}\frac{n_0}{\sqrt{\pi}\, v_T} \quad .$$

Inserting the above result for ϕ_0 in this equation we find, on integration, that

$$\frac{d\phi_1(z)}{dz} - \frac{d\phi_1(0)}{dz} = 4\pi e n_0 e\left[a_1\left(\frac{Lz^2}{2} - \frac{z^3}{3}\right) + \frac{a_2 z^2}{2}\right] \quad .$$

Integrating once again and using the boundary conditions $\phi_1(0) = \phi_1(L) = 0$ we eliminate $d\phi_1(0)/dz$ to obtain

$$\phi_1(z) = 4\pi e[2\pi n_0 e\, a_1(\frac{Lz^3}{6} - \frac{z^4}{12}) + \frac{a_2 z^3}{6}] + z\,\frac{d\phi_1(0)}{dz}$$

$$= 4\pi e[2\pi n_0 e\, a_1(\frac{Lz^3}{6} - \frac{z^4}{12} - \frac{L^3 z}{12}) + \frac{a_2}{6}(z^3 - L^2 z)] \quad .$$

To check the validity of the expansion procedure let us evaluate ϕ_1 at $z = L/2$ (where it attains its maximum value) and compare it to $\phi_0(L/2)$. We have

$$\phi_1(\frac{L}{2}) = -4\pi e[0.026 \times 2\pi n_0 e\, a_1 L^4 + 0.0625\, a_2 L^3]$$

whereas

$$\phi_0(\frac{L}{2}) = \frac{\pi\, n_0 e\, L^2}{4} \quad .$$

Hence,

$$\frac{\phi_1(\frac{L}{2})}{\phi_0(\frac{L}{2})} = 4\pi e[0.208\, a_1 L^2 + \frac{a_2 L}{4\pi n_0 e}] \quad .$$

Now,

$$a_1 \sim -\frac{e}{m_0}\frac{n_0}{v_T^2} \quad \text{and} \quad a_2 \sim -\frac{n_0}{v_0 \tau_p} \quad .$$

Thus, we have

$$\frac{\phi_1(L/2)}{\phi_0(L/2)} \sim [0.208(\frac{L\omega_0}{v_T})^2 + \frac{L}{v_0 \tau_p}] \quad .$$

The expansion is thus seen to be valid for the derived potential ϕ_1, the expansion parameters being

$$(\omega_0\tau_t)^2 << 1, \quad \tau_t/\tau_p << 1$$

where

$$\omega_0^2 = 4\pi n_0 e^2/m_0 \quad .$$

Collecting our results and expressing ϕ_0, ϕ_1 in volts, we have

$$\phi_0(\zeta) = 600\pi\, n_0 e L^2\, \zeta(1 - \zeta)$$

$$\phi_1(\zeta) = 600\pi\, n_0 e \left[\left(\frac{L\omega_0}{v_T}\right)^2 \frac{L^2}{6}(\zeta^3 - \tfrac{1}{2}\zeta^4 - \tfrac{1}{2}\zeta)\right.$$

$$\left. + \frac{1}{12n_0}\frac{\partial n_0}{\partial t}\frac{L}{v_T} L^2(\zeta^3 - \zeta)\right]$$

where $\zeta = z/L$.

The number density n_0 is given by

$$n_0 = \int dv_z\, f_0(v_z) \quad .$$

It is related to the current j_0, given by

$$j_0 = -e\int dv_z\, v_z\, f_0(v_z) \quad \text{esu} \quad .$$

It is more convenient to deal with currents j_{0A} expressed in amp/cm^2 and these are related to n_0 as follows:

$$j_{0A} = -\frac{10e}{c}\int dv_z\, v_z\, f_0(v_z) = -10\, n_0 e\, \frac{\bar{v}}{c} \quad \text{amps/cm}^2$$

where $e = 4.8 \times 10^{-10}$ esu. Thus,

$$n_0 e = \frac{0.1\left|j_{0A}\right|}{(\bar{v}/c)}$$

and

$$\bar{v} = \frac{2}{\sqrt{\pi}}\, v_T$$

is the mean velocity.

2.3.1 Summary of Results

The results of the first-order perturbation expansion analysis may now be assembled. They are summarized below. The potential $\phi(\zeta,\tau)$ is given by

$$\phi = \phi_0 + \phi_1$$

where

$$\phi_0(\zeta,\tau) = \frac{60\pi}{\bar{\beta}} j_{Am} L^2 \bar{\phi}_0(\zeta)\, g(\tau)$$

$$\phi_1(\zeta,\tau) = \frac{10\pi}{\bar{\beta}} j_{Am} L^2 g(\tau) \{ \left(\frac{L\omega_0}{v_T}\right)^2 \bar{\phi}_{1e}(\zeta)\, g(\tau)$$

$$+ \frac{1}{\sqrt{\pi}} \frac{L}{v_T \tau_p} \frac{1}{g} \frac{\partial g(\tau)}{\partial \tau} \bar{\phi}_{1p}(\zeta) \}$$

where

$$\zeta = z/L$$

$$\tau = t/\tau_p$$

$$\omega_0 = 5.64 \times 10^4 \, n_m$$

$$n_m = 6.25 \times 10^{18} \, j_{Am}/\bar{v}$$

$$\bar{v} = v_T \sqrt{2/\pi}$$

$$\bar{\beta} = \bar{v}/c \quad (c = 3 \times 10^{10})$$

$$v_T = 5.93 \, \varepsilon_T \quad (\varepsilon_T \text{ in eV}) \quad .$$

The pulse shape function $g(\tau)$ is arbitrary. The normalized potentials $\bar{\phi}_0$, $\bar{\phi}_{1e}$, $\bar{\phi}_{1p}$ are defined

$$\bar{\phi}_0(\zeta) = \zeta(1 - \zeta)$$

$$\bar{\phi}_{1e}(\zeta) = \frac{1}{2}\,\zeta(1 + \zeta^3 - 2\zeta^2)$$

$$\bar{\phi}_{1p}(\zeta) = \frac{1}{2}\,\zeta(1 - \zeta^2) \quad .$$

These functions are tabulated in Table 2.3.1 and are plotted in Figure 2.3.1.

In a similar fashion the electric field is given by

$$E = E_0 + E_1$$

where

$$E_0(\zeta,\tau) = -\frac{60\pi}{\bar{\beta}}\, j_{Am} L\, g(\tau)\, \bar{E}_0(\zeta)$$

$$E_1(\zeta,\tau) = \frac{10\pi}{\bar{\beta}}\, j_{Am} L\, g(\tau) \left\{ \left(\frac{L\omega_0}{v_T}\right)^2 g(\tau)\, \bar{E}_{1e}(\zeta) \right.$$

$$\left. + \frac{1}{\sqrt{\pi}}\, \frac{L}{v_T \tau_p}\, \frac{1}{g}\, \frac{\partial g(\tau)}{\partial \tau}\, \bar{E}_{1p}(\zeta) \right\} .$$

The functions $\bar{E}_0$, $\bar{E}_{1e}$, $\bar{E}_{1p}$ are defined

$$\bar{E}_0(\zeta) = 1 - 2\zeta$$

TABLE 2.3.1

NORMALIZED ZERO AND FIRST ORDER POTENTIALS AS FUNCTIONS OF THE NORMALIZED DISTANCE $\zeta = z/L$

ζ	$\bar{\phi}_0(\zeta)$	$\bar{\phi}_{1e}(\zeta)$	$\bar{\phi}_{1p}(\zeta)$
0.0	0.0	0.0	0.0
0.1	0.09	0.049	-0.05
0.2	0.16	0.093	-0.096
0.3	0.21	0.127	-0.137
0.4	0.24	0.149	-0.168
0.5	0.25	0.156	-0.188
0.6	0.24	0.149	-0.192
0.7	0.21	0.127	-0.179
0.8	0.16	0.093	-0.144
0.9	0.09	0.049	-0.085
1.0	0.0	0.0	0.0

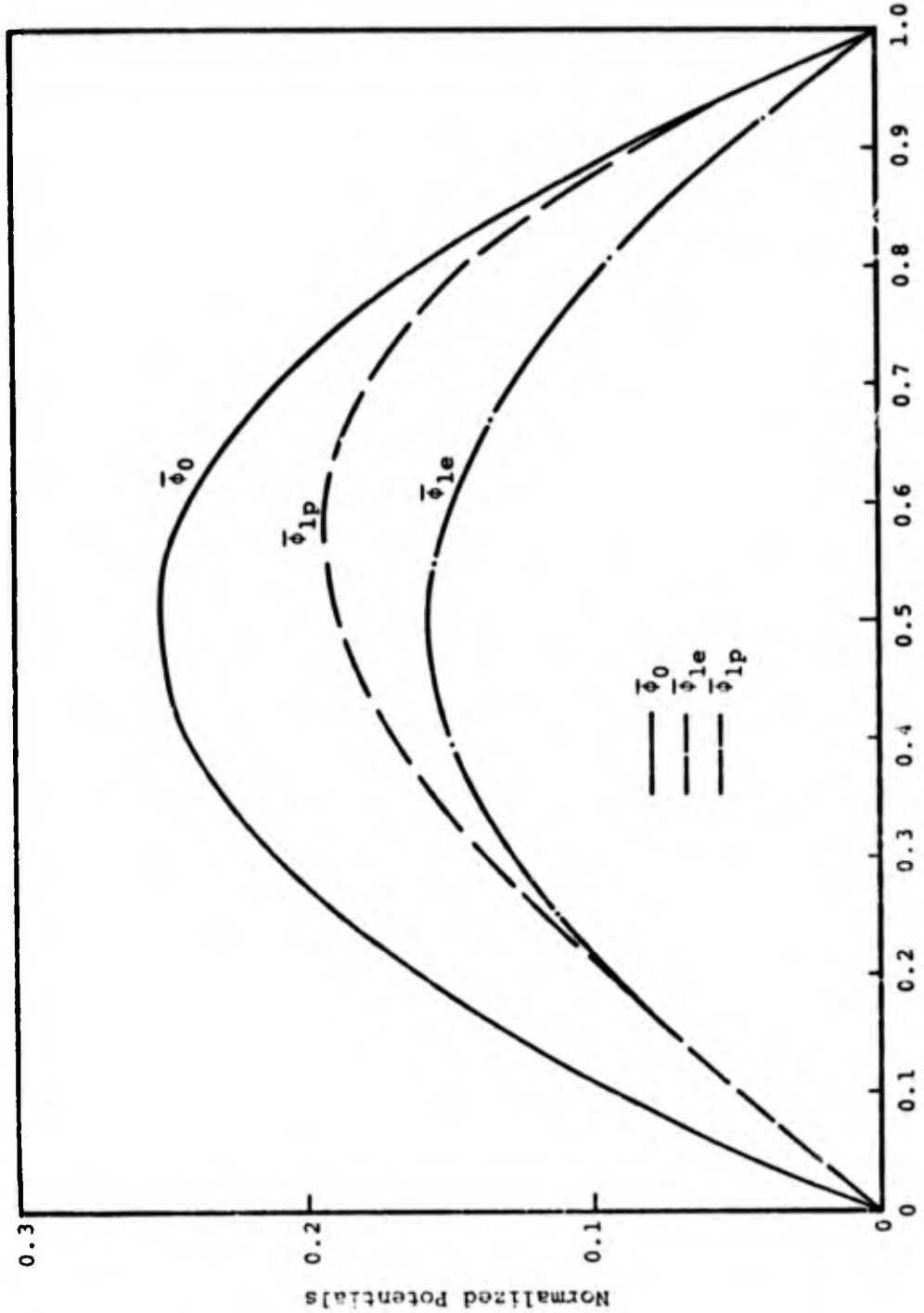

FIGURE 2.3.1 Normalized zero- and first-order potentials as functions of z/L.

$$\bar{E}_{1e}(\zeta) = \frac{1}{2}\,(1 + 4\zeta^3 - 6\zeta^2)$$

$$\bar{E}_{1p}(\zeta) = \frac{1}{2}(1 - 3\zeta^2) \quad .$$

They are tabulated in Table 2.3.2 and plotted in Figure 2.3.2.

In the results of the analysis presented here it has been assumed that the energy dependence of emitted electrons is of the form

$$f_0(\varepsilon) = n_0\,\sqrt{2/\pi}\,(\varepsilon/\varepsilon_T)^{3/2}\,\exp - \frac{\varepsilon}{\varepsilon_T} \quad .$$

Using a different form for f_0 would simply change the relation between v_T and $\bar{v}$.

TABLE 2.3.2

NORMALIZED ZERO AND FIRST ORDER ELECTRIC FIELDS AS FUNCTIONS OF THE NORMALIZED DISTANCE $\zeta = z/L$

ζ	$\bar{E}_0 = 1-2\zeta$	$\bar{E}_{1e} = \frac{1}{2}(1+4\zeta^3-6\zeta^2)$	$\bar{E}_{1p} = \frac{1}{2}(1-3\zeta^2)$
0.0	1.0	0.500	0.500
0.1	0.8	0.472	0.485
0.2	0.6	0.396	0.440
0.3	0.4	0.284	0.365
0.4	0.2	0.148	0.260
0.5	0.0	0.000	0.125
0.6	-0.2	-0.148	-0.040
0.7	-0.4	-0.284	-0.235
0.8	-0.6	-0.396	-0.460
0.9	-0.8	-0.472	-0.720
1.0	-1.0	-0.500	-1.000

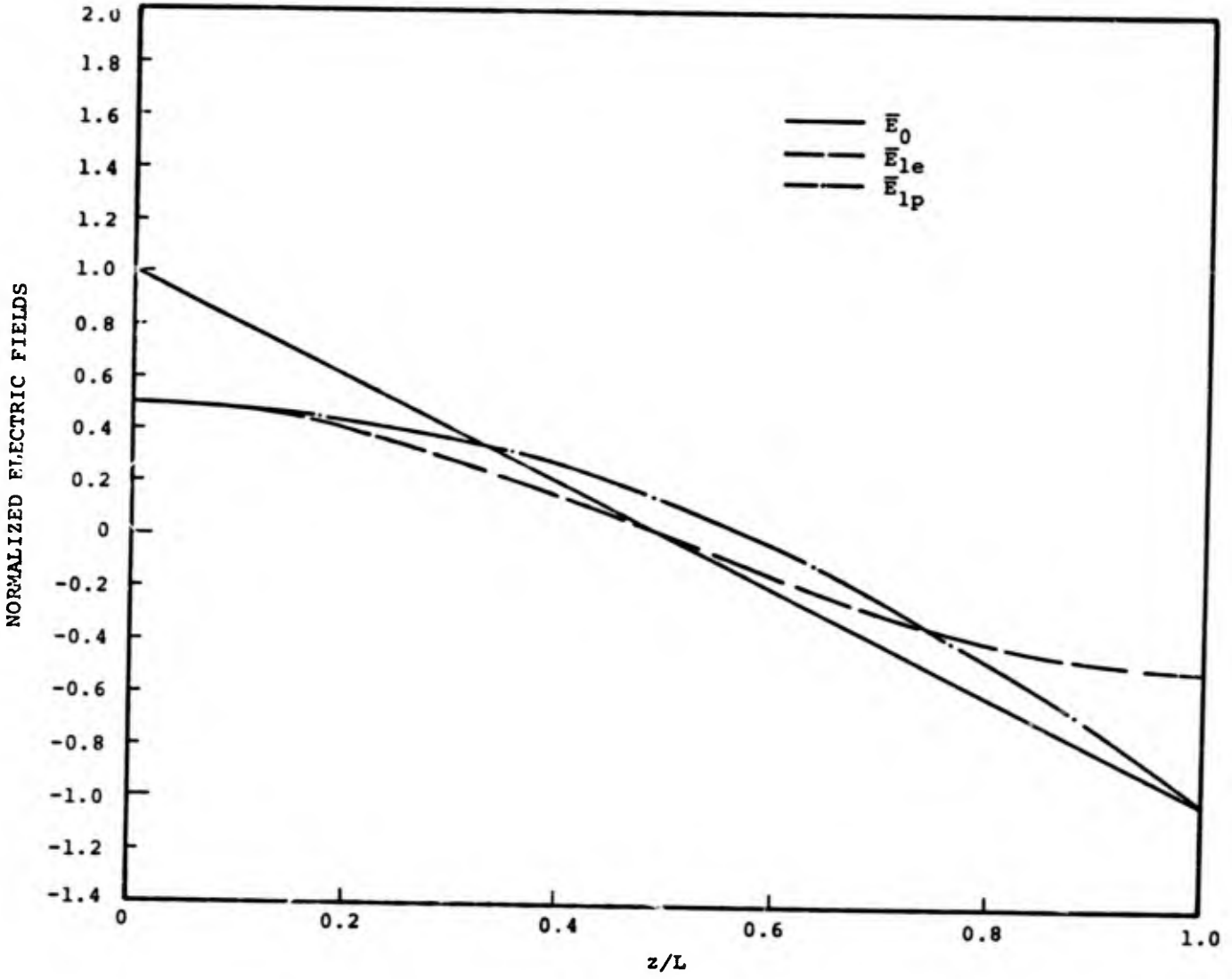

FIGURE 2.3.2 Normalized zero- and first-order electric fields as functions of z/L.

2.3.2 Numerical Example

The theory already described is best illustrated by means of a simple example.

A current is emitted into a diode space of width L = 8 cm. The emitted current is given by

$$j(t) = j_{Am}\, g(t/\tau_p)$$

where

$$j_{Am} = 0.5 \text{ A/cm}^2$$

$$g(\tau) = 2.33\, \tau^{1/2}\, e^{-\tau} , \quad \tau = t/\tau_p$$

$$\tau_p = 10^{-8} \text{ secs} .$$

The electrons have an energy distribution

$$f_0(\varepsilon) = \frac{n_0}{\varepsilon_T^{3/2}} \sqrt{2/\pi}\, \varepsilon^{3/2} \exp - \varepsilon/\varepsilon_T$$

which peaks at

$$\varepsilon = \varepsilon_T = 4 \times 10^4 \text{ eV} .$$

We then obtain from the results of the previous section

$$v_T = 1.19 \times 10^{10} \text{ cm/sec}$$

$$\bar{v} = 9.49 \times 10^9 \text{ cm/sec}$$

$$\bar{v}/c = 0.316$$

$$\omega_0 = 1.02 \times 10^9 \quad \text{sec}^{-1}$$

$$L/v_T = 6.72 \times 10^{-10} \quad \text{sec}^{-1}$$

$$(L\omega_0/v_T)^2 = 0.47$$

$$\frac{1}{\sqrt{\pi}} \frac{L}{v_T \tau_p} = 0.038 \quad .$$

The potential in the diode space ($0 < \zeta < 1$) at a time $t = \tau_p \tau$ is then given by

$$\phi = \phi_0 + \phi_1$$

where

$$\phi_0(\zeta,\tau) = 3.818 \times 10^4 \, \bar{\phi}_0(\zeta) g(\tau) \quad \text{volts}$$

$$\phi_1(\zeta,\tau) = -6.362 \times 10^3 \, g(\tau) [0.47 \, \bar{\phi}_{1e}(\zeta) \, g(\tau)$$

$$+ 0.038 \, \frac{1}{g} \frac{\partial g(\tau)}{\partial \tau} \, \bar{\phi}_{1p}(\zeta)] \quad \text{volts} \quad .$$

Quite analogously, the electric field is given by

$$E = E_o + E_1$$

where

$$E_o(\zeta,\tau) \simeq -2400\ g(\tau)\ E_o(\zeta)$$

$$E_1(\zeta,\tau) = -[188\ g(\tau)\ \bar{E}_{1\text{-}e}(\zeta) + 15.2\ \frac{1}{g}\frac{\partial g}{\partial \tau}\ E_{1p}(\zeta)]\ g(\tau).$$

The functions, $\bar{\phi}_0$, $\bar{\phi}_{1e}$, $\bar{\phi}_{1p}$, are listed in Table 2.3.1 and are plotted in Figure 2.3.1. In the same way the electric field can be evaluated, the normalized electric field functions $\bar{E}_0$, $\bar{E}_{1e}$, $\bar{E}_{1p}$ being listed in Table 2.3.2 and plotted in Figure 2.3.2.

At a time, t = 4 nsecs ($\tau = 0.4$), the pulse height function g is approximately

$$g \simeq 0.99$$

and

$$\frac{1}{g}\frac{\partial g}{\partial \tau} = \frac{\partial \ln g}{\partial \tau} = \frac{1}{2\tau} - 1 = 0.25 \quad .$$

We thus have at a position z = 0.16 cm ($\zeta = 0.2$):

$$\bar{\phi}_e = 0.16$$

$$\bar{\phi}_{1e} = 0.093$$

$$\bar{\phi}_{1p} = -0.096$$

$$\bar{E}_e = 0.60$$

$$\bar{E}_{1e} = 0.40$$

$$\bar{E}_{1p} = 0.44$$

$$g = 0.99$$

$$\frac{1}{g}\frac{\partial g}{\partial \tau} = 0.25 \quad .$$

Then the potential has the value

$$\phi = -5.78 \text{ kilovolts}$$

and the electric field is

$$E = 1.51 \text{ kilovolts/cm} \quad .$$

2.4 THE MONODE PROBLEM IN SGEMP

Up to now the stress in this report has been with regard to the internally generated field problem. However, in many cases of interest the emission of photoelectrons from surfaces into free space is important and will be addressed here.

Consider a surface being subjected to x-ray photons. The surface is part of a body in free space. On being emitted the electrons produce a space-charge field which tends to attract them back to the emitting surface--or monode. We are interested in determining the evolution of the space-charge field, the distance of maximum separation of the pulse of electrons from the monode, the time when this occurs and, indeed, whether the maximum separation is finite. All of these questions will be examined here, not only in plane geometry but also in cases where the monode can be more accurately termed cylindrical or spherical.

2.4.1 Plane Geometry

It is assumed that the electrons are generated by a square pulse (in time) of x-rays and that they are monoenergetic. For times $t > 0$, these electrons, of velocity v_0 and carrying a current $j(0)$ are emitted from a plane, conducting wall at $z = 0$. The equations describing the electron motion are

$$\frac{\partial n}{\partial t} + \frac{\partial}{\partial z}(nv) = 0 \qquad (2.4.1)$$

$$\frac{dv}{dt} = \frac{\partial v}{\partial t} + v\frac{\partial v}{\partial z} = -\frac{eE}{m_0} \qquad (2.4.2)$$

where n is the electron density. We also have, from Maxwell's equations

$$\frac{\partial E}{\partial z} = -4\pi ne \tag{2.4.3}$$

$$\text{div curl } \vec{B} = \frac{\partial}{\partial z}\left(\frac{4\pi}{c} j + \frac{1}{c}\frac{\partial E}{\partial t}\right) = 0$$

or,

$$\frac{\partial}{\partial z}\left(-4\pi nev + \frac{\partial E}{\partial t}\right) = 0 \quad . \tag{2.4.4}$$

The description of the system is completed by the initial conditions

$$\begin{aligned} E(z,0) &= 0 \\ n(z,0) &= 0 \\ v(z,0) &= 0 \end{aligned} \tag{2.4.5}$$

and the boundary conditions at $z = 0$

$$\begin{aligned} v(0,t) &= v_0 \\ n(0,t) &= n_0 = j(0)/v_0 \end{aligned} \tag{2.4.6}$$

and ahead of the beam front, $z > z_f(t)$

$$\begin{aligned} E(z,t) &= 0 \\ n(z,t) &= 0 \quad , \end{aligned} \qquad z > z_f(t) \; . \tag{2.4.7}$$

The equations (2.4.1, 2.4.2, 2.4.4) apply provided the velocity field is a single-valued function of position. They cease to apply when charge sheets (particles) cross one another. The

time at which such crossing occurs will be determined in due course.

From Eqs. (2.4.2), (2.4.6) and (2.4.7) it follows that

$$-4\pi env + \frac{\partial E}{\partial t} = 0 \quad . \tag{2.4.8}$$

From Eq. (2.4.3), namely

$$\partial E/\partial z = -4\pi ne$$

we then have

$$\frac{dE}{dt} = \frac{\partial E}{\partial t} + v \frac{\partial E}{\partial z} = 0 \quad . \tag{2.4.9}$$

This means that the electric field is constant along a particle orbit. The equation of motion (2.4.2) is immediately integrable and yields the velocity and position of a particle at time t

$$v = v_0 - (e/m_0)\, E(0,t_0)(t - t_0) \tag{2.4.10}$$

$$z = v_0\,(t - t_0) - \tfrac{1}{2}\,(e/m_0)\, E(0,t_0)(t - t_0)^2 \tag{2.4.11}$$

where t_0 is the time of emission of the particle.

To complete the solution we define the Lagrangian coordinate $\bar{z}$ of the particle by

$$n_0 \bar{z}(z,t) = M = n_0\, v_0 t - \int_0^z dz'\, n(z',t) \tag{2.4.12}$$

The Lagrangian mass constant satisfies

$$\frac{dM}{dt} = \frac{\partial M}{\partial t} + v \frac{\partial M}{\partial z} = 0 \qquad (2.4.13)$$

which can be seen by using the continuity equation (2.4.1) and the definition of M (see Eq. 2.4.12 below).

We now utilize the Lagrangian coordinate $\bar{z}$. For fixed t we have (see Eq. 2.4.12)

$$n_0 \, d\bar{z} = -n \, dz \qquad (2.4.14)$$

and the equation (2.4.3) can be written

$$\partial E/\partial \bar{z} = 4\pi n_0 e \quad . \qquad (2.4.15)$$

From Eq. (2.4.12), we have

$$\bar{z}(0,t) = v_0 t \qquad (2.4.16)$$

so that

$$t_0 = [\bar{z}(z,t)]/v_0 \qquad (2.4.17)$$

is the time at which the particle (currently at position z at time t) was emitted. We thus have, from Eq. (2.4.15), that

$$E(0,t_0) \equiv E(\bar{z}) = 4\pi n_0 e\bar{z} \quad . \qquad (2.4.18)$$

The particle position and velocity can now be written in terms of the Lagrange coordinate

$$v = v_0 - \omega_0^2 \bar{z} \left(t - \frac{\bar{z}}{v_0}\right) \tag{2.4.19}$$

$$z = v_0 \left(t - \frac{\bar{z}}{v_0}\right) - \frac{\omega_0^2}{2} \bar{z} \left(t - \frac{\bar{z}}{v_0}\right)^2 \quad (t \geq t_0) \tag{2.4.20}$$

where

$$\omega_0 = \left(\frac{4\pi n_0 e^2}{m_0}\right)^{1/2}$$

is the plasma frequency.

From Eq. (2.4.19), we see that the beam front $\bar{z} = 0$ moves forward with a constant velocity v_0 for all $t_0 \geq 0$. Other particles for which $\bar{z} > 0$) may reverse their velocity [see Eq. (2.4.19)] and eventually crossing of particle orbits will take place. The reversal time for any particle is given by

$$t_r = (v_0/\omega_0^2 \bar{z}) + (\bar{z}/v_0) \quad . \tag{2.4.22}$$

The first time $t_{r,min}$ any of the particles reverse velocity is given by

$$\partial t_r / \partial \bar{z} = 0 \quad . \tag{2.4.23}$$

Thus, we have

$$t_{r,min} = 2/\omega_0 \quad . \tag{2.4.24}$$

The corresponding value of $\bar{z}$ is

$$\bar{z}_{min} = v_0/\omega_0 \quad , \tag{2.4.25}$$

so that, from Eq. (2.4.20) this reversal occurs at the point

$$z_{min} = v_0/2\ \omega_0 \quad . \tag{2.4.26}$$

Having determined the position z_{min} and time $t_{r,min}$ when velocity reversal of any particle first occurs, we shall next turn to examine the question of particle crossing. The position z of a particle, given in Eq. (2.4.20) has a cubic dependence on $\bar{z}$. For small values of $\bar{z}$, z depends linearly on $\bar{z}$. For larger $\bar{z}$ values the quadratic and cubic dependence produce curvature, inflection and eventually double valuedness of the curve $z = z(\bar{z})$. When the curve ceases to be single valued the theory breaks down. At the point of inflection

$$\partial z/\partial \bar{z} = 0 \quad , \tag{2.4.27}$$

$$\partial^2 z/\partial \bar{z}^2 = 0 \quad . \tag{2.4.28}$$

This marks the onset of particle crossing. Using the above conditions in Eq. (2.4.20) yields the values of the time t_c of first crossing at the position z_c where it takes place. These values are

$$t_c = \frac{\sqrt{6}}{\omega_0} \quad , \tag{2.4.29}$$

$$z_c = \frac{\sqrt{6}}{9}\ \frac{v_0}{\omega_0} \quad . \tag{2.4.30}$$

For $t < t_c$, $\bar{z}$ is a single-valued function of z. For $t > t_c$ there are several solutions and Eq. (2.4.20) becomes invalid. However, comparison of the results (2.4.26) and (2.4.30) shows that the time of the earliest turnaround $t_{r,min}$ precedes the time t_c when particle crossing first occurs.

In order to obtain the electron density $n(z,t)$ we utilize the transformation (2.4.14), whereby

$$n(z,t) = - n_0 \frac{d\bar{z}}{dz}$$

$$= \frac{n_0}{\frac{\omega_0^2}{2} \left[(t - \bar{z}/v_0)^2 - (\bar{z}/v_0)(t - \bar{z}/v_0) \right] + 1} \qquad (2.4.31)$$

where $\bar{z} = \bar{z}(z,t)$ is found by solving Eq. (2.4.20). At the point of crossing (z_c, t_c) the electron density becomes infinite.

These results might be most easily appreciated with the help of a numerical example. An emission current density of 10^{-2} A/cm^2, composed primarily of 30 keV electrons ($\beta = 1/3$), gives rise to an electron number density n_0 at the point of emission which has the value

$$n_0 = \frac{0.1 \times 10^{-2}}{\frac{1}{3} \times 4.8 \times 10^{-10}} \approx 6 \times 10^6 \text{ cm}^{-3} \quad .$$

With $v_0 = \beta c = 10^{10}$ cm/sec and with the plasma frequency, given by (see Eq. 2.4.21)

$$\omega_0 \approx 5.6 \times 10^4 \, n_0^{1/2} \sim 1.4 \times 10^8 \text{ sec}^{-1} \quad ,$$

the time taken for the first turnaround due to space charge is

$$t_{r,min} = 14.2 \text{ nsec}$$

and the distance at which this occurs is at

$$z_{min} = 36 \text{ cm} \quad .$$

Finally, crossing first occurs at

$$z_c = 19 \text{ cm}$$

after a time

$$t_c = 17.4 \text{ nsec} \quad .$$

Thus, we see that 14.2 nanoseconds elapse before any electron is brought to a standstill by the space-charge field. This turnaround takes place at about 36 cm from the monode. Meanwhile the electrons at the front of the beam will have gone a distance $v_0 t_{r,min} = 2 v_0/\omega_0 = 142$ cm. Approximately 3 nsec after the first turnaround, bunching and overlapping of particles first takes place. This event occurs rather closer to the monode, at a distance of 19 cm.

The model presented here will become invalid sooner if the distance of the beam from the monode is comparable with or larger than the radius of curvature of the monode. In such cases, it must be reconsidered in cylindrical or spherical geometry.

2.4.2 Cylindrical Geometry

In this case, electrons are emitted normal to the surface of a cylinder of radius r_0. The other conditions of the model described already are unchanged. The electrostatic equation is now written

$$\frac{1}{r}\frac{\partial}{\partial r} rE = -4\pi ne \quad , \tag{2.4.32}$$

and the equation for electron conservation is

$$\frac{\partial}{\partial t}(ne) + \frac{1}{r}\frac{\partial}{\partial r}(nevr) = 0 \quad . \tag{2.4.33}$$

Thus, by inserting Eq. (2.4.32) into Eq. (2.4.33) we find

$$\frac{1}{r}\frac{\partial}{\partial r}\left(\frac{\partial rE}{\partial t} + v\frac{\partial rE}{\partial r}\right) = 0 \quad .$$

Using boundary conditions analogous to the plane geometry case, we find

$$\frac{d(rE)}{dt} = \frac{\partial(rE)}{\partial t} + v\frac{\partial(rE)}{\partial r} = 0 \quad . \tag{2.4.34}$$

In other words, rE is a constant along a particle trajectory. In the plane case above E was a constant. The equation of motion for an electron is

$$\frac{d^2r}{dt^2} = -\frac{e}{m_0}E(r,t) = -\frac{e}{m_0}\frac{E_0 r_0}{r} \quad , \tag{2.4.35}$$

where $E_0 = E(r_0,t_0)$ is the electric field at the monode at the time t_0 the particle was emitted. Rewriting the second

derivative in the form

$$\frac{d^2r}{dt^2} = \frac{1}{2}\frac{d(\dot{r}^2)}{dr}$$

the equation of motion can be integrated

$$\dot{r}^2(r) - \dot{r}^2(r_0) = -\frac{2eE_0r_0}{m_0}\ln(r/r_0) \quad , \qquad (2.4.36)$$

where

$$\dot{r}(r_0) = v_0$$

is the emission velocity. Evidently the electrons will eventually be stopped and turned around, since it is always possible to find a position

$$r = r_0 \exp\left(\frac{mv_0^2}{2E_0r_0}\right)$$

at which the velocity $\dot{r}(r)$ in Eq. (2.4.36) vanishes. It is possible to introduce the Lagrangian coordinate $\bar{r}$ in much the same way as was done in the plane geometry case (see Eqs. 2.4.12 through 2.4.18). Here the quantity $\bar{r}$ is defined

$$\bar{r} = r_0 + v_0t_0 \quad , \qquad (2.4.37)$$

where t_0 is the time that the particle (ring) in question is emitted. Thus, for the first particle emitted $\bar{r}$ is just the radius of the monode r_0. Equation (2.4.36) can be expressed

in integral form

$$\int_{t_0}^{t} dt' = t - t_0 = \int_{r_0}^{r} \frac{dr'}{\left(v_0^2 - \frac{2e}{m_0} E_0 r_0 \ln \frac{r'}{r_0}\right)^{1/2}} . \quad (2.4.38)$$

Analogous to Eq. (2.4.14) we have

$$n_0 r_0 d\bar{r} = - nrdr \quad (2.4.39)$$

so that Eq. (2.4.32) can be written

$$\frac{\partial(rE)}{\partial \bar{r}} = 4\pi n_0 e r_0$$

or

$$rE(\bar{r}) = 4\pi n_0 e r_0 (\bar{r} - r_0) \quad (2.4.40)$$

since the electric field before the pulse is initiated (at $\bar{r} = r_0$) is zero. On account of the constancy of rE along a particle trajectory the term on the left of Eq. (2.4.40) can be replaced by $r_0 E_0$, where $E_0 = E(0,t_0)$. Then Eq. (2.4.38) can be rewritten

$$t - t_0 = \int_{r_0}^{r} \frac{dr'}{\left(v_0^2 - 2\omega_0^2 r_0 (\bar{r} - r_0) \ln r'/r_0\right)^{1/2}} . \quad (2.4.41)$$

The point r' where velocity reversal takes place is given by

$$v_0^2 = 2\omega_0^2 r_0 (\bar{r} - r_0) \ln \frac{r'(t_r)}{r_0}$$

or

$$r'(t_t) = r_0 \exp\left(\frac{v_0^2}{2\omega_0^2 r_0 (\bar{r} - r_0)}\right) \quad .$$

Consequently, from Eqs. (2.4.37) and (2.4.41), t_r is given by

$$t_r - \frac{\bar{r} - r_0}{v_0} = \frac{v_0}{2\omega_0^2(\bar{r} - r_0)} \int_0^1 \frac{du}{(1-u)^{1/2}} \exp \frac{v_0^2 u}{2\omega_0^2 r_0 (\bar{r} - r_0)} \quad . \tag{2.4.42}$$

The time $t_{r,min}$ when reversal of velocity first occurs is defined by

$$\partial t_r / \partial \bar{r} = 0 \tag{2.4.43}$$

and hence, from Eq. (2.4.42), by

$$1 = \frac{v_0^2}{2\omega_0^2(\bar{r}-r_0)^2} \int_0^1 \frac{du}{(1-u)^{1/2}} \exp \frac{v_0^2 u}{2\omega_0^2 r_0 (\bar{r}-r_0)}$$

$$+ \frac{v_0^4}{4\omega_0^4 r_0 (\bar{r}-r_0)^3} \int_0^1 \frac{du\, u}{(1-u)^{1/2}} \exp \frac{v_0^2 u}{2\omega_0^2 r_0 (\bar{r}-r_0)} \quad . \tag{2.4.44}$$

This is a transcendental equation for $\bar{r}$ and cannot be solved, in general, in closed form. It is not so difficult to solve numerically. However, we shall content ourselves with the

examination of results in the limit

$$\alpha = \frac{v_0^2}{2\,\omega_0^2\, r_0\,(\bar{r} - r_0)} << 1 \quad . \tag{2.4.45}$$

To lowest order in this small quantity only the first term on the right of Eq. (2.4.44) appears. When the integral is expanded and the lowest order term retained the solution to that equation is

$$\bar{r} - r_0 = v_0/\omega_0 \quad .$$

Hence, from Eq. (2.4.42) we have

$$t_{r,min} = 2/\omega_0 \quad .$$

Thus, to the lowest order in the expansion parameter, we recover the same result as that obtained in the plane geometry case (see Eq. (2.4.24)).

The equation (2.4.44) can be solved numerically for arbitrary values of α. As pointed out already, even for large values of α, no electrons can escape from the space-charge field. That is, $t_{r,min}$ is always finite.

2.4.3 Spherical Geometry

In this case the product Er^2 is constant along any particle's trajectory. The equation of motion can be shown, in a manner analogous to that of the cylindrical and plane geometries, to be

$$\frac{d^2r}{dt^2} = -\frac{e}{m_0}\frac{E_0 r_0^2}{r^2} \quad . \tag{2.4.46}$$

This may be integrated

$$\dot{r}^2(r) = \dot{r}^2(r_0) - \frac{2eE_0 r_0^2}{m_0}\left(\frac{1}{r_0} - \frac{1}{r}\right)$$

$$= v_0^2 - 2\omega_0^2 r_0^2 (\bar{r} - r_0)\left(\frac{1}{r_0} - \frac{1}{r}\right) \qquad (2.4.47)$$

where v_0 is the velocity of emission at $r = r_0$ and where $\bar{r}$ is the analogous Lagrangian coordinate--this time in a spherical system.

Unlike the plane and cylindrical cases here, there is a possibility that electrons are not trapped in the space-charge field. In particular, the velocity of a particle vanishes at a point r given by

$$\frac{r}{r_0} = \left(1 - \frac{v_0^2}{2\omega_0^2 r_0 v_0 t_0}\right)^{-1} \qquad (2.4.48)$$

where we have used Eq. (2.4.37) to define $\bar{r}$. Thus, for

$$v_0/2\omega_0^2 r_0 t_0 > 1 \qquad (2.4.49)$$

there is no solution (no positive solution, that is). Particles having sufficient energy will thus escape. In fact, all particles emitted prior to the time

$$t_0 = v_0/2\omega_0^2 r_0$$

will escape.

To take the example cited earlier ($v_0 = 10^{10}$ cm/sec, $\omega_0 = 1.4 \times 10^8$ sec^{-1}), we see that particles emitted prior to $t_0 = 2.5 \times 10^{-7}/r_0$ sec will escape. If the radius of curvature is large ($r_0 = 100$ cm) the trapping begins after only 2.5 nsec. However, for smaller emitting surfaces a large fraction of the entire beam emitted may be lost (e.g., for $r_0 = 10$ cm in the case of a pulse of duration 1 to 2 shakes).

It is possible to pursue an analysis similar to that presented for the plane and cylindrical geometries. Indeed, the integrals are more tractable than in the cylindrical case. However, work on this topic will be pursued in a later effort.

2.4.4 Summary of Monode Analysis

The work discussed here is applicable to the problem of sheath formation around satellites in free space. Using an order of magnitude estimate of the conversion efficiency η of x-ray photons into photoelectrons we have

$$\begin{aligned}\eta &\sim 10^{-8} \text{ coulombs/calorie} \\ &= 10^{-8} \text{ (coul/cm}^2\text{/sec)/(cal/cm}^2\text{/sec)} \\ &= 1 \text{ amp/cm}^2\text{/(cal/cm}^2\text{)}\end{aligned}$$

if the pulse persists for 10^{-8} seconds. A fluence level of 10^{-4} cal/cm^2 will thus lead to an emission current in the range of 10^{-4} A/cm^2. The space-charge created by the emitted electrons will cause them to turn back toward the monode after a finite length of time. Repeating the numerical example presented in the plane geometry section, we see that the number density is $n_0 \sim 8 \times 10^4$ cm^{-3} if the emitted electrons have a velocity $\beta c = 7.5 \times 10^9$ cm/sec. The resulting plasma frequency is

$$\omega_0 \sim 1.6 \times 10^7 \text{ sec}^{-1} \quad .$$

Thus, turnaround first occurs at

$$t_{r,min} \sim 1.25 \times 10^{-7} \text{ sec}$$

at a distance of approximately 2.3 meters. This gives an indication of the size of the plasma sheath. The above estimate of photon conversion efficiency η is very crude. In general, it depends on the photon spectrum and the nature of the emitting material. If the radius of curvature of the emitting surface is comparable with or smaller than this distance the treatment given in the sections on cylindrical and spherical geometries must be used. If the surface from this distance away appears spherical, then the electrons may not be trapped by the space charge. In the case cited here, electrons emitted at a time t_0 after the initiation of the pulse will escape if (see Eq. 2.4.49)

$$\frac{7.5 \times 10^9}{5 \times 10^{14} \, r_0 t_0} > 1$$

where r_0 is the radius of curvature of the surface. Taking $r_0 = 100$ cm, it is clear that the electrons emitted prior to $t_0 = 1.5 \times 10^{-7}$ sec will be lost. In most cases of interest, this means that none will be retained by the space charge.

It must be stressed however, that the effects of finite pulse width, nonmonoenergetic electrons and angular dependence of the emission have not been taken into account. Nevertheless, for the case just cited, it is doubtful whether these will make the analysis essentially invalid.

3. IEMP PINCH EFFECT

3.1 BEAM PINCH

When a strong current I flows, it creates a magnetic field at radial position r

$$B_\theta(r) = \frac{0.2}{r} I(r) \tag{3.1}$$

where B is in gauss and I is in amperes. The electrons producing this current will tend to be deflected by this field and the radius of curvature of the electrons is

$$r_c = \frac{1}{300} (\varepsilon^2 + 2\varepsilon\varepsilon_0)^{1/2} \tag{3.2}$$

where $\varepsilon = (\gamma - 1)\varepsilon_0$ is the kinetic energy and $\varepsilon_0 = m_0c^2 = 5.1 \times 10^5$ eV is the electron rest energy. Thus,

$$r_c = \frac{\beta\gamma}{300} \frac{5.1 \times 10^5}{B_\theta} \tag{3.3}$$

where

$$\beta = \frac{v}{c}, \quad \gamma^2 = (1 - \beta^2)^{-1} \quad . \tag{3.4}$$

The beam is pinched fully if the radius of curvature of the motion is equal to that of the beam. Thus, from Equations 3.1 and 3.2 the critical current I_c is given by

$$I_c = 8.5\ \beta\gamma \ \text{kAmps} \quad . \tag{3.5}$$

This current I_c will be defined as the current necessary to deflect an electron onto the axis of the beam. As Equation 3.5 indicates the critical current is proportional to the velocity (βc) of the electrons. Thus, at first sight, the nonrelativistic electron beams generally encountered in IEMP environments, would appear to provide good candidates for pinching. Moreover, a total current of 5 to 10 kA is not impossibly large. For instance, a surface of one square meter ($=10^4$ cm^2), emitting a current density of only 1 ampere/cm^2 would provide a sufficiently large total current.

The effect of pinch on an IEMP environment could be important. Let us consider the following example. The magnetic field B_θ (gauss) associated with a current I (amps) carried by a beam of radius R is

$$B_\theta(R) = \frac{0.2I}{R} \quad .$$

The time rate of change of B is due to a change in both the total current as well as the radius. Thus,

$$\dot{B}_\theta = \frac{0.2}{R} (\dot{I} - I\dot{R}/R) \quad .$$

If $I(t) = I_m\, t/t_r$, we then have

$$\dot{B}_\theta = \frac{0.2}{Rt_r} I_m (1 + \frac{|\dot{R}|t}{R})$$

since $\dot{R} < 0$ when pinching takes place. An estimate of the second term can be obtained by assuming that pinching produces a minimum beam radius at the end of the current rise and that

$\dot{R} \sim (R - R_0)/t_r \sim -R_0/t_r$ if $R_0 >> R$ where R_0 is the initial radius. Then, we have

$$\dot{B}_\theta \simeq \frac{0.2\ I_m}{Rt_r}\left(1 + \frac{R_0}{R}\frac{t}{t_r}\right) \quad .$$

For a moderately strong pinch $R \sim 0.2\ R_0$ and $\dot{B}_\theta$ is enhanced six times. Consider a situation in which $R_0 = 50$ cm, $R = 10$ cm, $I_m = 10^4$ amp, $t_r = 10$ nsec. This gives rise to the magnetic field rate of change

$$\dot{B}_\theta \sim 120 \text{ gauss/nsec} \quad .$$

The electric field induced by the changing magnetic field is given by

$$E \sim 2R_0 \times 10^{-8}\ B = 2.4 \times 10^4 \text{ volts/cm} \quad .$$

In addition to the large induced field created by the pinch the current density is enhanced by pinching to a value of

$$j \sim \frac{10^4}{\pi R_0^2}\left(\frac{R_0}{R}\right)^2 \sim 300 \text{ A/cm}^2 \quad .$$

It is of interest to see how these values of E and j compare with those possible in a nonpinching environment. The current density enhancement, as already indicated, is a factor of $(R_0/R)^2 \sim 25$. The maximum electric field possible outside of the pinch environment is formed at very low pressures by the space charge. Under the conditions indicated above, that is, with an emitted current density of $10^4/\pi R_0^2 \sim 1.3$ amp/cm^2 the

maximum electric field possible in a system of linear dimension L is, approximately

$$E \sim 120\pi \times 1.3\ (L/\beta) \quad \text{volts/cm}$$

if the electrons have a velocity βc. For 30 keV electrons, $\beta \sim 1/3$ and hence

$$E \sim 1.3 \times 10^3\ L \quad \text{volts/cm} \ .$$

The system must be less than L = 8 cm in order that the electrons are not heavily space-charge limited, in which case the maximum space-charge is also limited and the maximum field possible is not given by the result above. Thus, the maximum field is about 1.2×10^4 volts/cm which is comparable with, but less than, the inductive field possible in the pinching case cited earlier.

3.2 PINCHING IN VACUO

There are conditions (other than those described in the previous section) to be satisfied for pinching to take place. Most important of these is the self electric field of the beam. An electron is subject to the accelerating force given by

$$\vec{F} = -e(\vec{E} + \frac{\vec{v}}{c} \times \vec{B}) \ . \qquad (3.6)$$

In the treatment given above only the magnetic force was taken into account.

At the very low gas densities frequently encountered in cases of interest the electric field arises from the space-charge $\rho = -ne$ of the electron beam. That is,

$$dE/dz = -4\pi ne \ ,$$

or,

$$E = -4\pi neL$$

$$= -0.4 \frac{\pi jL}{\beta}$$

where j is the emitted current density and βc is the electron velocity. The magnetic field, as already indicated, is given by

$$B(R) = \frac{0.2\ I(R)}{R}$$

$$= 0.4\pi jR \ .$$

Thus, in Equation 3.6 the magnetic and electric forces, on an electron (F_B, F_E respectively) are related by the ratio

$$\frac{F_B}{F_E} = 0.4\pi jR\beta \frac{\beta}{0.4\pi jL}$$

$$= \beta^2 \frac{R}{L} \ . \qquad (3.7)$$

Thus, in broad, short systems we expect pinching to be important provided the electrons are sufficiently energetic. On account of the factor β^2 it is now clear that the condition (3.5) is misleading since it suggested that low energy electron beam pinched most readily.

Thus, for 80 keV electrons ($\beta = 1/2$) the magnetic force is comparable with the electric field in geometries for which

the aspect ratio R/L is of order unity. However, for lower energies (ε = 30 keV, $\beta \sim 1/3$) the aspect ratio must be rather larger than unity. As a result, the effect of pinching is not expected to be dominant at very low pressures where space charge dominates.

3.3 PINCHING AT LOW PRESSURES

The presence of air permits neutralization of the space charge to take place. The primary electrons produce ionization and, while the heavy ions remain immobile in the space charge field the secondaries are driven out of such regions of high space charge, thus leaving the positive ions to neutralize the primary electrons. Of course, the secondaries themselves may cause ionization. However, we shall look only at the "low" pressure regime where this effect is negligible. The conditions under which this situation obtains will now be examined.

At "low" densities secondaries have long ranges, and, if strong local electric fields exist, it can be assumed they will undergo acceleration. Ranges increase with increasing energy, so it is likely that secondaries will escape to the walls, forming very few tertiaries on the way. Thus the number density of ion pairs created can be estimated from the primary ionization formula of Bethe[3.3.1] and the rate of neutralization will be given by multiplying the ratio of ion production by the fraction of secondaries that escape.

To examine the likelihood of escape we can look at the stopping power. From the tabulation of Nelms[3.3.2] we find that for a 10 keV electron the stopping power (-dε/dx) has the value of 19.5 MeV/gm/cm^2. With an NTP air density of 1.2 x 10^{-3} gm/cm^3 this corresponds to about 3 eV/cm at 0.1 torr (= 1/7600 atmospheres). This loss in energy is very small compared with the local field strengths to be expected in any SGEMP environment of interest. Thus, at such densities energetic secondaries will clearly escape and will create few tertiaries.

Quantitative estimates of energy loss rates for lower energy electrons are not readily available, but if we extrapolate the stopping power formula down to 1 keV we get

$$-\frac{d\varepsilon}{dx} \simeq 100 \text{ MeV/gm/cm}^2$$

or about 13 eV/cm, still a reasonably small number. Below 1000 eV, loss rates tend to flatten out (and ultimately decrease) because fewer electrons per atom are ionizable and because cross sections tend to peak. If we use a cross section of 1.5×10^{-16} (comparable to the ionization cross section of Ne at 100 eV) and an average energy transfer of about 100 eV per "collision" we get

$$-\frac{d\varepsilon}{dx} \simeq 150 \frac{\text{MeV}}{\text{gm/cm}^2}$$

as an estimate of the stopping power in the region around 100 eV electron energy. This corresponds to about 24 eV/cm at 0.1 torr.

On the basis of these rather crude estimates we see that at 0.1 torr all the secondaries escape if local field strengths are in excess of 100 V/cm or so. At about 10 V/cm substantial numbers of secondaries will not escape directly but will diffuse to the walls. Thus, for most cases of interest the streaming or runaway character of secondary electrons will dominate the diffusion-type behavior. Finally, if we use the data of McClure[3.3.3] for neon to estimate the number of ion pairs/cm created in air at 0.1 torr we obtain the following results.

TABLE 3.3.1

Primary Energy (eV)	Electron Produced (per cm)
5×10^4	.006
1×10^4	.021
1×10^3	.105
1×10^2	.263

Having indicated what is meant by the low pressure or secondary-escape regime we can now proceed to estimate the time for neutralization to occur. A primary beam, with an average electron number density n_B and with an average velocity βc moves through a gas containing n_0 atoms/cm^3. In a time t the beam creates

$$n_B n_0 \sigma \beta c t$$

secondary electrons. Here σ is the ionization cross section for primaries with velocity βc. As described above, only the formation of secondaries will be considered. Once formed, they escape from the region of the space-charge and that region becomes neutral when the number of secondaries produced is equal to the beam density. That is, for a constant beam density n_B, neutralization takes place in a time t_N given by

$$n_B = n_B n_0 \sigma \beta c t_N$$

or

$$t_N = \frac{1}{n_0 \sigma \beta c} .$$

The quantity $\sigma\beta c$ can be calculated from the Bethe formulation[3.3.1]. In air we have

$$\sigma\beta c = A(\sqrt{(1+x)/x}\ \ell nx - 1) + C\left(\frac{1+\sqrt{x}}{\sqrt{x(1+x)}}\right) ,$$

where

$$A = 1.26 \times 10^{-9}$$

$$C = 1.08 \times 10^{-8}$$

$$x = \gamma^2 - 1 = \varepsilon/m_0c^2(2 + \varepsilon_0/m_0c^2)$$

ε = kinetic energy (in eV)

$$m_0c^2 = 5.1 \times 10^5 \text{ eV} .$$

In Table 3.3.2 the quantity $\sigma\beta c$ is tabulated as a function of energy.

TABLE 3.3.2

Kinetic Energy (eV)	$\sigma\beta c$ (cm^3/sec)
4×10^4	2.9×10^{-8}
5×10^4	2.6×10^{-8}
6×10^4	2.4×10^{-8}
8×10^4	2.2×10^{-8}
1×10^5	2.0×10^{-8}
1.5×10^5	1.7×10^{-8}
2×10^5	1.5×10^{-8}

The neutralization time t_N is plotted as a function of the air gas density (n_0, cm^{-3}) for several values of the kinetic energy

of the primaries in Figure 3.3.1. As an example, we consider a pulse with a duration of 2 shakes (2×10^{-8} secs). With pressures less than 0.05 torr only partial neutralization of the space charge is possible, even for 40 keV electrons.

The estimate of the neutralization time is subject to several sources of error. For instance; (a) the pulse is not constant in time – a triangular pulse could increase the estimate by as much as a factor of 2; (b) the slowing of the primary electrons in the partially neutralized space charge field would tend to enhance ionization and hence lead to a decrease in t_N; (c) the drift velocity of the secondaries decreases as neutrality is approached, thus leading to an increase in t_N.

3.4 PINCH CONDITIONS

At gas densities such that space charge neutrality can be achieved for the primary beam, pinching will take place if the total current flowing, I, is comparable with or greater than 8.5 $\beta\gamma$ kA (see Eq. (3.5)). As was pointed out earlier this constraint is quite possible in IEMP situations. However, as it stands, it is oversimplistic. Implicit in its derivation is the assumption that all the electrons are moving parallel to the direction of the current beam. This is unlikely either on account of curvature of the emitting surface or the nearly isotropic angular emission frequently encountered.

The effect of angular spreading of the emitted beam electrons can have important consequences for beam pinching. The numerical treatment described later in this report can be used to address this question, although this has not been carried out in the work reported here. The results of a simple fluid beam model are illustrated in Figure 3.4.1.

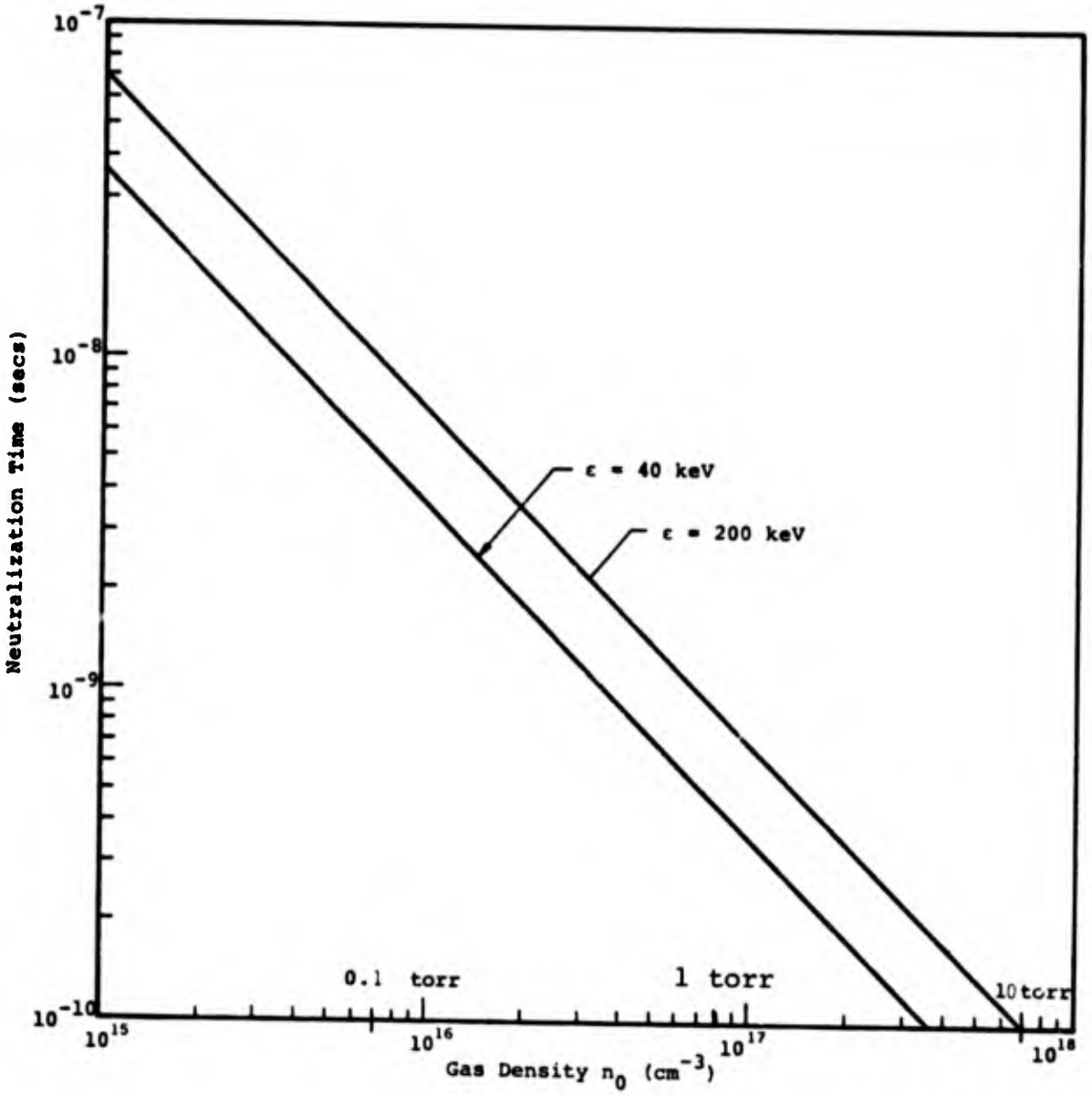

Figure 3.3.1 Space-charge neutralization time as a function of density.

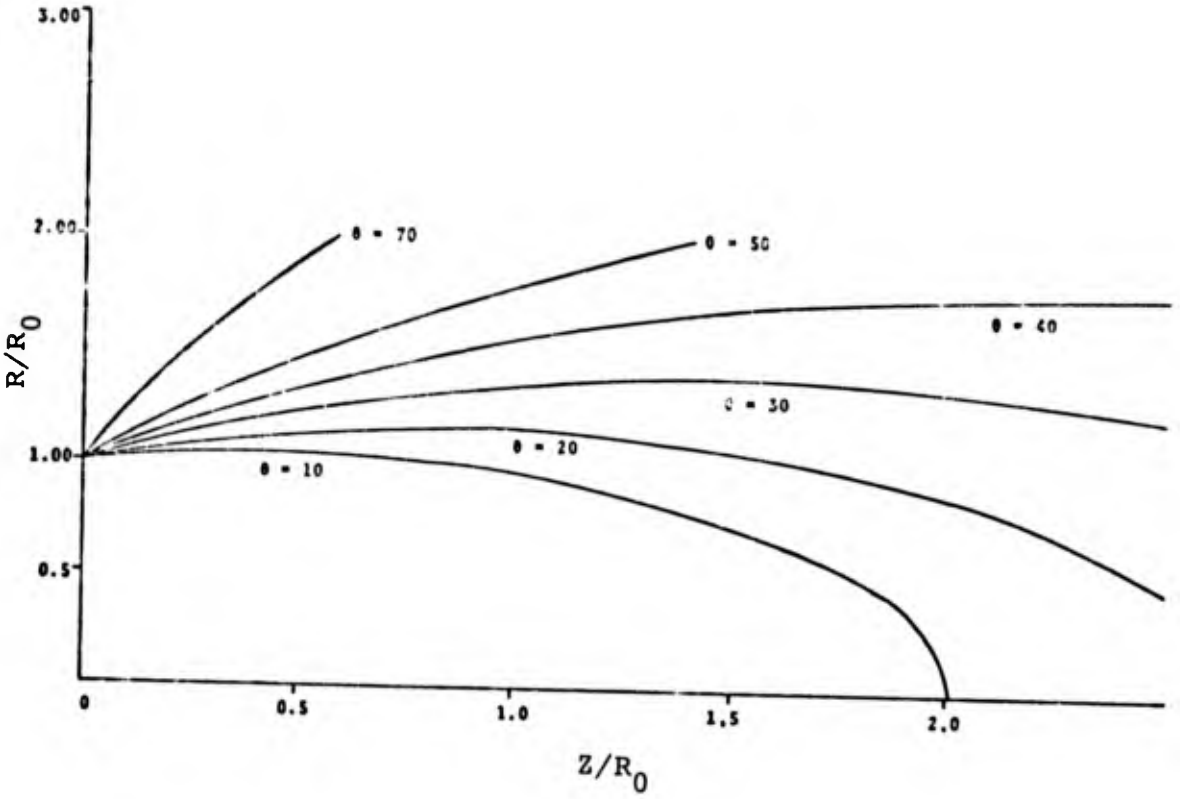

Figure 3.4.1 Showing the influence of the initial emission angle θ on the pinching distance. R_0 is the initial beam radius. The current flowing is equal to 0.4 I_c.

In order to achieve space charge neutrality, finite gas pressure in excess of 0.05 torr is necessary for pulses with a 2 shake duration. Depending on the energies and current density of the primary electrons, pressures much greater than 1 - 10 torr can provide conditions which lead to gas breakdown. Thus, pressures between 0.1 - 1 torr are most favorable to pinch conditions although they do not guarantee that pinching will occur. Sufficient conditions are provided by constraints on the total current flowing and on the degree of spreading of the beam.

These features are not amenable to simple analysis. To illustrate how pinching might occur in representative situations a computer code was developed to investigate the effect. A description of the code is given in the next section. Briefly, it solves Poisson's equation

$$\nabla^2\psi = 4\pi ne$$

from which is obtained the electric field

$$\vec{E} = -\nabla\psi \quad .$$

It also calculates the magnetic field from Ampere's Law

$$\oint \vec{B} \cdot d\vec{s} = 0.4\pi \ I$$

where I is the current (in amperes) and $d\vec{s}$ is an element of the current loop.

Two sample calculations were performed. In the first of these a current of uniform beam density j = 5 A/cm is injected from the z = 0 end of a right cylinder. The length L of the cylinder is 16 cm and the radius R = 16 cm also. The injected particles have an energy ε = 100 keV ($\beta \sim 0.5$). In

Figures 3.4.2 - 3.4.5 the progress of the beam in the tank is shown. By the time it has crossed the tank ($t \sim 1$ nsec) some pinching of the beam is apparent. In this case strong pinching is not expected since (see Equation 3.7) the ratio $\beta^2 R/L$ is much less than unity (where R is the beam radius) and because the total current $I \sim 250$ A is so low. It is clear that (see Figures 3.4.4 and 3.4.5) neutralization of the beam is also important for pinching to take place. In these figures the presence of the space charge field is still evident as electrons are turned back. If the same calculation were carried out later in time greater neutralization would be achieved and the constriction would be more pronounced.

In the second calculation a more space-charge neutralized situation is considered. With quasi-neutrality taking place in less than a nanosecond and with a much broader beam carrying a larger total current the pinch effect is much more evident (see Figures 3.4.6 - 3.4.9). Here again the electrons emitted have an energy of 100 keV. The current density is 10 A/cm^2 and the total emitted current is 1.77 kiloamps. The strength of the pinch is determined by (a) the ratio of the total current I to the critical current I_c (see Equation 3.5) and (b) by the rate at which secondary electrons are created to neutralize the higher charge densities that occur near the neck of the pinch.

As regards (a) the ratio $I/I_c \sim 0.21$ so that the pinching, even if the space-charge were totally neutralized, would not be expected to be complete. As regards (b), the potential contours show that even though the space-charge field is somewhat less than it would be under vacuum conditions it is still fairly large ($\sim$60 kV) primarily because the tank is large (L = 32 cm). However it is not sufficiently strong to slow many electrons appreciably.

Conditions such as this might be encountered in simulation experiments where direct beam injection takes place. At

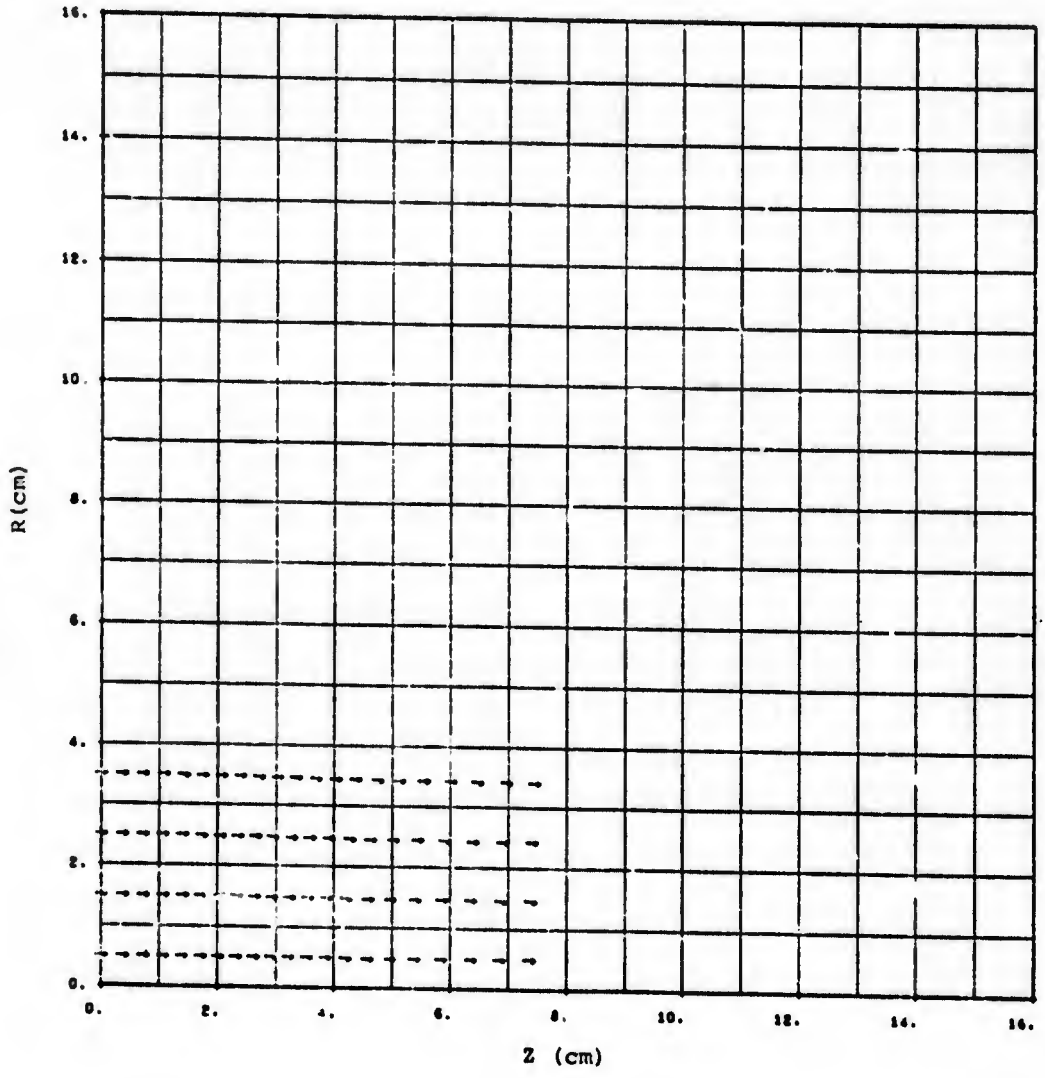

Figure 3.4.2 Beam electrons at 0.4 nsec.

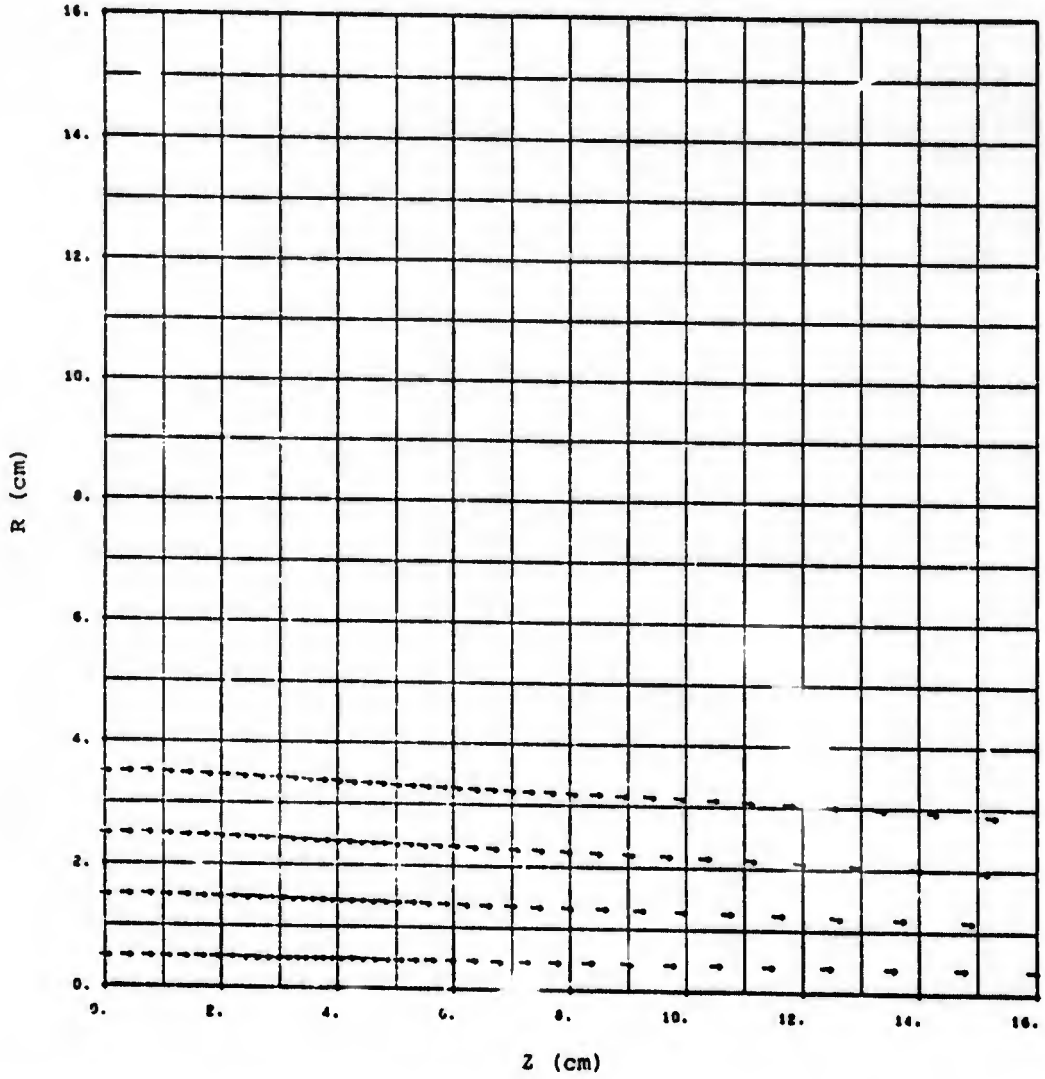

Figure 3.4.3 Beam electrons at 0.8 nsec. Space-charge is slowing electrons in the neighborhood of peak potential (at z ∿ 4 cm) while the beam is pinching in regions of smaller potential.

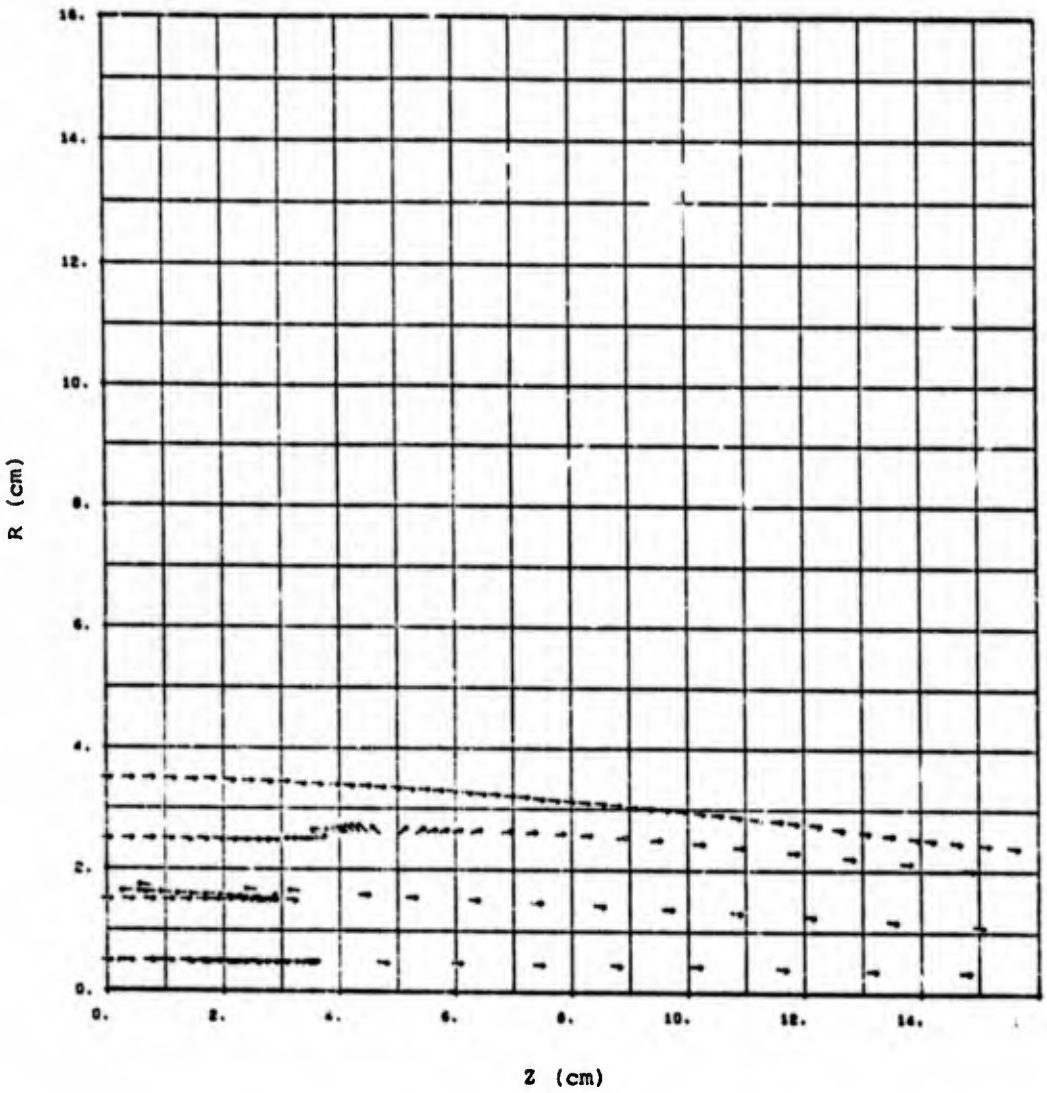

Figure 3.4.4 Beam electrons at 1.6 nsec. Pinching is maximum at the exit face where space-charge is least. Electrons are being reversed at z ∿ 5 cm where the potential is greatest.

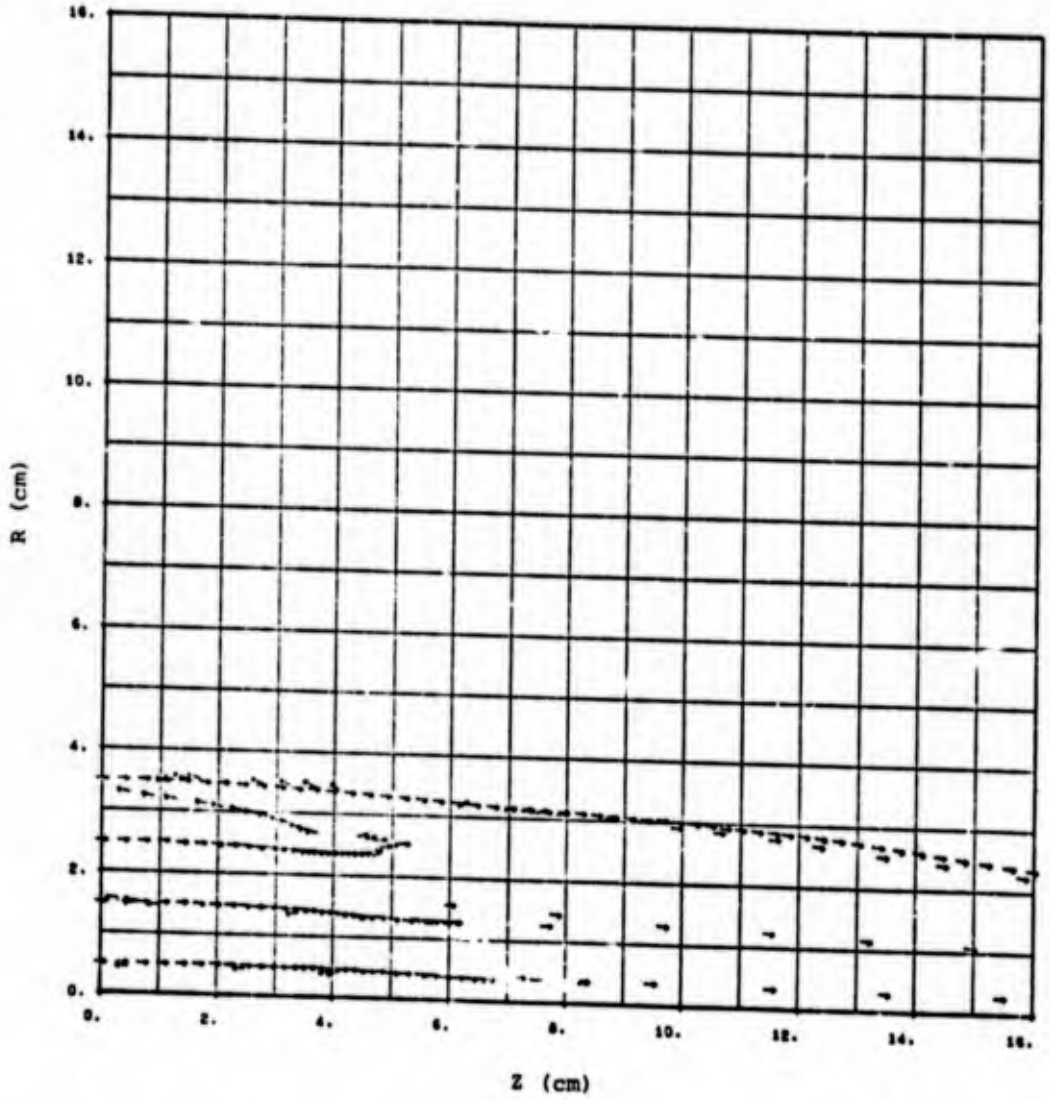

Figure 3.4.5 Weak pinch at t = 2 nsec near the exit face. Neutralization of space charge has not yet taken place and the current transmitted is limited.

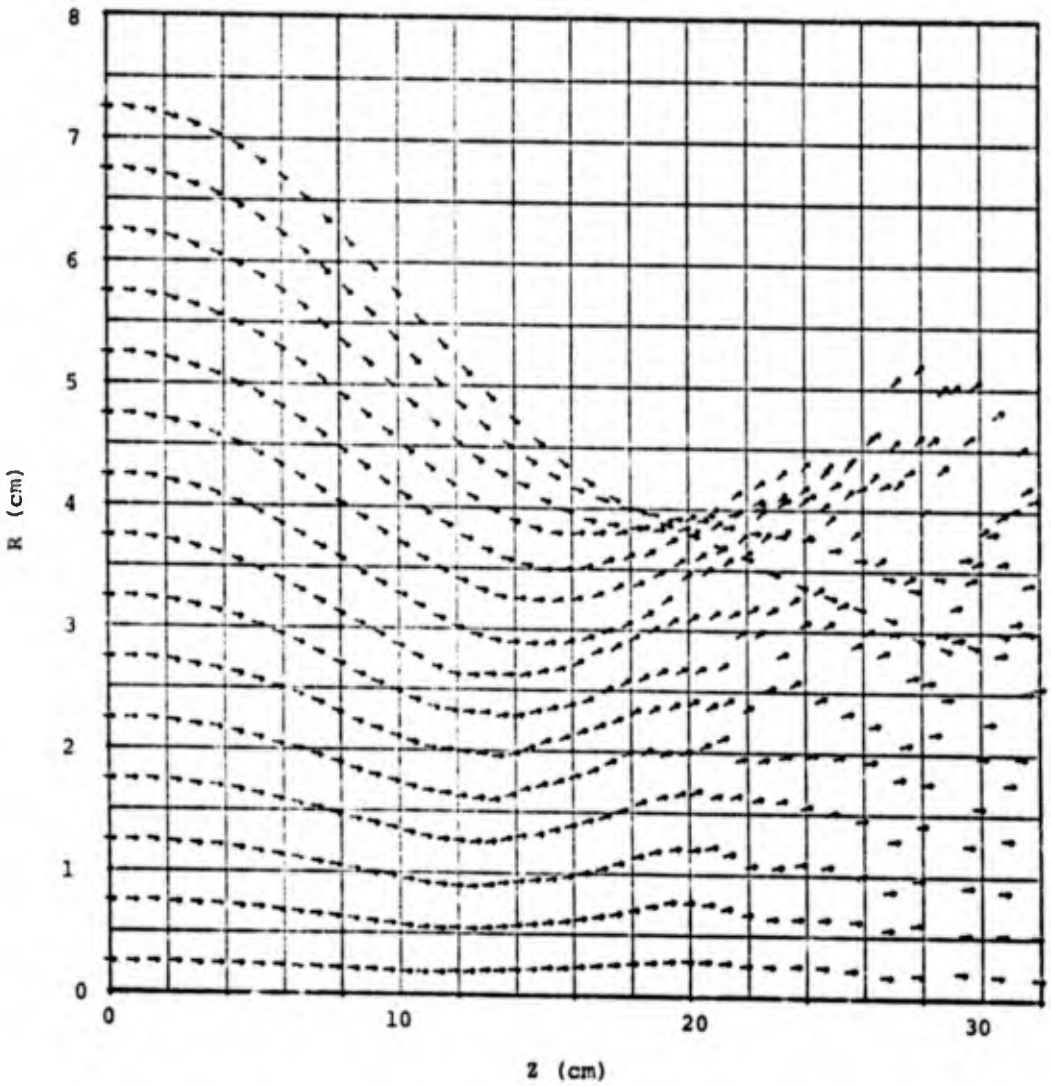

Figure 3.4.6 Beam electrons at t = 3 nsec. Beam constriction at z = 20 cm is limited by the space charge present.

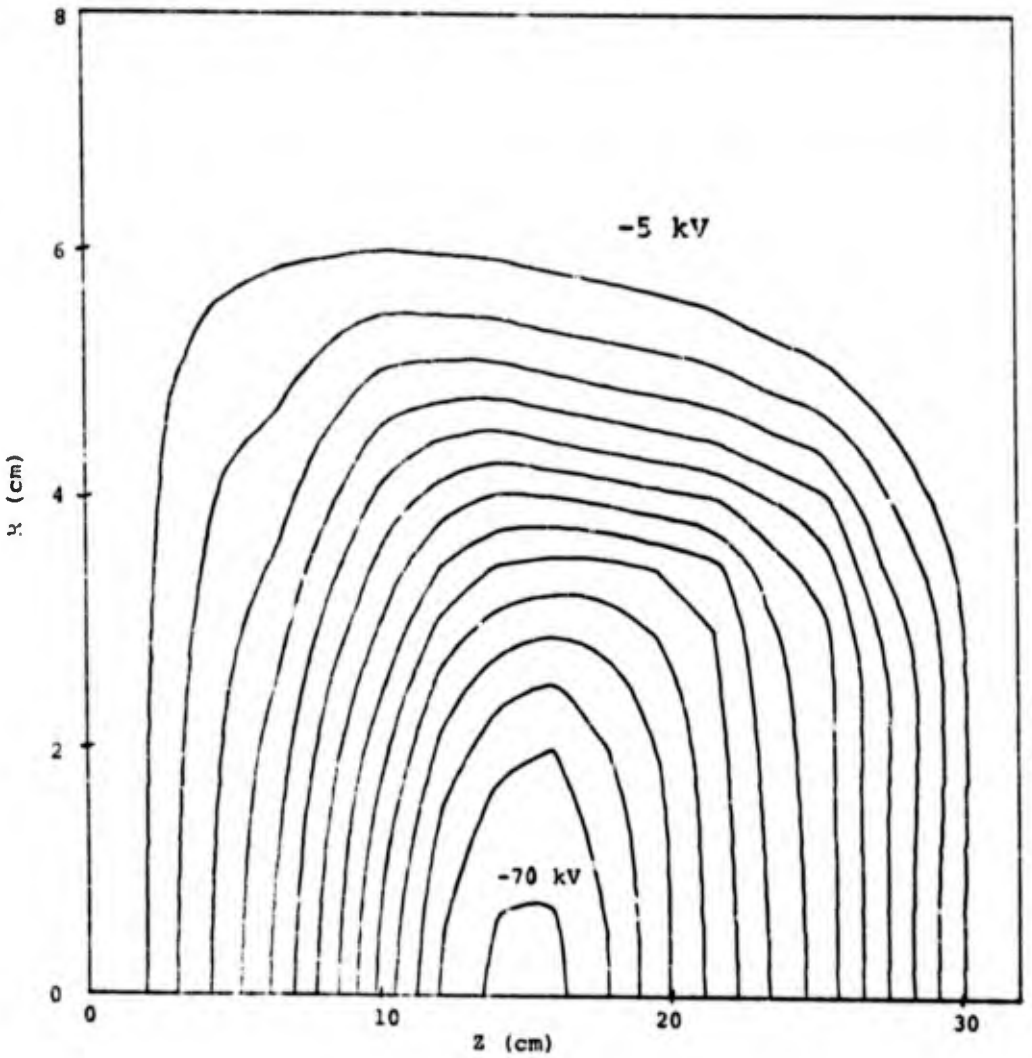

Figure 3.4.7 Field potential contours at t = 3 nsec, ranging from -5 kV to -70 kV.

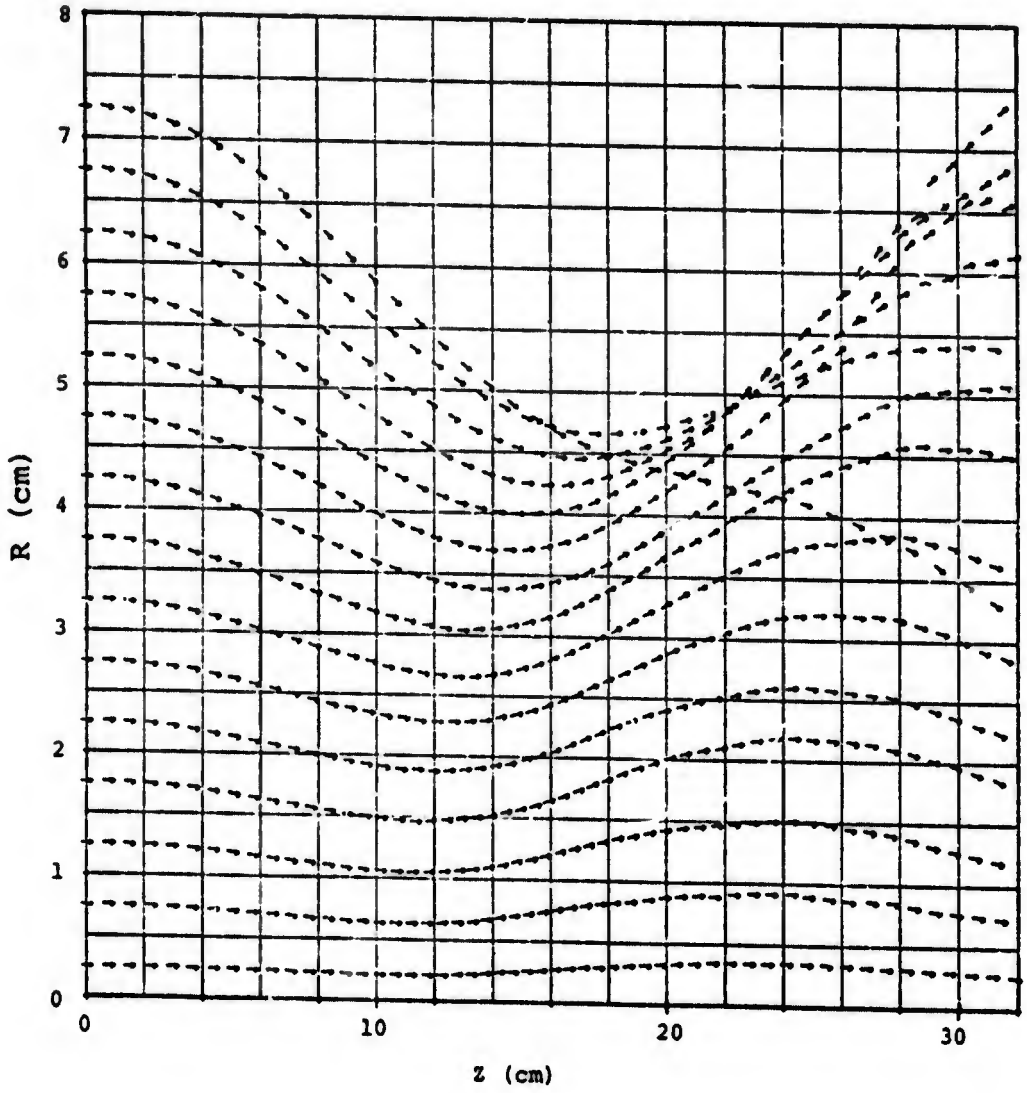

Figure 3.4.8 Beam electrons at t = 9 nsec. The space charge is still present. It does not lead to considerable slowing of electrons, but it causes deflection of trajectories in the region where beam constriction is greatest - where space charge is maximum.

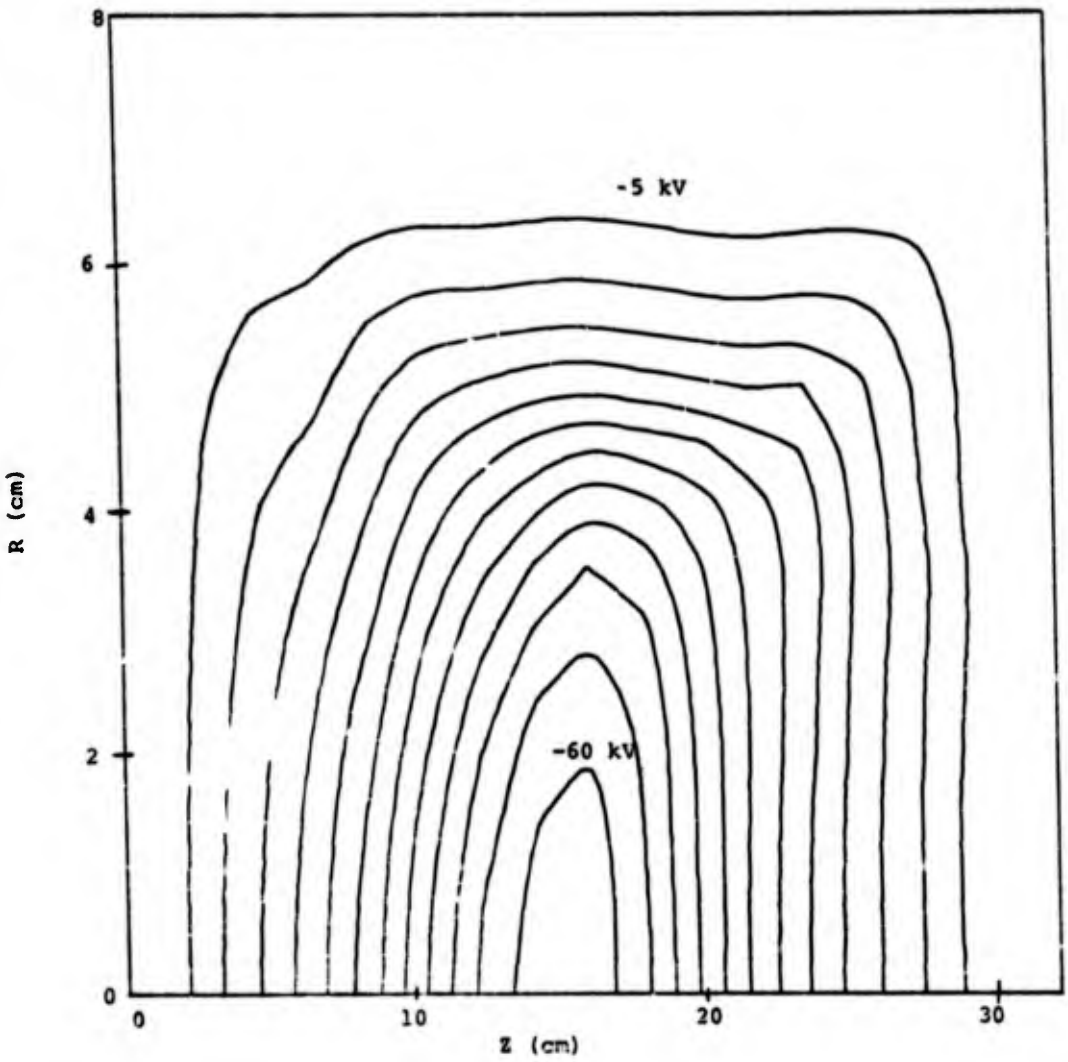

Figure 3.4.9 Field potential contours at t = 9 nsec, ranging from -5 kV to -60 kV.

the time of writing this report, work is in progress on electron transport at finite pressures under conditions where appreciable beam pinching is important.

While finite gas pressure enhances the self-pinching of a beam it is of greater importance for SGEMP applications to examine the weaker pinching that occurs under vacuum or low pressure conditions. It is for such cases that the code developed here is useful.

4. COMPUTATIONAL DEVELOPMENT

4.1 FAST-RUNNING ELECTRODYNAMIC (FRED) CODES

Much of the basic IEMP phenomenology is amenable to analytic treatment. However, the analysis of real, as distinct from idealized, problems requires numerical treatment. Existing IEMP computer codes deal with the generation of fields in simple 1-D and 2-D cavities. During the present contract period a family of computer codes has been developed which are (1) fast, (2) modular and (3) applicable, in principle, to arbitrary 2-D geometries.

A description of the theory underlying the FRED (Fast-Running-Electro-Dynamic) series of codes is presented in the following section. Some effort has been expended toward understanding the physics relevant to a variety of IEMP field generation problems instead of developing a generalized IEMP code which would be cumbersome and slow running. The result of this work has culminated in a series of codes which are, at once, much more rapid computationally than even the simpler electrostatic IEMP codes currently in use and, in addition, are less cumbersome that the fully electromagnetic versions.

These codes have been applied to a variety of test problems (see Chapters 3 and 5), such as the pinch effect at finite gas pressures and the transmission of space-charge dominated beams in evacuated cavities. Little progress can be made analytically in understanding these problems as the beam transport is two dimensional and strongly coupled to the self-generated fields.

4.2 ELECTROMAGNETIC FIELD MODELS

For many situations relevant to SGEMP the electric field is longitudinal (curl free) and may be calculated from

$$\nabla \cdot \vec{E}_\ell = 4\pi\rho$$

where ρ is the charge density. This is valid whenever the length scale of the system is small in comparison with the distance $\beta c t_r$ travelled by electrons (with velocity βc) in a time t_r characteristic of the pulse that creates the electrons. Thus, for 30 keV electrons ($\beta \sim 1/3$) and with a pulse time $t_r \sim 10^{-8}$ sec, it is apparent that for systems smaller than 1 meter the longitudinal field model constitutes a reasonable approximation.

For systems larger than this or for less energetic electrons errors may, in principle, be appreciable. However, the argument given above requires some qualification if space-charge limiting and turn-around of electron trajectories are important. In most SGEMP situations this is the case and there the length scale of the system is characterized by the distance traveled by the electrons from the emitting surface to the turn-around point. Thus, the longitudinal field model has a wider range of application than that indicated above.

The generation of magnetic fields is less frequently discussed in SGEMP problems. Provided the transverse electric fields are negligible the magnetic fields are calculated from

$$\nabla \cdot \vec{B} = 0 \quad ,$$

$$\nabla \times \vec{B} = \frac{4\pi}{c} \vec{j} + \frac{1}{c} \frac{\partial \vec{E}_\ell}{\partial t} \quad .$$

It is important to retain the longitudinal displacement current in the above displacement since it guarantees charge conservation

$$\frac{\partial \rho}{\partial t} + \nabla \cdot \vec{j} = 0 \quad .$$

Its neglect introduces spurious charge fluctuations in SGEMP problems as currents are not divergence-free, in general.

To summarize, the equations to be solved are:

Poisson's Equation

$$\nabla^2 \psi = -4\pi\rho \tag{4.1}$$

from which we obtain the longitudinal electric field

$$\vec{E}_\ell = -\nabla\psi \quad ,$$

and Ampere's Law

$$\nabla \times \vec{B} = (4\pi/c)\ \vec{j}_t \tag{4.2}$$

where

$$\vec{j}_t = \vec{j} - (\partial/\partial t)\ \nabla\psi$$

is the divergence-free part of the net current (conduction + longitudinal displacement).

Finally, if the transverse electric field $\vec{E}_t$ is not negligible, we must solve

Faraday's Law

$$\nabla \times \vec{E}_t = - (1/c)(\partial \vec{B}/\partial t) \quad .$$

These equations comprise the full set of Maxwell's equations if the transverse displacement current can be neglected. Generally speaking, many SGEMP problems involve knowing only the longitudinal field $\vec{E}_\ell$. However, it is not consistent to move electrons in the field $\vec{E}_\ell$ alone since the equation of motion (nonrelativistic) is

$$m \frac{d\vec{V}}{dt} = q\left(\vec{E}_\ell + \frac{\vec{V}}{c} \times \vec{B} \right) \quad .$$

The ratio of the electric and magnetic forces in this equation can be shown to be of order β^2 times a geometrical factor. Thus, if the electrons are more energetic than $\sim$30 keV ($\beta \sim 1/3$) then the magnetic forces may be appreciable in certain geometries (see Chapter 3).

In the work performed the electromagnetic models have been based on:

(a) Poisson's equation alone, i.e., only longitudinal electric field acceleration on the electrons.

(b) Poisson's equation and the divergence-free current form of Ampere's Law, i.e., inclusion of magnetic forces. It should also be stated that if we are interested in calculating currents flowing in struts of an assembly then this model should be used for consistency.

(c) Inclusion of Faraday's Law has not yet been carried out but should be considered in future work.

In the next three sections the emphasis is entirely upon the model (a) above, as applied to complex two-dimensional geometries. However, the method described applies to model (b) also.

4.3 POSING THE PROBLEM

Given an initial source function, the electric and magnetic fields that influence electron motion can be found from the electron spatial and velocity distributions. For many cases the influence of magnetic fields on the electron motion can be neglected, and the problem reduces to solving the following equations:

$$\nabla^2\psi = -4\pi\rho \tag{4.3}$$

$$m\frac{d\vec{v}}{dt} = F = q\vec{E} = q\ (-\nabla\psi) \tag{4.4}$$

Equation (4.3) is Poisson's equation and must be solved with the appropriate boundary conditions which, for conducting walls, is

$$\psi = 0$$

on the walls. Equation (4.4) is just Newton's second law for charged particles in an electric field. For the case in point the particle motion has only the added requirement that particles disappear when they hit the wall. However, the calculation of the fields can be extremely tedious if proper care is not taken to organize the problem efficiently. Below we describe a procedure that would enable one to calculate fields within an arbitrarily shaped two-dimensional region with either

cylindrical or Cartesian symmetry. This procedure in general would offer greater spatial resolution and greater computational speed than the currently used Green's Function technique of dePlomb and Woods[4.1] as well as having the added advantage of being able to treat cavities of arbitrary (noncylindrical or rectangular) shapes. This includes conducting objects within the cavity.

4.4 CALCULATION OF THE POTENTIAL

When setting up a problem, we construct a rectangular grid that entirely contains the region of interest. When finding the charge density on the grid, each particle's charge is shared among the cells surrounding the particle's position as if the particle was a finite rectangular charge cloud. This is the usual cloud-in-cell model[4.2] used to minimize finite grid noise and "shot" noise due to the small number of simulation particles compared with a real system.[4.3]

There are extremely fast transform and direct methods for solving potentials with periodic or regular zero boundary conditions, e.g., that $\psi(r_{max}) = 0$ on a cylinder.[4.4] For example, to solve the potential on a 32 x 32 mesh with periodic boundary conditions takes about 0.5 seconds of Univac 1108 time.

The solution to the problems proceeds as follows. It is a well-known mathematical device to replace boundary conditions on the solution of Poisson's equation

$$\nabla^2\psi = -4\pi\rho_p \tag{4.5}$$

by introducing a surface layer of charge ρ_b in the boundary of the system under consideration. Here ρ_p is the charge

density in the system. Then, instead of solving Eq. (4.5) subject to ordinary conducting boundary conditions, we solve the equation:

$$\nabla^2\psi = -4\pi\ (\rho_p + \rho_b) \tag{4.6}$$

subject to the boundary conditions that are the grid coordinate system. By "grid boundary conditions" we mean those conditions that permit the simplest solution of Poisson's equations. Thus, with rectangular coordinates, periodic boundary conditions are appropriate. In cylindrical (r,z) coordinates the conditions are that ψ be periodic with respect to z and that $\psi = 0$ at $r = R$ and $\psi'(r) = 0$ at $r = 0$ where $r = R(z)$ is the radial boundary surface. The actual choice of the grid boundary conditions is arbitrary, but those described here permit use of the Fast Fourier method[4.5] on at least one of the coordinates [on z in the (r,z) system and on either y or z in the rectangular system]. The boundary charge density ρ_b will depend on the actual conditions chosen.

The latter is calculated as follows. If we solve

$$\nabla^2\psi_p = -4\pi\rho_p \tag{4.7}$$

subject to the grid boundary conditions, we then have the potential along the boundary. That is, in r,z coordinates

$$\psi_p\ [\vec{s}(r,z)] = \psi_b(\vec{s})$$

where $\vec{s}$ is the curve defining the boundary. For computational purposes $\psi_b(\vec{s})$ is evaluated at a number of points

along the boundary and so is stored as a column vector and denoted by $\vec{\psi}_b$. In the same way, the boundary charge density is denoted by $\vec{\rho}_b$.

The remaining part of the problem is to calculate $\vec{\rho}_b$. This is done using the capacitance method of Hockney.[4.4] We place an arbitrary charge distribution, $\vec{\rho}_a$, on the boundary. Then the potential distribution on the boundary, $\vec{\psi}_a$, that results from the surface charge is given by

$$A \ \vec{\rho}_a = \vec{\psi}_a \qquad (4.8)$$

where A is obtained either analytically in simple geometries or numerically in an arbitrary geometry. It results from a simple superposition of the Coulomb fields of individual charges on the boundary. The inverse of A is termed the capacitance matrix C, where

$$C = A^{-1} \quad . \qquad (4.9)$$

The capacitance matrix is purely a function of geometry and is calculated only once. Thus, having calculated the boundary potential $\vec{\psi}_b$ from Eq. (4.5) we obtain the effective boundary charge distribution $\vec{\rho}_b$ from

$$\vec{\rho}_b = C \ (-\vec{\psi}_b) \quad . \qquad (4.10)$$

Finally, we calculate the total charge density ρ, given by

$$\rho = \rho_p + \rho_b \quad . \qquad (4.11)$$

The circle is now closed and the potential ψ is found by solving Eq. (4.6) subject to the grid boundary conditions.

The basic idea behind the method outlined here is to solve Eq. (4.6) subject to simple grid boundary conditions rather than to solve Eq. (4.5) with the ordinary conducting boundary conditions. The reason for this is numerical efficiency. Using the Fast Fourier Method for linear coordinates and finite differences for the curvilinear coordinate renders the computation very rapid.

Thus, a cycle of computation involves (a) computing the potential, given the particle charge distribution (Eq. 4.3) and (b) moving the particles in accordance with the new charge distribution (Eq. 4.4). The potential is found by first solving Eq. (4.7) (using grid boundary conditions) for the boundary potential density, ψ_b, created by the particle charge distribution ρ_p, by then computing the boundary charge distribution, ρ_b, using the capacitance matrix, and finally by solving the Poisson equation (4.6) using the grid boundary conditions. Thus, two solutions of Poisson's equations are involved in each cycle, but as already indicated they are performed very rapidly.

The particle-moving part of the problem is straightforward. However, for efficiency it is important to avail of a variety of computational techniques--binary arithmetic, parallel processing and assembler routines for operations that are performed very frequently.

4.5 COMPARISON WITH CURRENT METHODS

The method described here for calculating the electric field and potential and derived quantities (such as transmission factor and magnetic field) is new in the

IFMP/SGEMP area. It enables calculations to be performed in realistic geometries. Such calculations would form part of future work in this area.

In addition, the method is superior to other currently available schemes (such as those of the TEDIEM codes) for simple geometries. In Ref. 4.1 it is stated that to perform a calculation with a mesh of 20 x 20 points requires 25 minutes of Univac 1108 time to set up a 4-D table of the Green's Function $G(r,r',z,z')$. Each cycle then involves the integral

$$\psi(r,z) = 4\pi \int_0^R dr'\, r' \int_0^L dz'\, \rho(r',z')\, G(r,r',z,z')$$

where L, R are the axial and radial dimensions, respectively. While this integral appears to involve a similar number of operations as the method described here, the Fast Fourier Transform method needs only operations proportional to $mn \log_2 n$ to solve for the potential with m radial mesh points and n axial points as opposed to m^2n^2 for the Green's Function technique. This will show up as a significant time savings when the number of cells is very large. Since, in addition, performing the integral (in TEDIEM) requires very much less time (by several orders of magnitude) than the preparation of Green's Function tables, it is clear that the method proposed here is decidedly faster than the TEDIEM or other schemes. The advantage of the new method becomes increasingly superior for larger grids since the size of the Green's Function table grows as the fourth power of the linear number of cells.

Our method can be applied to complicated geometries. Consider the situation illustrated in Figure 4.1. There, on a 32 x 64 mesh a considerable amount of detail is possible. To solve for the potential on such a large mesh about two seconds of Univac 1108 time is involved. This must be done twice per cycle. Add to this one second (or rather less) to move particles (about 100 μsec per particle with efficient coding) and to perform the matrix multiplication (Eq. 4.10). It is clear that even with such a large mesh and with several thousand particles a calculation of over 100 cycles takes on the order of 10 minutes or less of 1108 time.

It is interesting to note that the Green's Function scheme, which cannot be easily applied to such a complex geometry, would require in addition to a comparable time for performing the calculation, a set-up time for the Green's Function of order

$$\left(\frac{32 \times 64}{20 \times 20}\right)^2 \times 25 \text{ minutes}$$

or approximately 11 hours!

4.6 SUMMARY OF CURRENT CAPABILITY

The current capability includes (a) two-dimensional electrostatic code in (r,z) geometry (FRED/E) and (b) two-dimensional nonradiative electromagnetic code at zero or finite gas pressures in (r,z) geometry (MANFRED). These codes are based on fast numerical techniques, as described already. This method has the following advantages over other IEMP/SGEMP codes.

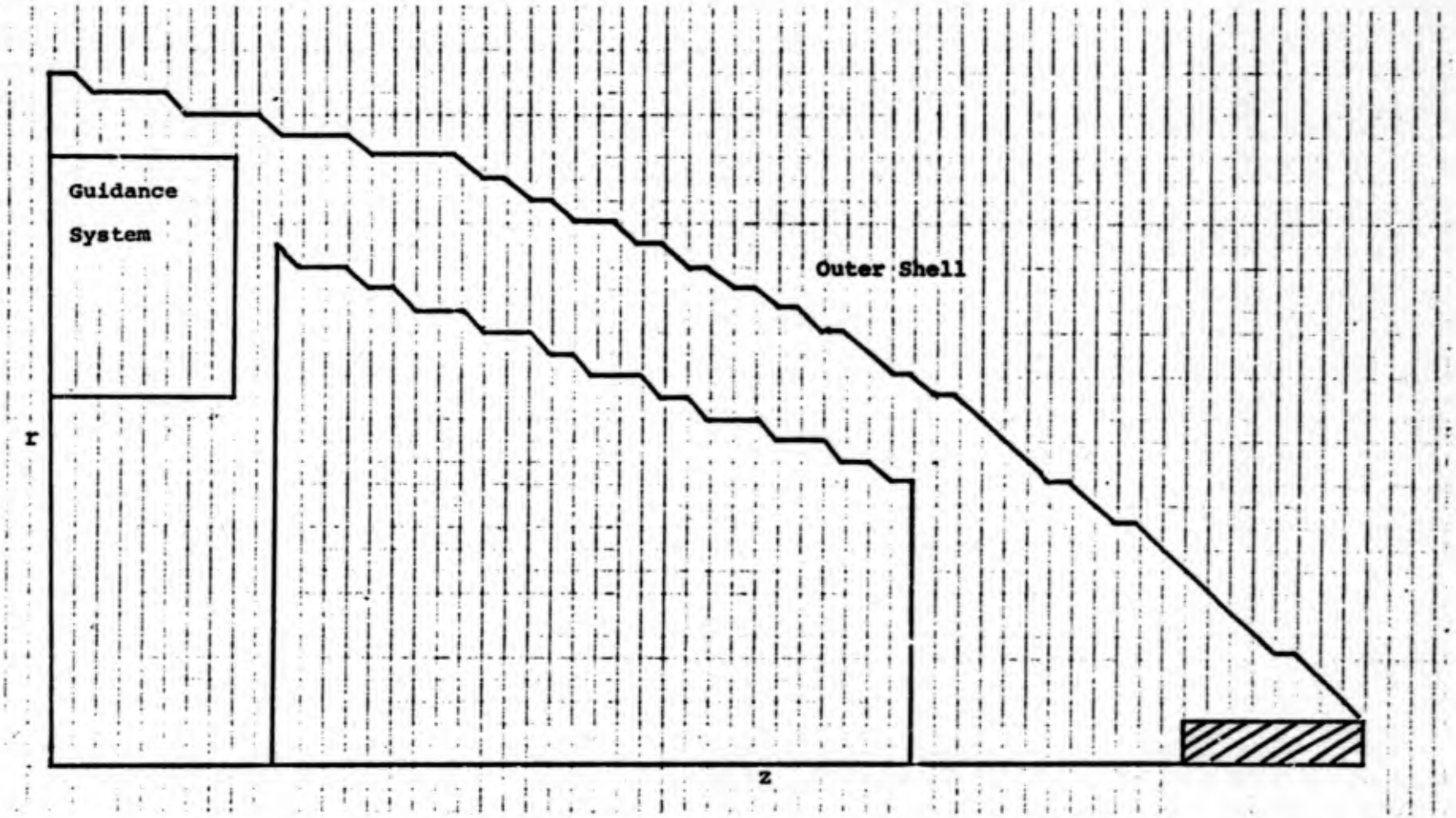

Figure 4.1 Sample problem in cylindrical r-z geometry indicating the detail possible in a 32×64 mesh.

(1) It is much faster (by an order of magnitude in typical problems) and the relative speed increases as the size of the problem grows. The reason for this is the smaller number of operations required with the Fast Fourier Technique.

(2) It is applicable to a general two-dimensional geometry of arbitrary shape.

(3) The electrical properties of the problem might be those of a conductor (uniform potential on the walls), a dielectric (nonuniform potential) or a section of the boundary might be a vacuum.

(4) It is applicable to both electrostatic and nonradiative electromagnetic field problems.

It should be emphasized, however, that so far the code development has not led to implementing the generality indicated in points 2 to 4 above.

5. BEAM INJECTION CALCULATIONS

The electrostatic code FRED/E was used to calculate the current transmitted and the fields produced by a beam of electrons injected into a cavity. The experiments considered were performed at the SPI facility by Osborn (unpublished).

A beam of electrons is injected through a fine wire mesh anode into a chamber of which the pertinent dimensions are

Anode--Faraday cup separation $L = 14$ cm

Cathode (i.e., beam) radius $R_B = 15.24$ cm (6 in.)

The chamber cross section is octagonal with the centers of opposite forces separated by a distance

$$d = 45.72 \text{ cm (18 in.)} \quad .$$

For the purposes of the calculation the octagonal cross section was replaced by a circle of the same area, that is, the average radius R of the cavity is given by

$$\pi R^2 = 8(d/2)^2 \tan \pi/8$$

or

$$R = 24.11 \text{ cm} \quad .$$

The electrons injected into the cavity (Figure 5.1) are created in the anode-cathode space (not shown) of the electron beam machine. The voltage $V_D(t)$ and current $I_D(t)$ in that region are plotted as functions of time in Figures 5.2, and 5.3, respectively. Much of that current

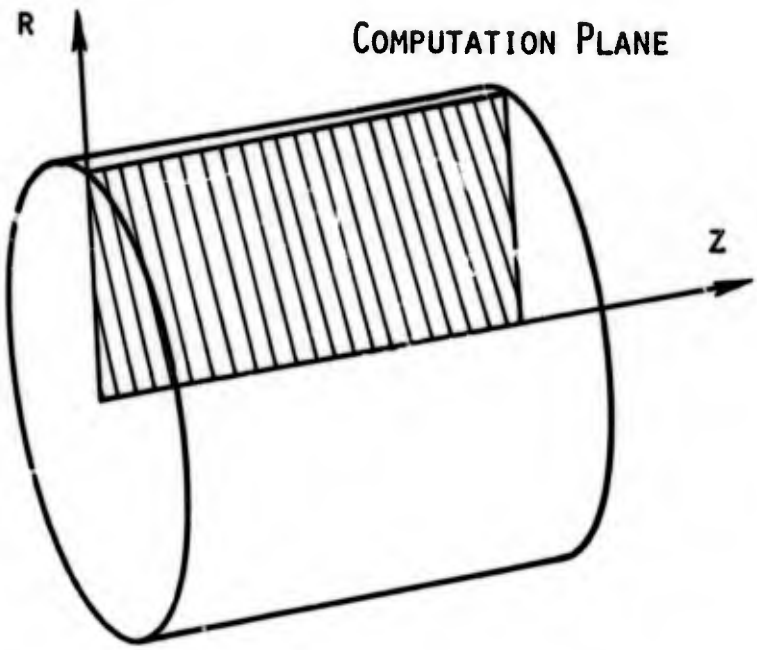

Figure 5.1 Showing the (R,Z) geometry and the computation plane used in calculations. Electrons are injected into the $Z = 0$ plane as a beam of radius R_B. The transmitted current is received at the exit face $Z = L$ on Faraday cups.

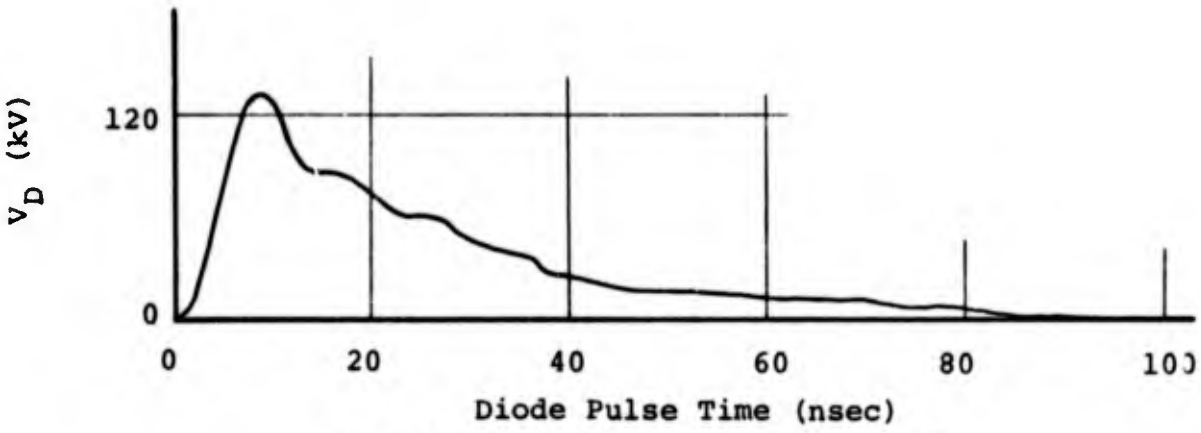

Figure 5.2 SPI diode voltage, V_D.

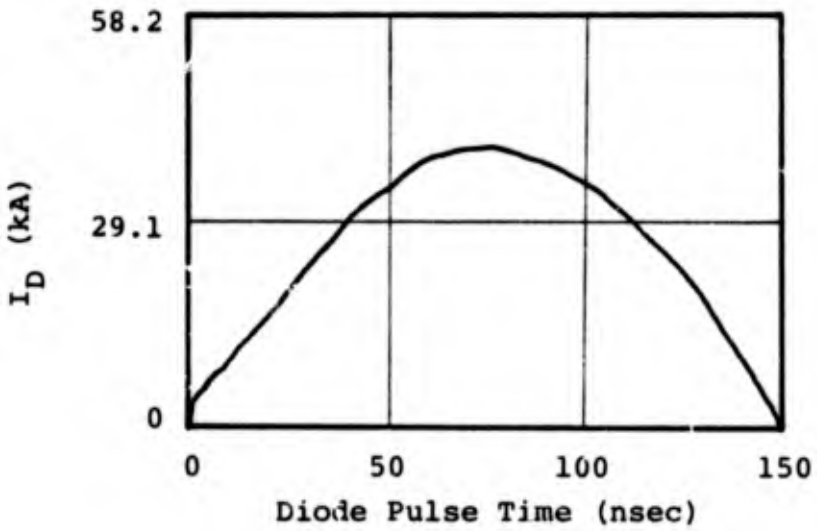

Figure 5.3 SPI diode current, I_D.

is not transmitted by the grid. The beam current injected $I_{inj}(t)$ is measured separately (Figure 5.4).

The following assumptions were made in connection with the electron emission:

1. The energy ε (in volts) of the electrons emitted is given by

$$\varepsilon(t) = v_D(t) - L_D \, (dI_D/dt)$$

where the diode inductance L_D is taken to have the value of 20 nanohenries.

2. The injected current I_{inj} is assumed to be initiated 5 nanoseconds after the beginning of the diode pulse (Figure 5.1, 5.2).

3. At any instant t the electrons injected into the cavity are monoenergetic with energy $\varepsilon(t)$.

4. The injected current density $j_{inj}(t)$ is uniform over the emitting surface and is given by

$$j_{inj}(t) = I_{inj}(t)/\pi R_B^2 \quad .$$

5. The electrons are injected normal to the emitting surface.

In the above assumptions no account is taken of the loss in energy of electrons in passing through the mylar wire mesh. Also, no account is taken of the beam transport in the diode region which, in the experiment, contained gas at finite pressure.

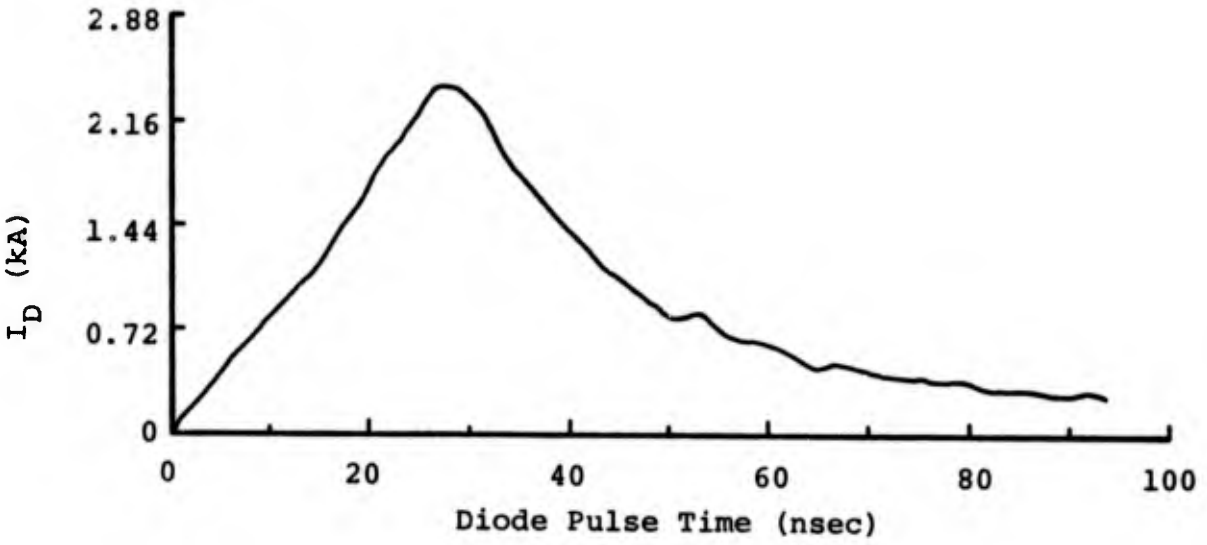

Figure 5.4 Injected current I_{inj}.

Other assumptions include:

6. The anode mesh and the other walls of the cavity are assumed grounded.

7. The cavity is evacuated.

8. Electrons, once they strike a wall, are absorbed.

9. The electrons are treated classically.

10. The chamber, with octagonal cross section, is replaced by a cylinder with circular cross section. Also, the recess at the receiving end of the cavity (not shown in Figure 5.1) is not taken into account.

With these assumptions three calculations were performed (termed I, II and III). In I a mesh of 16 x 16 cells was used and 10 particles were injected per time-step ($\Delta t = 2.5 \times 10^{-11}$ sec). In II the same mesh was used but three times as many particles were injected (so that the average charge per particle is 3 times smaller). Comparison of these two calculations indicates the degree of approximation associated with the number of particles followed. Finally, in III a finer 32 x 32 mesh was used ($\Delta t = 1.25 \times 10^{-11}$ sec) and 40 particles were injected per cycle. This resulted in having as many as 4000 particles present in the mesh at any time.

The results of these calculations are shown in Figure 5.5. They are quite similar except near the tail of the pulse where fluctuations in the transmitted current in I were greater than either II or III. The rise of the pulse is similar in all three calculations. The peak current is slightly less in III than in I or II. The abrupt fall off in current which follows the onset of space-charge limiting (at approximately 19 nanoseconds) differs slightly in the three calculations

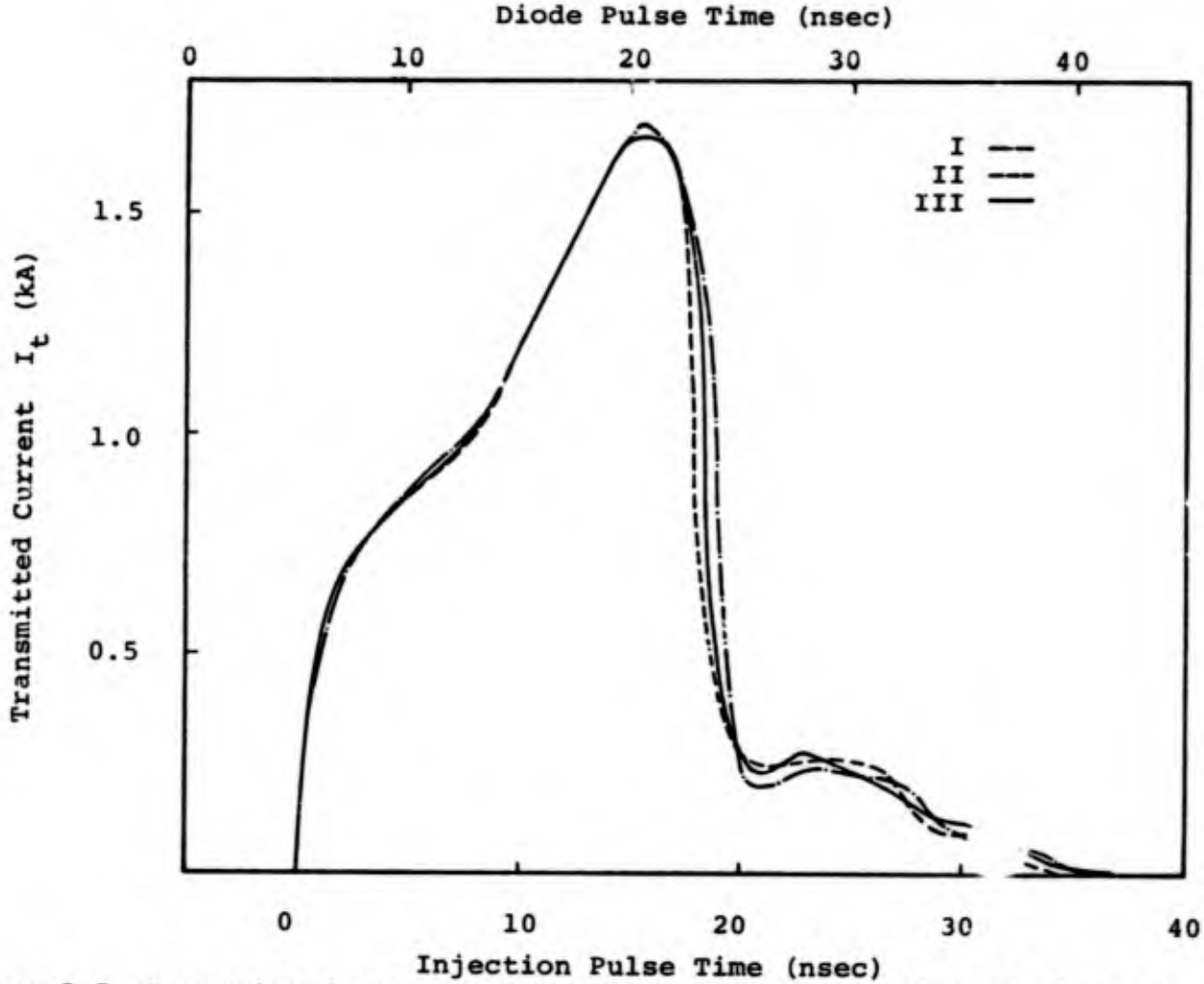

Figure 5.5 Transmitted current (in kiloamps) as a function of time for the three calculations performed. I has a 16 x 16 mesh with a low particle injection rate (i.e., larger charge per particle). II uses the same mesh but the injection rate is 3 times higher. III uses a 32 x 32 mesh and the injection rate is four times that of I. The time scale indicated begins at the initiation of injection which is taken to be 5 nsec later than the diode pulse initiation.

with the result of III being intermediate between the two others.

The dynamics of the beam transmission are illustrated in Figures 5.6 through 5.8. Before the onset of space-charge limiting the flow is laminar with some radial expansion taking place. The maximum potential at this time (~ 16 nsec) is approximately 65 kV and this is less than the energy of the electrons being injected. At ~ 19 nsec the energy of the electrons falls below this potential and space-charge limiting ensues. By 31.9 nsec (Figures 5.7, 5.8) the current injected is very low and the maximum potential is no greater than 32 kV. However, the emitted electron energy is rather less than this and the transmission is limited by space-charge.

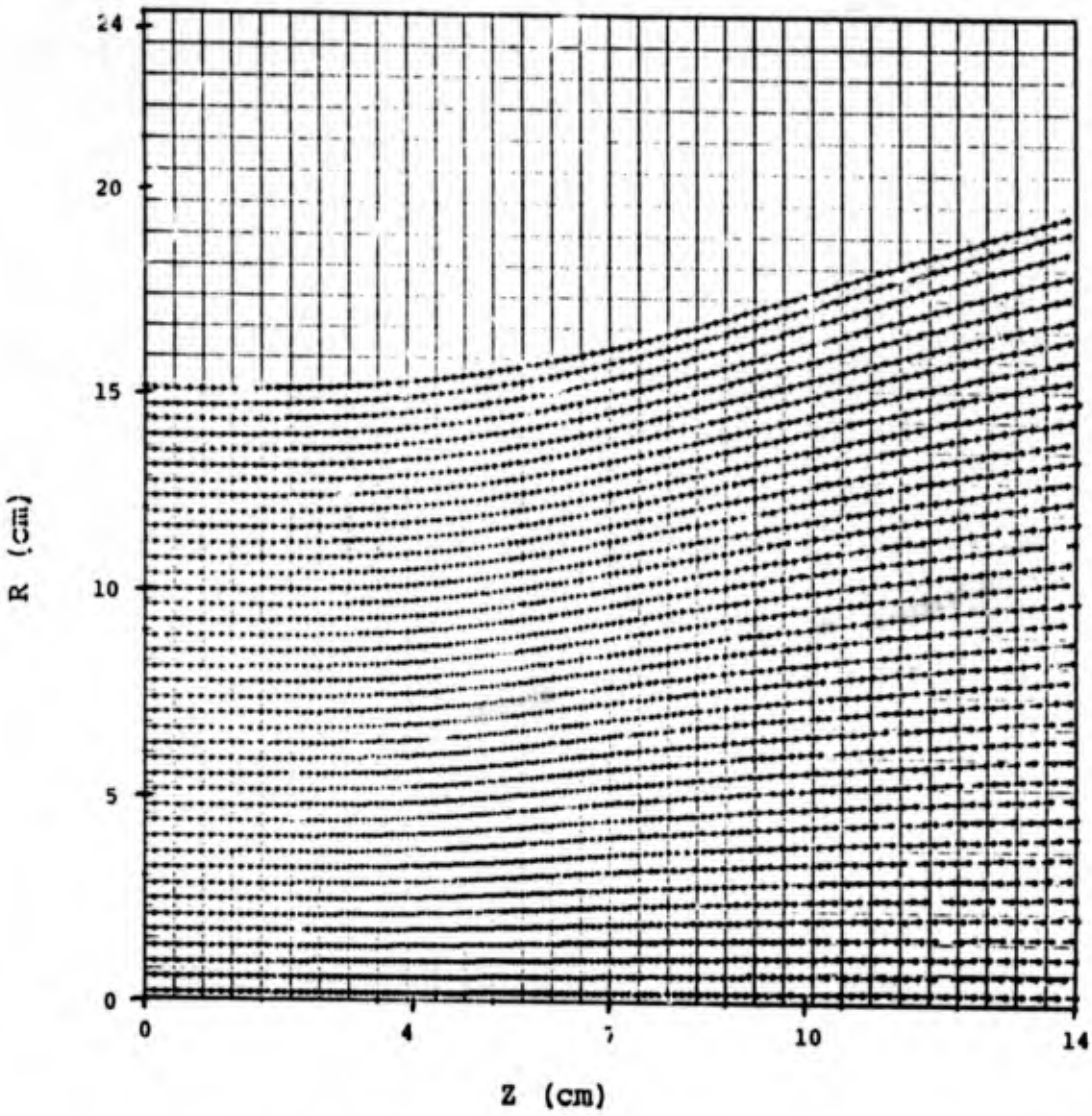

Figure 5.6 Electron flow after 16 nsec. The electrons between Z = 4 and Z = 7 cm are moving most slowly and are most densely bunched.

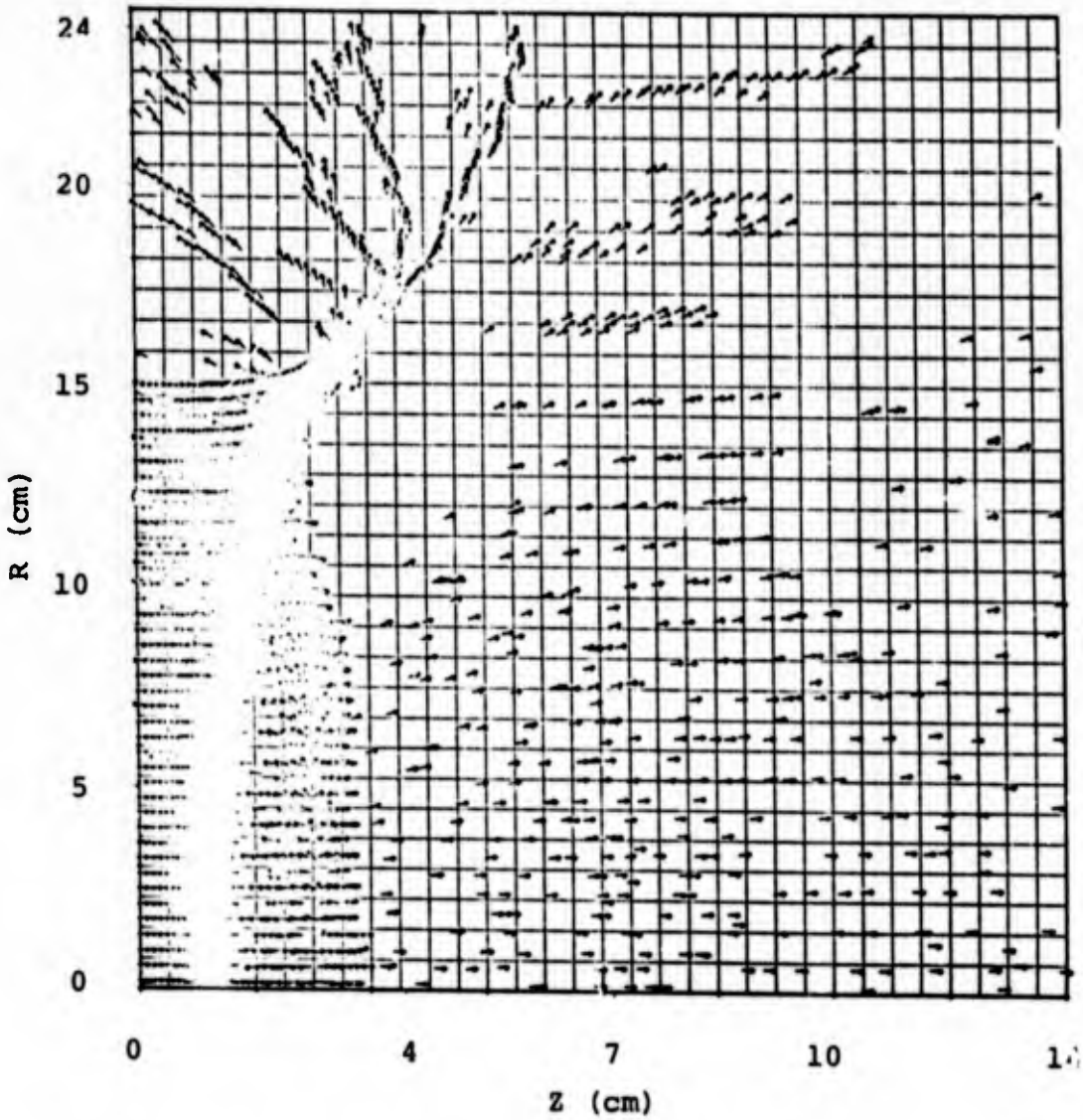

Figure 5.7 Electron flow after 31.9 nsec. The transmission is still limited by space charge.

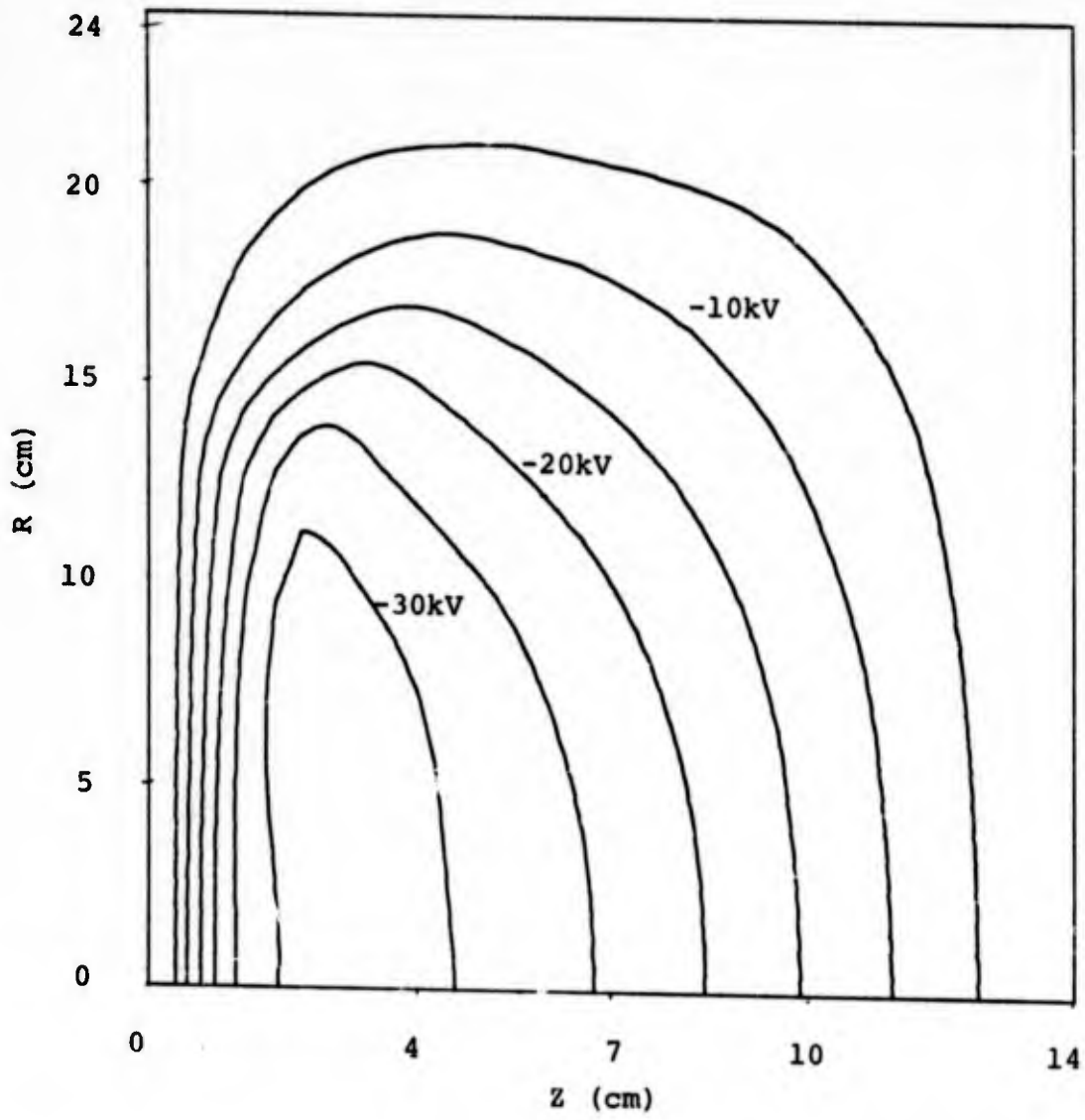

Figure 5.8 Potential contours at 31.9 nsec.

REFERENCES

2.1.1 Osborn, D. C. and A. R. Wilson, DNA 3094F, October 1973 (U).

2.2.1 Morse, P. M. and H. Feshbach, Methods of Theoretical Physics, Chapter 10, McGraw-Hill, New York, 1953.

2.3.1 Dellin, T. A. and C. J. McCallum, IEEE Trans. Nuc. Sci., NS-20, 91, 1973.

3.3.1 Mott, N. F. and M. S. W. Massey, The Theory of Atomic Collisions, p. 503, Oxford, 1965.

3.3.2 Nelms, A. T., NBS Circular 577, 1956.

3.3.3 McClure, G. W., Phys. Rev. 90, 796, 1953.

4.1 dePlomb, G. and A. Woods, DNA Report 3140?, March 1973 (U).

4.2 Birdsall, C. K., A. B. Langdon and M. Okuda, p. 241, Vol. 9, Methods in Computational Physics (Alder, B., S. Fernbach, M. Rotenberg), Academic Press, New York, 1970.

4.3 Birdsall, C. K. and K. Fuss, J. Comp. Phys. 3, 494, 1969.

4.4 Hockney, R. W. P., p. 135, Vol. 9, Methods in Computational Physics, Academic Press, New York, 1970.

4.5 Cooley, J. and J. W. Tukey, Math. Comp. 297, 19, 1965.